# DESIGN AND DEVELOPMENT OF FIBER BRAGG GRATING SENSOR FOR DETECTING OF HYDROGEN GAS IN TRANSFORMER OIL

**MOHD RAFFI BIN SAMSUDIN**

**FACULTY OF ENGINEERING**
**UNIVERSITY OF MALAYA**
**KUALA LUMPUR**

**2020**

# DESIGN AND DEVELOPMENT OF FIBER BRAGG GRATING SENSOR FOR DETECTING OF HYDROGEN GAS IN TRANSFORMER OIL

**MOHD RAFFI BIN SAMSUDIN**

**THESIS SUBMITTED IN FULFILMENT OF THE REQUIREMENTS FOR THE DEGREE OF DOCTOR OF PHILOSOPHY**

**FACULTY OF ENGINEERING**
**UNIVERSITY OF MALAYA**
**KUALA LUMPUR**

**2020**

**UNIVERSITY OF MALAYA**

**ORIGINAL LITERARY WORK DECLARATION**

Name of Candidate: Mohd Raffi bin Samsudin

Registration/Matric No: KHA 120052

Name of Degree: Doctor of Philosophy

Title of Project Paper/Research Report/Dissertation/Thesis ("this Work"):

Design and development of fiber Bragg grating sensor for detecting of hydrogen gas in transformer oil

Field of Study: Engineering, Photonics

I do solemnly and sincerely declare that:

(1) I am the sole author/writer of this Work;
(2) This Work is original;
(3) Any use of any work in which copyright exists was done by way of fair dealing and for permitted purposes and any excerpt or extract from, or reference to or reproduction of any copyright work has been disclosed expressly and sufficiently and the title of the Work and its authorship have been acknowledged in this Work;
(4) I do not have any actual knowledge nor do I ought reasonably to know that the making of this work constitutes an infringement of any copyright work;
(5) I hereby assign all and every rights in the copyright to this Work to the University of Malaya ("UM"), who henceforth shall be owner of the copyright in this Work and that any reproduction or use in any form or by any means whatsoever is prohibited without the written consent of UM having been first had and obtained;
(6) I am fully aware that if in the course of making this Work I have infringed any copyright whether intentionally or otherwise, I may be subject to legal action or any other action as may be determined by UM.

Candidate's Signature Date:

Subscribed and solemnly declared before,

Witness's Signature Date:

Name:

Designation:

**DESIGN AND DEVELOPMENT OF FIBER BRAGG GRATING SENSOR FOR DETECTING OF HYDROGEN GAS IN TRANSFORMER OIL**


## ABSTRACT

Hermetically sealed oil-immersed transformers are the key to electricity distribution networks. They are also one of the most expensive facilities in the electricity supply network. Immediate replacement is expected for this type of transformer upon failure because it is directly connected to the customer. Transformer oil acts as insulation, coolant and condition indicator. To date, there is no economical real-time monitoring system available to monitor the transformer oil condition. Therefore, there is a need to develop a cheap, non-intrusive and non-electrical sensor to monitor the health of the transformer by measuring the amount of dissolved hydrogen gas in oil, which is an early indicator for electrical fault in the transformer. In this research, sixteen fiber Bragg gratings (FBG) sensors which are based on different palladium (Pd) coatings ratios and thicknesses were developed to detect dissolved hydrogen gas content in transformer oil. All the coatings were prepared by using physical vapour deposition technique with a combination of RF and DC methods. All samples have palladium-chromium ratios of 100:0 ($Pd_{100}$), 88:12 ($Pd_{88}Cr_{12}$), 75:25 ($Pd_{75}Cr_{25}$) and 67:33 ($Pd_{67}Cr_{33}$) and for each composition, four (4) samples were prepared with different coating thicknesses which were 970 nm, 1060 nm, 1180 nm and 1300 nm. $TiO_2$ was used as the adhesion layer between FBG and the Pd-Cr coatings. Initially, the adhesion layer on a test fiber was tested inside heated transformer oil for 40 days before the palladium and chromium coating. The $TiO_2$ coating showed excellent adhesion properties to the fiber because it did not show any signs of surface roughness, uneven thickness, peeling off or micro-cracking after it was immersed in transformer oil. Transformer oil samples with different dissolved hydrogen contents were then prepared by diffusing hydrogen gas into the oil. The samples were tested by using a portable dissolved gas analyser. All the

FBG sensors were tested with separate transformer oil with different levels of dissolved hydrogen, and the wavelength shifts were recorded. The measurement of coating thicknesses and compositions were done by scanning electron microscopy (SEM) and energy dispersive x-ray (EDX) method. On the other hand, a high voltage generator and a spark gap were developed to generate partial discharge in the oil for validation purpose. All sensors were tested with hydrogen gas generated by partial discharge activity, and the errors were less than 10%. $Pd_{100}$ sensor showed average induced strains of 0.1801 pm/ppm (970 nm of coating thickness) whereas $Pd_{67}Cr_{33}$ sensor showed the lowest strain of 0.0137 pm/ppm (970 nm of coating thickness). This work has demonstrated a potential of using alloy metal like chromium to the palladium metal to enhance dissolved hydrogen detection range. Different ranges of saturation were shown for all FBG sensors due to different palladium-chromium composition. This sensor has the potential to be used inside the hermetically sealed transformer to detect electrical fault at the early stage. The sensor can be made as a standalone module which may be used to produce fault alarm once hydrogen exceeded specific preset value.

Keywords: Fiber Bragg gratings, fiber optics sensors, hermetically sealed transformer

**REKABENTUK DAN PEMBANGUNAN SENSOR FIBER BRAGG GRATING UNTUK MENYUKAT GAS HIDROGEN DI DALAM MINYAK ALATUBAH**

**ABSTRAK**

Alatubah minyak adalah kunci kepada rangkaian pengedaran elektrik. Ia juga merupakan salah satu fasiliti yang paling mahal dalam rangkaian bekalan elektrik. Penggantian segera dijangka untuk alatubah jenis ini apabila gagal kerana ia secara langsung disambung terus dengan pelanggan. Minyak alatubah bertindak sebagai penebat, penyejuk dan penunjuk keadaan. Sehingga kini, tidak ada sistem pemantauan masa nyata yang boleh digunakan untuk memantau keadaan minyak pengubah. Oleh itu, terdapat keperluan untuk membangunkan sensor murah yang bukan konduktif dan tidak menyebabkan gangguan pada sistem elektik untuk memantau keadaan pengubah dengan mengukur jumlah gas hidrogen terlarut dalam minyak. Sensor ini merupakan penunjuk awal untuk kerosakan elektrik dalam pengubah. Dalam kajian ini, enam belas gentian Bragg gratings (FBG) yang disalutkan pada nisbah kandungan palladium (Pd) dan ketebalan yang berbeza dibangunkan untuk mengesan kandungan gas hidrogen yang terlarut dalam minyak alatubah. Semua salutan disediakan dengan menggunakan teknik pemendapan wap fizikal dengan gabungan kaedah RF dan DC. Semua sampel mempunyai nisbah paladium-kromium iaitu 100:0 ($Pd_{100}$), 88:12 ($Pd_{88}Cr_{12}$), 75:25 ($Pd_{75}Cr_{25}$) dan 67:33 ($Pd_{67}Cr_{33}$) dan bagi setiap komposisi, 4 sampel disediakan dengan ketebalan lapisan salutan yang berbeza iaitu 970 nm, 1060 nm, 1180 nm dan 1300 nm. $TiO_2$ digunakan sebagai lapisan lekatan antara FBG dan lapisan Pd-Cr. Pada mulanya, kualiti lapisan lekatan pada gentian biasa telah diuji dalam minyak alatubah dengan memanaskannya selama 40 hari. Ini dilakukan sebelum lapisan palladium dan kromium disalut keatas gentian Bragg grating. Lapisan $TiO_2$ telah menunjukkan sifat lekatan yang sangat baik untuk gentian kerana salutan tidak menunjukkan tanda-tanda kekasaran

permukaan, ketebalan yang tidak rata, pengelupasan atau retakan mikro selepas ia direndam di dalam minyak alatubah. Selain itu, sampel minyak alatubah dengan kandungan hidrogen yang berbeza telah disediakan dengan melarutkan gas hidrogen ke dalam minyak. Kemudian, sampel telah diuji dengan menggunakan penganalisis gas terlarut mudah alih. Semua sensor FBG diuji dengan minyak alatubah berasingan dengan tahap hidrogen yang berbeza dan perubahan panjang gelombang telah direkodkan. Pengukuran ketebalan salutan dan komposisi dilakukan oleh kaedah SEM-EDX. Sebaliknya, penjana voltan tinggi dan celah percikan telah dibangunkan untuk menghasilkan pelepasan separa dalam minyak untuk tujuan pengesahan. Semua sensor telah diuji dan disahkan dengan gas hidrogen yang terhasil daripada aktiviti discaj separa dan ralat ialah kurang daripada 10%. Sensor $Pd_{100}$ menunjukkan ketegangan teraruh purata iaitu sebanyak 0.1801 pm/ ppm (970 nm ketebalan salutan) manakala sensor $Pd_{67}Cr_{33}$ menunjukkan ketegangan terendah iaitu 0.0137 pm / ppm (970 nm ketebalan salutan). Kajian ini telah menunjukkan potensi mengabungkan logam aloi seperti kromium ke logam paladium untuk meningkatkan jangkauan pengesanan hidrogen yang terlarut. Tahap tepu yang berbeza telah ditunjukkan oleh semua sensor FBG kerana komposisi palladium-kromium yang berbeza. Sensor ini mempunyai potensi untuk digunakan di dalam alatubah minyak kedap untuk mengesan kerosakan elektrikal pada peringkat awal. Sensor ini juga boleh dibuat sebagai modul mandiri yang boleh digunakan untuk menghasilkan penggera kerosakan apabila gas hidrogen di dalam minyak melebihi nilai pratetap tertentu.

Kata kunci: Gentian Bragg gratings, sensor gentian optik, alatubah kedap minyak

## ACKNOWLEDGEMENTS

Alhamdulillah, gratitude to the most merciful Allah for guiding me to complete this study successfully. Thanks for the support and love given by my parents, Mr Sumsudin bin Naji Bulhak and Madam Azrah binti Moiden. I would like to express my gratitude to my wife Madam Zeenath Begum binti Akbar Khan for being patient and supported me in completing this study for the past 7 years.

Thanks to my supervisors, Prof Faisal Rafiq Mahamd Adikan and Dr Shee Yu Gang, for guiding me throughout the project. Besides, I would like to thank my lab members for providing me with data and facilities to perform the experiments successfully.

Finally, I would like to thank the University of Malaya for giving me the opportunity and funding to carry out this challenging project.

## TABLE OF CONTENTS

## LIST OF FIGURES

## LIST OF TABLES

## LIST OF SYMBOLS AND ABBREVIATIONS

**Symbols**

| | |
|---|---|
| $R$ | Resistor |
| $\theta_0$, $\theta_1$ | Incident and refraction angle |
| $n_0$ ,$n_1$ | Refractive index |
| $K_\varepsilon$ | Strain sensitivity |
| $p_{11}$ | Pockel's coefficient |
| $v$ | Poisson's ratio |
| $\omega$ | Angular frequency |
| $\beta$ | wave propagation constant |
| $P$ | Pressure |
| $\Phi$ | Incident angle |
| $A$ | Ampere |
| $M$ | Molar |
| $V$ | Voltage |
| $d$ | Thickness |
| $t$ | Time |
| $E$ | Electric Field |
| $U$ | Potential difference |
| $\varepsilon_r$ | Relative Permittivity |
| $C$ | Capacitor |
| $Z$ | Impedance |
| $L1$ | Minimum Gas Concentration |
| $x$ | x-coordinate |
| $y$ | y-coordinate |

| | | |
|---|---|---|
| AC | : | Alternating Current |
| $Al_2O_3$ | : | Aluminium Oxide |
| AI | : | Artificial Intelligence |
| ANN | : | Artificial Neural Network |
| ASE | : | Amplified Spontaneous Emission |
| $B_2O_3$ | : | Boron Trioxide |
| $C_2H_2$ | : | Acetylene |
| $C_2H_4$ | : | Ethylene |
| $C_2H_6$ | : | Ethane |
| $CdCl_2$ | : | Cadmium Chloride |
| CdS | : | Cadmium Sulfide |
| $CH_4$ | : | Methane |
| Cr | : | Chromium |
| CrH | : | Chromium Hydride |
| CIGRE | : | International Council on Large Electric Systems |
| cm | : | centimeter |
| CO | : | Carbon Monoxide |
| CVD | : | Chemical Vapour Deposition |
| DGA | : | Dissolved Gas Analysis |
| EDX | : | Energy Dispersive X-ray |
| EMI | : | Electromagnetic Interference |
| FBG | : | Fiber Bragg Gratings |
| fm | : | femtometer |
| GC | : | Gas Chromatography |
| GIS | : | Gas Insulated System |
| $GeO_2$ | : | Germanium dioxide |

| | | |
|---|---|---|
| $H_2$ | : | Hydrogen |
| $H_2S$ | : | Hydrogen Sulfide |
| HOPG | : | Highly Oriented Pyrolytic graphite |
| HV | : | High voltage |
| Hz | : | Hertz |
| IEC | : | International Electrotechnical Commission |
| IEEE | : | Institute of Electrical and Electronics Engineers |
| ISO | : | International Organization for Standardization |
| KrF | : | Krypton Flouride |
| LV | : | Low Voltage |
| MIS | : | Metal-Insulator-Semiconductor |
| mm | : | milimeter |
| MTM | : | Malaysian Transformer Manufacturing |
| MVA | : | Mega-Voltage-Ampere |
| NA | : | Numerical Aperture |
| $NaBH_4$ | : | sodium borohydride |
| NIR | : | Near-infrared spectroscopy |
| nm | : | nanometer |
| OCEF | : | Overcurrent and earth fault protection |
| PAS | : | Photo-acoustic gas spectroscopy |
| PD | : | Partial discharge |
| Pd | : | Palladium |
| Pd-H | : | Palladium hydride |
| PEO | : | Polyethyleneoxide |
| PLC | : | Power line carrier |
| pm | : | picometer |

| | | |
|---|---|---|
| ppm | : | Parts per million |
| ppb | : | Parts per billion |
| PVD | : | Physical vapour deposition |
| RF | : | Radio Frequency |
| SEM | : | Scanning electron microscopy |
| $SnO_2$ | : | Tin dioxide |
| sccm | : | Standard cubic centimetre per minute |
| TDCG | : | Total Dissolved Combustible Gas |
| TNB | : | Tenaga Nasional Berhad |
| UV | : | Ultraviolet |
| $WO_3$ | : | Tungsten Trioxide |
| XRD | : | X-ray powder diffraction |

# CHAPTER 1: INTRODUCTION

## 1.1 Background

Hermetically sealed transformers are major power distribution system equipment. Their reliability not only affects the electric energy availability of the supplied area but also influences the optimal operation of the utility. For example, the fault of a distribution transformer may leave thousands of homes without heat and light, and the failure of a step-up transformer in a power generation plant may cause the forced outage of the attached generation unit. Figure 1.1 shows the transformer reliability survey worldwide conducted by the International Council on Large Electric Systems (CIGRE) (Petersen, 2010). It shows that the winding and insulation failure contributed to 40% of the transformer failure. Besides, in Malaysia, there were 450 hermetically sealed transformers which had failed prematurely over the past 15 years. The failure modes are insulation (paper and oil) failure and mechanical failure (tap changer, contacts) (Mohd Iqbal Ridwan, 2011).

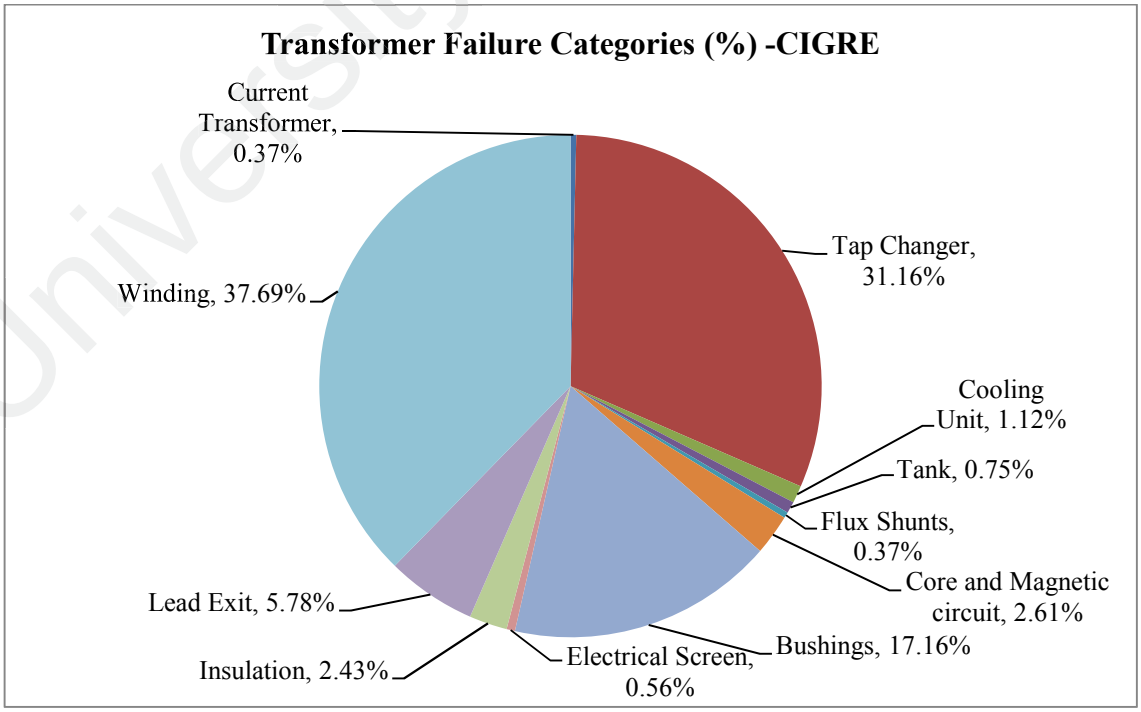


**Figure 1.1: Transformer failure categories**

If the protection system operates quickly, damages of the transformer could be minimised. However, sophisticated protection systems such as arc protection will cost higher than basic overcurrent and earth fault protection (OCEF) for a transformer. Although the collateral damage can be avoided, carbon contamination can be extensive and destructive. Tiny particles of carbon may travel into the winding and cause surface tracking and reduce the insulation integrity. Figure 1.1 shows the hermetically sealed transformer and its internal construction

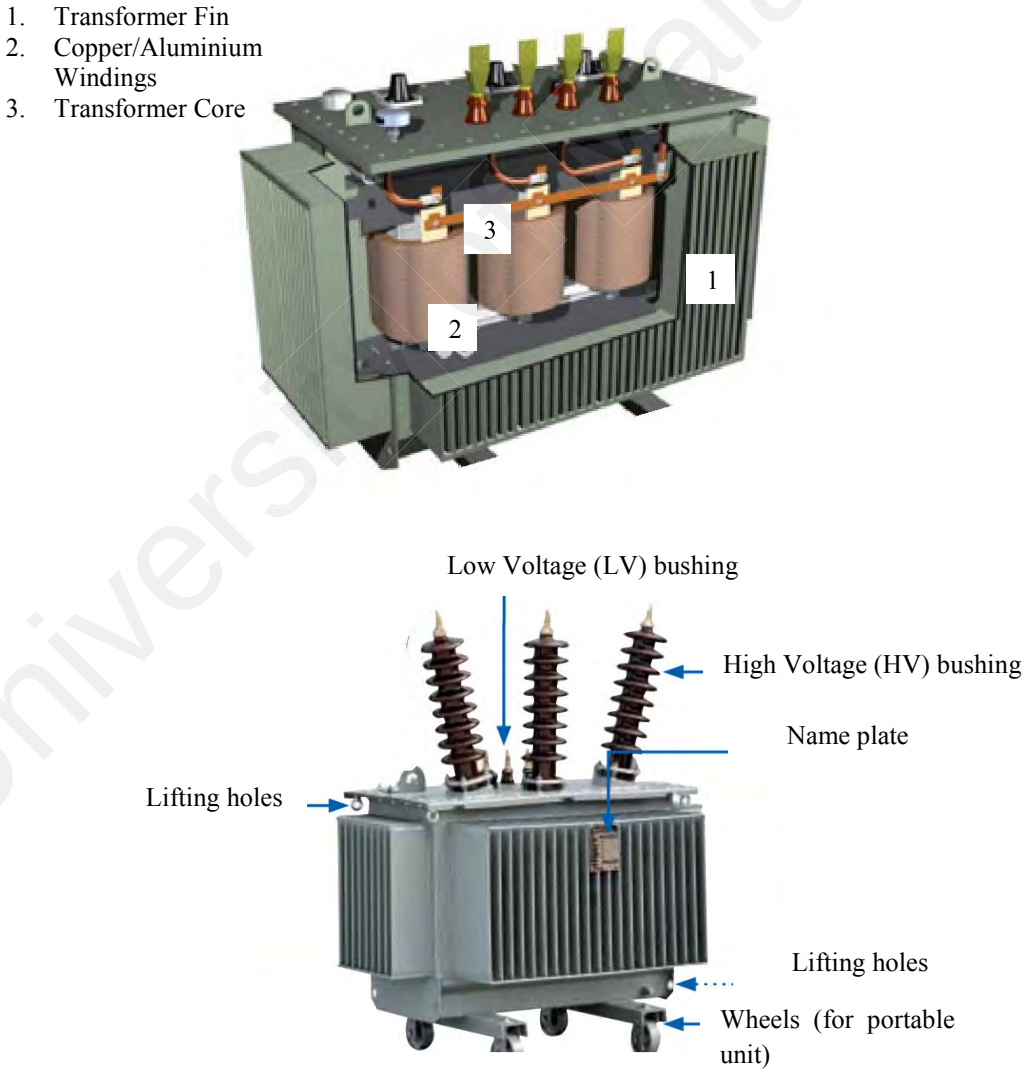


**Figure 1.2: Hermetically sealed transformer (Picture courtesy of TNB Research Sdn. Bhd.)**

Hermetically sealed transformers mainly consist of three components, which are core and windings, paper insulation and oil (Figure 1.1). The winding winded with an insulating paper and immersed in transformer oil. The paper-insulated winding, which is immersed in the transformer oil, will have higher dielectric strength. The thickness of the insulating paper will determine the insulation strength, whereas the size of the winding conductor will decide the capacity of the transformer (Naphthenics, 2008).

Transformers have two sets of winding, known as primary winding and secondary winding. The number of winding depends on the intended supply, either three-phase or single-phase. For a three-phase system, the number of windings on the primary and the secondary side is 6, and for single-phase system, the number of windings on the primary and secondary is one each (Kulkarni, 2004). All of the transformers manufactured are subjected to routine tests following IEC 60076-1: 2011 standard.

Dissolved Gas Analysis (DGA) method is the current practice to monitor the condition of the power transformer for the past five decades. Usually, the DGA test is done in the lab by using the extracted oil from the power transformer. Seven key gasses are used in determining the condition of the power transformers. These are Hydrogen, Methane, Acetylene, Ethane, Ethylene, Carbon Monoxide and Carbon Dioxide (IEC, 2015). This conventional method will require more than a week to obtain the lab test result due to transportation and stock stacking. The delay in processing the samples may cause a catastrophic failure to the transformer. Dissolved hydrogen in transformer oil is the vital gas for incipient electrical fault in the transformer. Earlier signs of failure, such as winding and insulation deterioration can be detected by monitoring the amount of hydrogen inside the transformer oil.

The future transformer condition assessment will be based on the online condition monitoring technique. The data from an online condition monitoring system will be

used as a part of the smart grid system, thus will enable real-time monitoring of the transformer and severe fault can be prevented or minimised. An online system will support the operation manager to make a decision on the maintenance regime of a transformer based on the real-time data. The real-time data can be obtained by installing one or more sensors inside the transformer. Besides, fiber optics sensors are preferred because they can produce a faster response than other types of sensor. At the same time, it also has higher electrical resistance as well (Haema, 2012).

The major concern of incipient fault inside the transformer is that it may decrease the electrical and mechanical integrity of the insulation system. This may progress to a condition that the insulation cannot withstand transient over-stresses caused by through-fault current (mechanical forces on windings) and electrical over-voltages (temporary, switching or lightning). Therefore, incipient fault diagnosis is closely related to insulation condition assessment.

## 1.2 Hydrogen as the key gas for electrical fault in transformer oil

Thermal and electrical stresses can occur in a transformer in normal operating conditions. However, elevated stresses can generate hydrocarbon gases which indicate a potential problem in the transformer. The gas generation varies with transformer design, loading, and the type of insulation materials. Figure 1.2 shows the gas generation chart for a transformer.

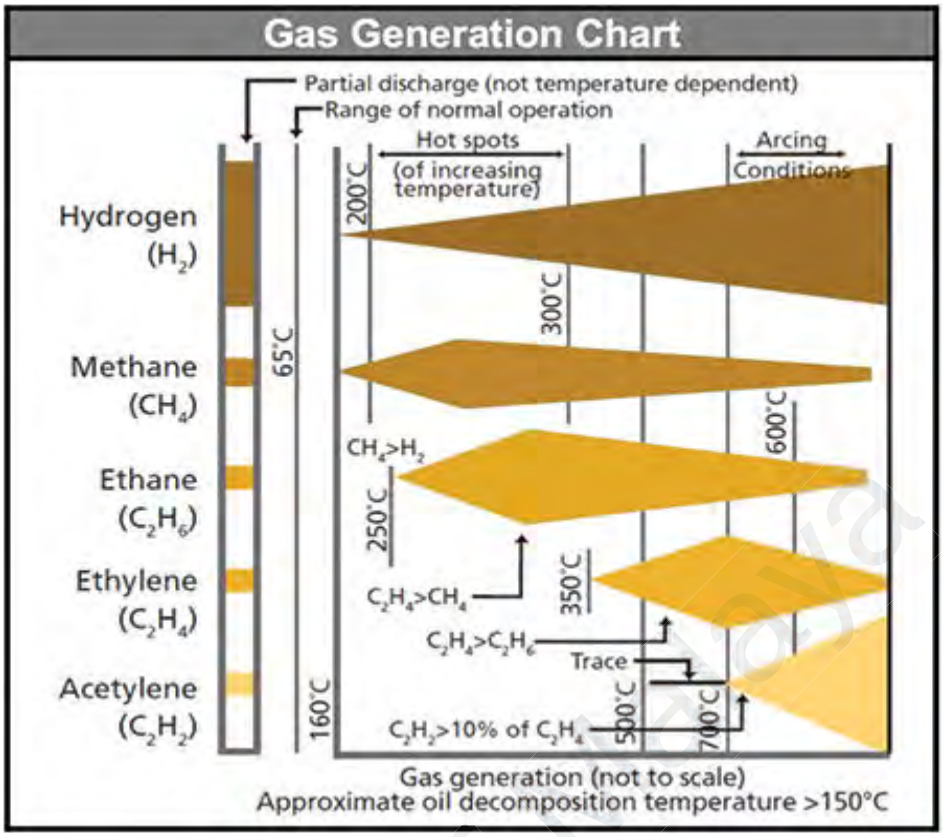


**Figure 1.3: Gas generation chart (Arvind, Khushdeep, & Deepak, 2008)**

Hydrogen is the vital gas to indicate faults in transformers. Hydrogen and methane begin to form in small amounts at around 150°C. As the temperature increases, the amount of hydrogen will increase significantly. At all temperature of faults, hydrogen will still be formed (Bandyopadhyay, 2007). The formation of the acetylene is an indication of high-temperature discharge in the transformer. Acetylene is produced at temperatures between 500 to 700°C. At this temperature, hydrogen will be formed too.

Monitoring the amount of dissolved hydrogen in the transformer oil will give an early indication of the electrical fault inside the transformer. Therefore, monitoring hydrogen in the hermetically sealed transformer will be a right approach in providing an early indication on the incipient and fault inside a transformer because it is not economical to install a complete range of DGA online system due to size and the cost. In addition, the dissolved hydrogen gas content cannot be used to evaluate the cellulose ageing of the transformer. However, this study only covers the electrical fault inside the

transformer. Table 1.1 shows the typical fault in a transformer and the corresponding gasses dissolved in oil.

**Table 1.1: Typical faults in the transformer and corresponding fault gasses (Arvind et al., 2008)**

| Indication / Faults | $H_2$ | CO | $CO_2$ | $CH_4$ | $C_2H_2$ | $C_2H_4$ | $C_2H_6$ | $O_2$ | $H_2O$ |
|---|---|---|---|---|---|---|---|---|---|
| Cellulose aging | | • | • | | | | | | • |
| Mineral oil decomposition | • | | | • | • | • | • | | |
| Leaks in oil expansion systems, gaskets, welds, etc. | | | • | | | | | • | • |
| Thermal faults – Cellulose | • | • | • | • | | | | • | |
| Thermal faults in oil @ 150 °C – 300 °C | • | | | • | | TRACE | • | | |
| Thermal faults in oil @ 300 °C - 700 °C | • | | | • | TRACE | • | • | | |
| Thermal faults in oil @ 700 °C | • | | | • | • | • | | | |
| Partial Discharge | • | | | • | TRACE | | | | |
| Arcing | • | | | • | • | • | | | |

## 1.3 Online Monitoring system

In recent years, utility managers are putting more attention on online monitoring approach for dissolved gas analysis (DGA) techniques. The DGA online monitoring system is an independent system which is mounted to the transformer to extract the oil in situ and measure the amount of fault gasses. Gas chromatography (M. Duval, 2002) is the most common technique used for online DGA. In addition, there are other techniques which are claimed to give consistent results such as the gas chromatography (GC) technique, photo-acoustic gas spectroscopy (PAS) (Y. Yun, 2008), and near-infrared spectroscopy (NIR) (M. Benounis, 2008). All these techniques can monitor transformer continuously despite there is a long time delay between the fault initiation and the fault detection. However, each unit is comparatively expensive to be installed in a hermetically sealed transformer. The cost of the hermetically sealed transformer, which is less than 5 MVA is almost equal to the cost of an online monitoring system. Besides, there is no possibility to locate the exact fault location (J. Deng, 2001). Figure 1.4 to Figure 1.6 show the commercially available online monitoring system by Morgan

Shaffer (gas chromatography), Kelman (photo-acoustic spectroscopy) and LumaSense (near-infrared spectroscopy) respectively. The photoacoustic method and the near-infrared spectroscopy are using the optical method where light waves are directed into a gas chamber containing gasses, and the power absorption at the specific wavelength are measured (Y. Yun, 2008) .


**Figure 1.4: Morgan Shaffer Callisto using gas chromatography technique (Picture courtesy from Morgan Shaffer website)**


**Figure 1.5: Kelman Transfix using photo-acoustic gas spectroscopy technique (Picture courtesy from Kelman GE. website)**

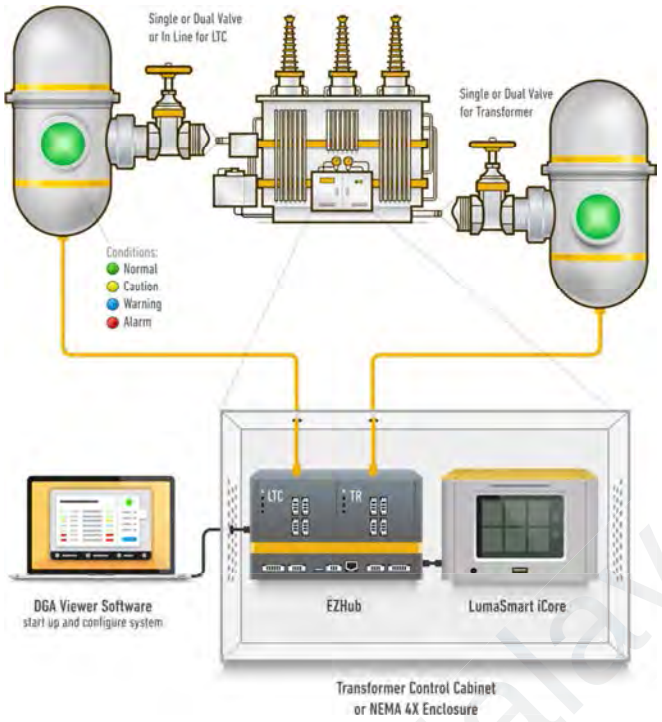


**Figure 1.6: LumaSense online DGA using near-infrared spectroscopy technique (Picture courtesy from LumaSense website)**

## 1.4 Optical Measurement

The key gas for partial discharge occurrence detection in a transformer is hydrogen. In this research, there is a need to develop a non-electrical sensor to place inside a hermetically sealed transformer to monitor the level of hydrogen developed due to electrical fault. Fiber optic has been identified as one of the candidates to develop the sensor in this study. Fiber optic is widely used in the power system for communication purpose (Palais, 2001; R. Schwarz, 2005). Recently, fiber optics are used in arc protection for vacuum circuit breaker, temperature sensors for transformer windings (Cheng et al., 2012) and partial discharge sensors in power transformer (Kulkarni, 2004). They are preferred in the power system because they are not susceptible to noise and other frequency components in the power system. Besides, fiber optic is used in detecting gases in the air, such as hydrogen and methane. For instance, a fiber optic cable with palladium cladding can detect hydrogen in the air (Takeshita, Tanaka, Ishizaki, & Stanbury, 1993).

One of the earliest research was to evaluate the change of resistivity of the thin palladium film to detect the presence of hydrogen gas (A. D'Amico, 1982; I. Lundstrom, 1975; M.C. Steele, 1976). Palladium will expand when it is exposed to hydrogen gas naturally (Ma, Li, Luo, Mu, & Wang, 2012). A palladium metal which reacts with hydrogen will produce palladium hydrides which have larger lattice dimension and reduced conductivity (M. D. Yang, Jixiang, 2012). The lattice dimension difference between the palladium and palladium hydride is in nano-scale; thus, it can be measured by using an optical method (Xue, 2013). Palladium, when is coated on the fiber Bragg gratings (FBG), will expand and cause strain on the FBG when it is exposed to hydrogen gas (Dai, Yang, Yu, & Lu, 2013; M. H. Yang, Dai, Cao, Liao, & Zhang, 2012). The strain of FBG will cause Bragg wavelength shift and the wavelength shift can be measured by using an optical spectrum analyser. Palladium coated FBG sensor offers accurate and sensitive remote sensing as well as volumetric detection of hydrogen with no risk of ignition (X. Bevenot, 2000). It was also shown that the Pd-coated FBG sensor's response was linear for a hydrogen concentration of 0.3-1.8% in air. However, these measurements were taken at room temperature, and the response time was not mentioned (B. Sutapun, 1999).

Apart from palladium coated on FBG, there are other optical methods in detecting hydrogen. Those methods are based on the direct interaction of hydrogen gas with a transducer and interaction between hydrogen and the optical wave (Slaman, Westerwaal, Schreuders, & Dam, 2012). The direct interaction of the hydrogen with the optical wave was analysed by using infrared absorption technique or Raman scattering. Besides, the interaction between the hydrogen and a transducer will cause fiber crystalline structure modification and change its effective refractive index (A. D. Kersey, 1997). Besides, there were other approaches used to detect hydrogen such as using Pd mirrors and interferometers, surface plasmon resonance (X. Bevenot, 2002),

measurement of the real and the imaginary components of the palladium hydride by using tapered fiber (Hernández, 2005; M. Tabib-Azar, 1999), and evanescent wave changes by the palladium hydride when it is exposed to hydrogen (B. Sutapun, 1999; F. Yang, Jung, & Penner, 2011).

The interferometric sensor operation is based on optical path length changes when the coated palladium film is exposed to hydrogen or if there is a change of temperature. However, this type of sensor does not offer multiplexing capability, and it has a complex design (B. Sutapun, 1999). Apart from that, the sensor built by using Pd micro-mirror coated on the end of a multimode fiber performed well between the temperatures of -196ºC to 23ºC. For hydrogen concentration of 100% in air, the response time was 5 seconds, whereas, for 4%, the response time was 40 seconds (X. Bevenot, 2000). In addition, micro Michelson interferometer with palladium film deposited on fiber showed a higher sensitivity to detect hydrogen from 0% - 16 % (M. Wang et al., 2012). Besides, the palladium-silver composition of 76:24 showed a detection limit of 4% of hydrogen (Dai, Yang, Chen, et al., 2012). Besides, hydrogen sensor with side-polished FBG with thin Pd film coated with magnetron sputtering showed Bragg wavelength shift of 15 pm with 0.01% of hydrogen (246 ppm) (Liu, 2011).

Furthermore, side polished sensors have showed higher sensitivity in detecting hydrogen concentration of 4-8%. The palladium-hydrogen system response was shown reversible (M. D. Yang, Jixiang, 2012). In this study, FBG sensor was used with the palladium-chromium coating with various thicknesses and composition to establish wider detection range. Palladium, when it is exposed to hydrogen, will produce palladium hydride. The palladium hydride has a different conductivity, and the change of the conductivity will indicate the presence of hydrogen. When the hydrogen content

is reduced, the palladium hydride beads will shrink and revert to palladium. Concurrently, the electrical conductivity will reduce as well (M. H. Yang et al., 2012).

## 1.4 Problem Statement

Tenaga Nasional Berhad (TNB) is the national electricity utility provider in Malaysia. There are around 65,000 of hermetically sealed transformer owned and installed by TNB throughout Malaysia. The voltage ratings for these transformers are 11kV, and the capacities are 100 kVA, 350 kVA, 500 kVA and 1000 kVA. Currently, there is no monitoring system available for these transformers. All of the transformers are protected with overcurrent and earth fault (OCEF) protection. However, the OCEF protection is a post fault protection to avoid further damages to the transformer once there is a short circuit due to insulation failure. Thus, it does not serve to proactive replacement of the transformer when it showed an abnormal sign of a fault. Besides, transformer oil is also not monitored by performing the dissolved gas analysis (DGA). The DGA serves as a condition indicator for transformer electrical fault and thermal fault. There are a few major gasses that have been identified to determine the health of a transformer which are hydrogen ($H_2$), ethane ($C_2H_6$), methane ($CH_4$), acetylene ($C_2H_2$), ethylene ($C_2H_4$), carbon monoxide (CO) and carbon dioxide ($CO_2$). Hydrogen gas is the condition indicator for partial discharge activities in a transformer. The partial discharge causes further damage to the insulation and finally causes the transformer to fail. It is not advisable to take an in-situ oil sample from hermetically sealed transformer because the transformer tank is sealed with a nitrogen blanket, thus will cause a reduction of the oil level and the refilling process needs vacuum equipment. Usually, the refilling of the hermetically sealed transformer is done in the factory. Therefore, there is a need to access the condition of the transformer at the site without extracting the oil out.

In addition, TNB is working on smart grid system which complies to IEC 61850. The initiatives under the smart grid are self-healing network, substation automation, smart home and nationwide smart meter installations. The smart grid requires secure communication and network architecture. Therefore, TNB will need to upgrade the existing fiber network to cater for more communication. For example, TNB will install radio frequency (RF) towers and power line carrier (PLC) exchanges throughout the nation for the smart meter project. These communication networks will cover the whole of Malaysia. Besides, smart meters will be installed in all substation contained hermetically sealed transformer.

The existing designs of the hermetically sealed transformer are optimised to capacity, material and resources. Therefore, it is not advisable to install any conductive sensor inside the transformer, which can jeopardise live conductor safety clearance. So, it is crucial to identify a small and non-conductive material to embed into the transformer as a sensor. Fiber optic has fulfilled the criteria for becoming the base material for sensor development. Besides, fiber optics can be connected and integrated to TNB fiber network when they are available at substations. Meanwhile, the sensor can utilise the RF and PLC networks for communication purposes. Besides, the sensor needs to have the capability for embedded temperature compensation and more straightforward integration interface with the existing network architecture.

## 1.5 Purpose of the study

This research is to explore the potential use of optical FBG based sensor as an alternative and supplementary to the commonly used techniques of detecting dissolved hydrogen gas in transformer oil. The current studies have four objectives which are as follow:

i. To investigate the feasibility of using FBG as the base material to detect dissolved hydrogen in transformer oil;

ii. To evaluate the performance of the 16 units of FBG sensors coated with $TiO_2$ as adhesive material in addition to various thicknesses and compositions of palladium- chromium alloy against hydrogen gas dissolved in transformer oil and to assess the accuracy of the palladium-chromium sensors against dissolved hydrogen generated by the sharp edges.

## 1.6 Organisation of the thesis

This thesis includes five chapters. **Chapter 1** provides a brief and concise overview of the hermetically sealed transformer and its components, conventional gas sensors and optical sensors for transformers. Besides, this chapter covers the current researches on optical sensing briefly. The research questions are clearly addressed, and objectives are outlined. Besides, explanations of the thesis organisation are described in this chapter.

**Chapter 2** presents an in-depth state of art and state of practice of ongoing research works related to conventional gas sensing transducers for transformer for the past 20 years. It includes the current monitoring system, which is widely used for gas in oil detection. Besides, past research work related to hydrogen monitoring, selection of coating materials, coating techniques and results were discussed. It also includes the advantages of using optical sensors which are based on FBG for the application inside the hermetically sealed transformer. In addition, the working principle of FBG based sensors and the applications in dissolved hydrogen gas detection were discussed. At the same time, the novelty of this research is briefly explained in this chapter.

**Chapter 3** presents the detailed research methodology of this work in order to conduct the research objectives and test the research framework effectively. Both quantitative

and qualitative approaches were used. This chapter covers the design of the testbed for optical and chemical parameter measurement, design of the experiment tank, high voltage generator, spark gap and preparation of dissolved hydrogen samples. Besides, coating techniques and parameter used to coat the FBG are also discussed in this chapter. Thus, experiments were designed to measure the wavelength shift of the FBG with respect to the dissolved hydrogen in transformer oil.

**Chapter 4** discusses the results of the experimental measurements. Meanwhile, the discussion covers the correlation between the wavelength shift and the amount of dissolved hydrogen in transformer oil. The selection of the best coating thickness and the composition of the FBG sensors based on the detection range are also discussed in this chapter.

**Chapter 5** concludes the findings of the research and recommendation for future studies in gas in oil detection. There are a few recommended studies which can be conducted to enhance and value add to the findings of this work.

# CHAPTER 2: LITERATURE REVIEW

This research is focussed on developing a sensor which can be used to detect dissolved hydrogen in transformer oil. The concept of the transformer insulation system needs to be understood. In addition, the working principle of the optical-based sensor will be discussed.

## 2.1 Transformer Insulating Oil as Insulator and Coolant

The oil in the transformer acts as the insulation, coolant and condition indicator. Table 2.1 summarises the specification, test method and typical values for the newly manufactured transformer oil (Naphthenics, 2008). New transformer oil should withstand a voltage of more than 30 kV in order to provide the insulation to the transformer (IEC, 2015). Degraded oil will lead to insulating paper degradation and failure. The failure of the paper causes the winding turns to short-circuit. The shorted winding turns will lead to transformer breakdown (N.H. Malik, 1997).

The secondary function of transformer oil is as a coolant for the transformer. The liquid serves a good conductor of heat (Pradhan, 2006). The heat from the winding and the core are transferred to the oil and will be dissipated to the surroundings through the transformer radiator (Naphthenics, 2008). The dissipation of the heat is also further enhanced with the presence of cooling fans mounted to the transformer radiator (Figure 2.1).

**Table 2.1: Specifications of transformer oil**

| Properties | Test Method | Specification | Typical Value |
|---|---|---|---|
| Kinematic Viscosity<br>@40ºC<br>@100ºC | ISO 3104 | 12 (max)<br>N/A | <br>9.24<br>2.36-3.0 |
| Flash Point ºC | ISO 2719 | 135 (min) | 145 |
| Pour Point ºC | ISO 3016 | -40 (min) | -50 |
| Appearance | - | Clear<br>Sediment – Free<br>Particulate - Free | Clear<br>Sediment – Free<br>Particulate - Free |
| Density @ 20ºC, kg/dm$^3$ | ISO 3675 | 0.895 (max) | 0.875 – 0.88 |
| Acidity mgKOH/s | IEC 62021-1 | 0.01 (max) | <0.01 |
| Corrosive Sulphur | DIN 51353 | Non-corrosive | Non-corrosive |
| Water Content, ppm<br>Bulk<br>Drum | IEC 60814 | <br>30 (max)<br>40 (max) | <br>< 20<br>< 30 |
| Anti-Oxidant Additive | IEC60666 | Not-Detectable | Not-Detectable |
| Oxidation Stability,<br>164 hr, 120 ºC, Method C<br>Sludge (%)<br>Acidity mgKOH/g | IEC61125<br>Method C | <br><br>0.8 (max)<br>1.2 (max) | <br><br>0.4<br>1.0 |
| Breakdown Voltage, kV | IEC 60156 | 30 (min) | >50 |
| Interfacial Tension, mN/m | ISO 6295 | 40 (min) | 46 |
| Dissipation Factor, tangent delta @ 90 ºC, 40 Hz – 60 Hz | IEC 60247 | 0.005 (max) | 0.0005 |
| Gassing tendency at 50 Hz after 120 min, mm$^3$/min | IEC60628,A | Not required | ≤+5 |
| Total furan, mg/kg | IEC61198 | 0.1 (max) | Not Detectable |
| Total PCB content, mg/kg | BS EN61619 | Not Detectable | Not Detectable |
| Polycyclic aromatics (PCA), % mass | BS2000 part 346 | 30 (max) | 0.2 |

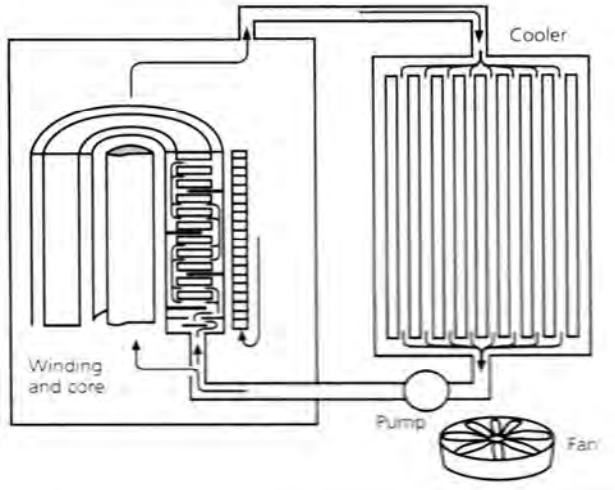


**Figure 2.1: Transformer cooling system (Naphthenics, 2008)**

## 2.2 Transformer Oil as Condition Indicator

The transformer oil-paper insulation system is subjected to degradation due to the electrical, mechanical and thermal stresses (M. Wang, 2002). The degradation will be further accelerated with the presence of an electrical, mechanical and thermal fault. The faults in the transformer will decompose the insulation to a few decomposition products such as dissolved gasses, acids and solids (IEEE, 2015). Measuring the amount dissolved gasses in transformer oil serves as an indicator on the transformer health (Haema, 2012).

## 2.3 Insulating Paper

Paper is used as an insulating material in the transformer because it is cheaper and can provide the best insulation for the price. It is a mat of cellulose that is originated from plant sources, mainly wood. The cellulose molecules are a cyclic hexagonal glucose rings with different length and arranged adjacently. The glucose rings are bonded together by hydrogen bonds involving the hydroxyl (-OH) groups (Figure 2.2). The integrity of the paper is determined by measuring the length of cellulose molecules. This method is known as the degree of polymerization (DP) (N.H. Malik, 1997).

The paper used in the transformer is known as electrical paper which has to meet specific physical and chemical standards. The chemical and the physical properties will determine the electrical properties of the paper. The electrical properties are; high dielectrics strength (high breakdown voltage), lower power factor (dielectric loss). In addition, the dielectric constant has to match to transformer oil and free from particles (Rojas, 2006).

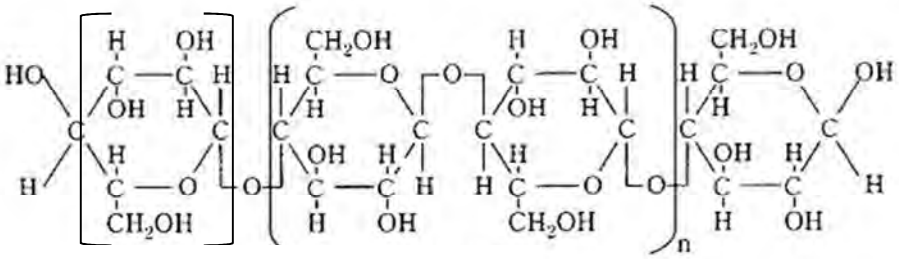

Glucose Cellulose

**Figure 2.2: Structural formula for cellulose and glucose (Naphthenics, 2008)**

The paper which is impregnated in transformer oil is known as oil-impregnated Kraft paper (Vecchio, 2001). The impregnated paper is electrically stronger, and it can withstand continuous electrical stressing. The role of the paper in a transformer is crucial, where the operation of the transformer would be impossible without it. When the cellulose chain breaks due to fault and degradation, the hydrocarbon components will get released into the oil as gasses and liquids.

The pressboard is used where insulating support and structure are needed. The pressboard thickness is around 2 mm and builds in sheets. The sheets will be used to provide clearance between the windings. The pressboard and paper are excellent electrical insulating material when impregnated in transformer oil. They serve as a good insulator with the presence of oil (Vecchio, 2001).

When a transformer is loaded to its maximum capacity, the winding and the core will get hotter. Besides, the transformer can also get hotter when there is no proper ventilation or oil circulation. The paper can only withstand a specific temperature before it loses its physical and chemical properties (Pradhan, 2006). Once the paper loses its physical and chemical properties, the electrical properties will be affected (M. Mirzaie1, 2007).

In addition, insulating paper can absorb a significant amount of moisture whenever moisture presents in the transformer oil. At the same time, the transformer oil absorbs the moisture from the surroundings. The amount of moisture absorbed in the paper is

directly related to the amount of moisture in the oil. As the moisture in the oil and the paper increased, the degradation of these materials will become faster with the presence of thermal and electrical stress (N.H. Malik, 1997).

## 2.4 Degradation of Transformer Paper and Oil

The transformer insulation, which consists of paper and oil, might degrade with the presence of moisture and oxygen. The degradation of these insulating materials is a function of temperature and time. The temperature is determined by the loading and the cooling mechanism of the transformer. Once the insulation degraded, it will lose its dielectric strength, thus will cause a higher risk of inconvenient outages of the transformer. The degraded paper insulation will produce sludge, which will be deposited at the bottom of the transformer tank. The sludge formation is an indication of deteriorated paper insulation (IEC, 2015).

The most critical part of the transformer insulation system is the paper which is winded intimately around the copper or aluminium conductors of the windings because the deterioration of the paper at these regions is difficult to repair or replace. On the other hand, the oil is not as critical as the paper because the deteriorated oil due to moisture contents and other contaminants can be filtered to remove the degradation products or the oil is replaced. The by-products in the oil due to degradation are used to estimate the condition of the paper. The health of the transformer is primarily dependent on the condition of the paper (Kulkarni, 2004).

### 2.4.1 Degradation of Oil Insulation

The heat in the transformer will deteriorate the insulating oil. The most dominant deterioration of the oil is caused by oxidation, which happens in the presence of oxygen

and moisture. The by-products of the oxidation process are hydrogen, sludge, acids and water. In addition, the presence of dissolved metals such as iron and copper will act as a catalyst to degrade the oil further (Arshad & Islam, 2011).

### 2.4.2 Effect of Oxygen on Transformer Oil

Oxygen can enter a transformer through the leaky gaskets. The oxidation process of the transformer oil may produce lighter molecules (hydrogen, acids and water) as well as heavier molecules (sludge) depending on the reaction conditions.

The sludge in the transformer will form a blanket barrier which will block the oil flow through the radiator ducts and windings. If this condition remains for a longer time, the insulation will get heated due to improper heat dissipation from the transformer. With higher temperature and the presence of more oxygen, the oxidation process will become more rapid. An increase of 10ºC will double the rate of oxidation of insulating materials. As the insulation deteriorates due to oxidation, the lifetime of the transformer will be shortened (Flanagan, 1992).

The sludge in the transformer can be removed by flushing transformer with a high stream of oil. However, this process needs to be done in the factory due to the complexity of work. So it is recommended that the amount of oxygen in the transformer to be as low as possible to extend the life of transformer due to minimized insulation oxidation rate (H.Harlow, 2004).

### 2.4.3 Effect of Moisture on Transformer Oil

Moisture contamination in transformer oil is the common cause of the deterioration of the transformer insulation system. The allowable moisture content in the transformer is 30 ppm. The moisture is needed in transformer oil to prevent the insulating paper from becoming brittle. The paper which has become brittle will lose its dielectric

strength due to micro-cracking. Moisture can exist in the transformer in various forms such as free water, emulsified water (suspension) and dissolved water (Naphthenics, 2008).

Generally, free water presents in new clean transformer oil during the shipment. The water which enters the transformer will settle down at the bottom of the tank when the interfacial tension of the oil is high (30-50 dynes/cm). Free water that settles down at the bottom of the transformer can be seen when drawing the oil sample from the bottom sampling valve. However, water in oil which is free from solid suspensions is not dangerous to the transformer because it will quickly settle down at the bottom of the transformer (Godswill, 2008).

The concern on the water in the transformer will become significantly dangerous in the presence of solid contaminants such as cellulosic fibers and oxidation products. The water tends to grasp the contaminants and form the heterogeneous mixture. The heterogeneous mixture is known as emulsified water or suspension. The water in the suspension will combine with acids and sludge in transformer oil thus will increase the rate of insulation deterioration. The water in the suspension is not visible to the naked eyes, and can't be detected by using the breakdown voltage test alone. This is because there are many factors which will affect the breakdown voltage of the transformer oil such as particles, acids and dissolved gasses (Mayoux, 2000).

On the other hand, the nature of the transformer oil is that it can absorb some amount of water due to temperature and the condition of the oil. The absorbed water is known as dissolved water/moisture. As the transformer temperature increases, the amount of moisture in the oil will increase too. This happens due to the moisture migration from the insulating paper to the oil. The measurement of the moisture content in the transformer is in parts per million (ppm). The dissolved water has little or no effect on the dielectric strength of the oil compared to the emulsified water (Naphthenics, 2008).

### 2.4.4 Degradation of Paper Insulation

The ageing of the paper in the transformer is not uniform and depends on thermal and moisture gradients. The external layers of the paper are subjected to a higher concentration of oxygen and byproducts of oil, thus will degrade faster than the internal layers of the paper insulation. The actual mechanism of the paper deterioration is quite complex and mainly depends on heat, oxygen, moisture and acid (M. Mirzaie1, 2007).

#### 2.4.4.1 Paper Degradation by Heat

The rate of degradation of the insulating paper is highly dependent on the temperature of the transformer. For every 10ºC of increase of temperature, the degradation rate doubles. The temperature rise is dependent on transformer loadings as well as faults in transformer such as partial discharge and arcing. The partial discharge and the arcing will accelerate the insulation degradation thus will cause localized overheating. A study showed that a temperature of 200ºC tends to break the glycosidic bonds and break the glucose rings. Once the glucose bond is broken, the byproducts such as glucose, moisture, acids and carbon oxides will present in the transformer oil (M. Mirzaie1, 2007).

#### 2.4.4.2 Paper Degradation by Oxygen

The oxygen presence in transformer oil will oxidize the cellulose. Oxidation is a part of transformer wear and tear, but it can be managed. The oxidation will produce moisture and a group of carbonyl (aldehydic) and carboxyl (acid). This will further weaken the glycosidic bond and may lead to chain scission (N.H. Malik, 1997).

#### 2.4.4.3 Paper Degradation by Moisture

Transformer paper has a high tendency of holding moisture. Water held in the transformer will migrate to the oil as the transformer temperature increases and vice versa. Typically, the recommended moisture content level for new transformer paper which is immersed in the oil should be lesser than 0.5% by weight.

Although the transformer is perfectly sealed, the oxidation of the cellulose will also release the moisture in the transformer oil. The rate of generation of moisture in the transformer is dependent on the oxidation and the temperature of the system (N.H. Malik, 1997).

#### 2.4.4.4 Paper Degradation by Acid

The cellulose degradation can happen due to hydrolysis. Hydrolysis is a process where water consumed by the insulation will break the polymeric chains in the cellulose molecules. This process is further catalysed by acids. Carboxylic acids are produced in the oil by the oxidation process. As the amount of the acids increases, the rate of degradation of the paper will be increased too (H.Harlow, 2004).

## 2.5 Gas formation in Transformer due to Fault

The gases are generated in transformer oil due to the breaking of chemical bonds that were formed by hydrocarbon molecules. The nature of the fault and its respective energy will determine the type of gasses that will be generated. The generated gasses are Hydrogen ($H_2$), methane ($CH_4$), ethane ($C_2H_6$), Ethylene ($C_2H_4$), Acetylene ($C_2H_2$), Carbon Monoxide (CO) and Carbon Dioxide ($CO_2$) (IEC, 2015). The generated gasses are dissolved in oil. The amount of the gasses dissolved in the oil is directly related to the amount of the gasses generated. As the dissolved gasses get saturated in the oil, the gasses will be released from the oil.

Lower energy or temperature is required to create or break single C-H bonds, whereas, a higher temperature is required to create or break a higher molecular bond. At a lower temperature, around 300ºC, methane and ethane will be formed. In addition, hydrogen will be formed too if there are low energy electrical discharges. Meanwhile, at a higher temperature of more than 500ºC, ethylene will be formed. Besides, even at a higher temperature of at least 800ºC to 1200ºC, acetylene gas will be produced. The faults in transformers are divided into thermal and electrical types. Table 2.2 summarizes the faults in the transformers(IEC, 2015).

**Table 2.2: Typical faults in power transformers**

| Fault | Examples |
|---|---|
| Partial discharge | • Discharge in the gas-filled cavities resulting from incomplete impregnation, high humidity in the paper, oil super-saturation or cavitation. |
| Discharge of low energy | • Sparking or arcing between bad connections of different of floating potential, from shielding rings,toroids, adjacent disks or conductors of winding, broken brazing or closed-loop in the core. Discharge between clamping parts, bushing and tank, high voltage and ground within windings, on tank walls<br>• Tracking in wooden blocks, the glue of insulating beam, winding spacers, breakdown of oil, or selector breaking current. |
| Discharges of high energy | • Flashover, tracking or arcing of high local energy or with power flow through.<br>• Short circuit between low voltage and the ground, connectors, windings, bushings and tank, copper bus and tank, winding and core, in oil duct, turret. Closed-loop between two adjacent conductors around the main magnetic flux, insulated bolts of the core, and metal rings holding core legs. |
| Thermal fault<br>t < 300ºC | • Overloading of the transformer in emergency situations<br>• Blocked item restricting oil flow in windings<br>• Stray flux in damping beams of yokes |
| Thermal fault<br>300ºC< t < 700ºC | • Defective contacts between bolted connections (particularly between aluminium busbar), gliding contacts, contacts within selector switch connection form cable and draw rod of bushings.<br>• Circulating currents between yoke clamps and bolts, clamps and laminations, in-ground wiring, defective welds or clamps in magnetic shields.<br>• Abraded insulation between adjacent parallel conductors in windings. |
| Thermal fault<br>t >700ºC | • Large circulating currents in tank and core<br>• Minor current in tank walls created by a high uncompensated magnetic field<br>• Shorting links in core steel laminations |

## 2.6 Dissolved Gas-in-Oil Analysis (DGA)

Dissolved gas-in-oil analysis (DGA) is an online technique to detect the incipient fault in the transformer based on the amount of dissolved gases in transformer oil. The oil sample is extracted out from the transformer and sent to the lab for gas chromatography analysis (M. T. Yang, Hu, L. S., 2013).

This technique has been in practise for 30 years and has gained tremendous success compared to the other techniques. The main reason for the success is the sampling and the analyzing procedures which are more straightforward and cheaper, and there are many established standards related to the testing methods and analysis (Duval., 1989).This conventional method will require more than a week to obtain the lab test result due to transportation and stock stacking. The delay in processing and test the samples may cause a catastrophic failure to the transformer (IEC, 2015).

There are a few major gasses that have been identified to determine the health of a transformer which are hydrogen ($H_2$), methane ($CH_4$), ethane ($C_2H_6$), ethylene ($C_2H_4$), acetylene ($C_2H_2$), carbon monoxide (CO) and carbon dioxide ($CO_2$). Table 2.3 summarizes the gasses typically found in transformer oil under fault condition (IEEE, 2015).

**Table 2.3: Gasses typically found in transformer insulating liquid under fault conditions (Suwanasri, 2009).**

| Gas | Chemical Formula | Predominant Source |
|---|---|---|
| Nitrogen | $N_2$ | Inert gas blanket or atmosphere |
| Oxygen | $O_2$ | Atmosphere |
| Hydrogen | $H_2$ | Partial Discharge |
| Carbon dioxide | $CO_2$ | Overheated cellulose or atmosphere |
| Carbon monoxide | CO | Overheated cellulose or air pollution |
| Methane | $CH_4$ | Overheated gas (hot metal gas) |
| Ethane | $C_2H_6$ | Overheated oil |
| Ethylene | $C_2H_4$ | Very overheated oil |
| Acetylene | $C_2H_2$ | Arcing in oil |

The analysis of the amount of dissolved gas in transformer oil is done by using 6 methods which are key gas method (IEEE), Duval Triangle, Logarithmic Nomograph, Doernenburg ratio, Roger ratio and IEC ratio (Bandyopadhyay, 2007). The ratios method is the most common method in analyzing the dissolved gases. A few key gasses are selected as nominator and denominator to establish the ratios. The ranges of each ratio are categorized into different codes to determine the types of fault in the transformer. The only drawback of the ratio method is the ambiguity problem associated with some cases which are covered out of the specified codes (Micheal Duval, 2003).

In addition, the DGA methods are very dependent on analytical experts. Since transformers of different sizes, structures, manufacturers, loadings and maintenance histories may have different gassing characteristic, they need to be considered differently in most cases. DGA is thus often referred to as "art" instead of "science". However, the DGA method is still widely used, and the need to get instant dissolved gas data from transformer oil is arising; thus, an area of online DGA has emerged.

## 2.7 Online Dissolved Gas-in-oil Analysis (DGA)

On-line gas-in-oil monitors appeared soon after the introduction of the DGA technology. An advantage of on-line monitors is the continuous measurement of one or more gases, so that any gassing trend, which is critical information for incipient fault screening, can be easily obtained. Problems with these monitors are related to selectivity and durability of the gas molecule screening membrane, field calibration, measurement range and resolution. Poor selectivity lowers measurement accuracy. Membranes with poor durability deteriorate faster, especially under field conditions where temperatures vary greatly between day and night. Since the inputs of the monitors are non-electrical quantities, while the readout device of the monitors contained an electronic circuit that

is subject to offset and characteristic shift due to factors like temperature and humidity, field calibration of the device could be a big problem. Generally, the measurement range and resolution of on-line monitors are far behind that of laboratory tests. With the new generation of monitors being developed, the gap is becoming narrower. For all these reasons, on-line monitors are usually used as screening tools to identify possible abnormal units. Detailed fault diagnosis is still then left to conventional method (Haema, 2012).

## 2.8 Partial Discharge in Transformer

One of the causes of the transformer dielectric breakdown is partial discharge. Arcing in the transformer is preceded by partial discharge activity. The level and rate of partial discharge activities are the indications of developing fault in the transformer. Early detection of the partial discharge activity will prevent catastrophic failure of the transformer. The partial discharge will generate hydrogen in transformer oil and thus can be detected by dissolved gas analysis method. The PD in the transformer can be caused by cavities in the insulation, gas bubbles, embedded metal chip in the insulation and moisture. However, the detection of the PD created by floating component and sharp edges did not yield any useful information about the insulation because its appearance is not directly related to the condition of the insulation. Insulation breakdown happens mainly due to PD in voids, surface discharge and small cracks. Voids are defined as gaps in a dielectric material which are less denser than the dielectric material itself such as gas bubbles in oil that fill the transformer tank, or cracks in the paper insulation. The void region has a lower dielectric constant than the surrounding material, which creates capacitance. Partial discharge can then occur when the electric field difference across the void exceeds minimum breakdown field strength (Boggs, 1990).

### 2.8.1 Theory of Discharges

The partial discharge phenomena can be explained by using the Townsend theory of breakdown and Streamer discharge theory. However, Townsend theory failed to explain some experimental observations such as zigzag and branching paths of the spark channel, and short breakdown times when the gaps are overstressed. Due to these limitations, the Streamer Theory was proposed (E. Kuffel, 2000).

#### 2.8.1.1 Townsend Theory of Breakdown

By referring to Figure 2.3, the high electric field between the plates will ionize the air and produce free electron and ions. Free electrons are accelerated under the electric field and collided with the neutral gaseous molecules. If the kinetic energy of the free electrons is sufficiently high, the collision will produce a new free electron and a positive ion. The new electron and the original free electron will continue to be accelerated and collided with other electrons, hence produced new electrons.

This process continues and leads to electron avalanche. Similarly, the newly formed positive ions will move towards the cathode and increase the electric field around the cathode. The accelerated positive ion will bombard the cathode, which will cause the cathode to emit free electron that is called secondary electrons. Eventually, the electron avalanche is independent of the free electron, and gaseous discharge will become self-sustaining.

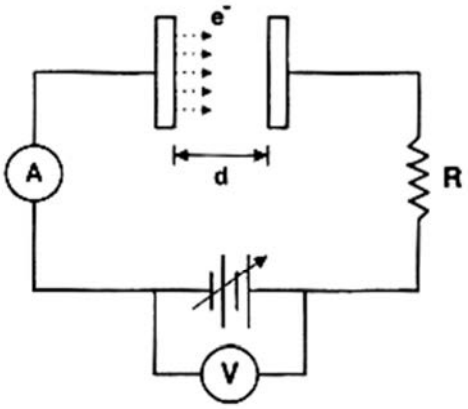


**Figure 2.3: Circuit model for Townsend theory of breakdown (N.H. Malik, 1997)**

### 2.8.1.2 Streamer Theory of Breakdown

In Streamer theory, the initiating electrons start the avalanche by simple Townsend mechanism. As the electrons move faster, they are concentrated at the head of the electron avalanche and followed by positive ions. The space charges strengthen the electric field at the head of the electron avalanche. The middle part of the avalanche is considered as a plasma column with a weaker electric field which makes the recombination of the ions and electrons easier. The recombination process produces a lot of photons. The photons ionize the neutral molecules in the avalanche head with a high electric field and emit electrons. The electrons move towards the anode, and second electron avalanche is formed. The second electron avalanche will combine with the first one and enlarge the plasma column. When the plasma has bridged the anode and cathode, gaseous discharge with a narrower width occurs. This is called the streamer discharge. The speed of photon-induced ionization is faster than electron-induced ionization. This concludes that Streamer discharge is more rapid than Townsend discharge (Figure 2.4).

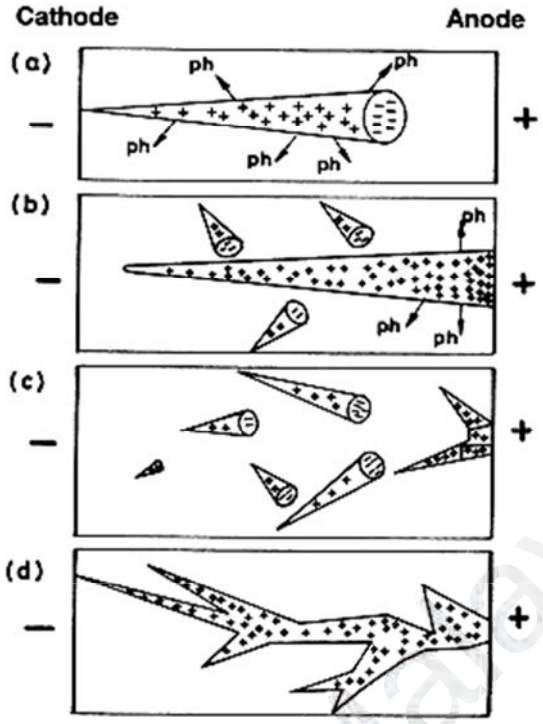


**Figure 2.4: Streamer theory of breakdown(N.H. Malik, 1997); (a) Electrons concentrated at the head of the electron avalanche and followed by positive ions; (b) The photons ionize the neutral molecules and emit electrons; (c) The electrons move towards the anode and second electron avalanche is formed; (d) The Streamer discharge**

### 2.8.1.3 Paschen Law

Based on Townsend breakdown criterion, a relationship between breakdown voltage $V_s$ and the product of pressure (P) and gas spacing (d) can be established. Figure 2.5 shows that the breakdown voltage is a unique function of the product of gas pressure and gap length. This relationship is known as Paschen law.

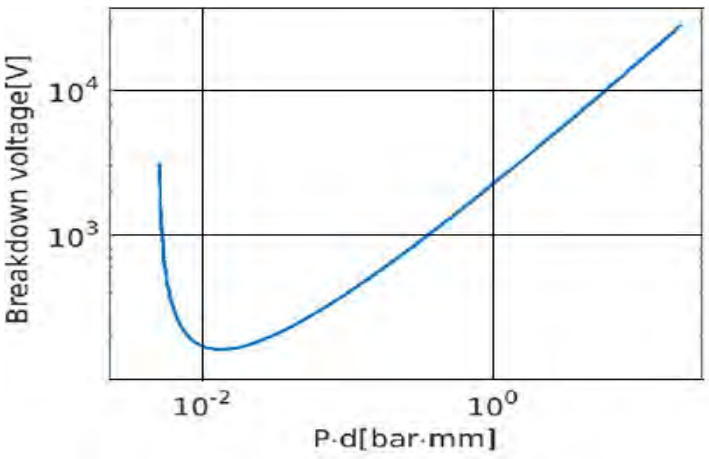


**Figure 2.5: Paschen curve for air (N.H. Malik, 1997)**

### 2.8.2 Internal Discharge at AC Voltage due to Voids

A partial discharge occurs within an area of the insulation material exposed to high electric stress. The space charges accumulated in this area disturb the electric field distribution. This condition will generate intermittent discharges and a series of discharge pulses (F.H.Kreuger, 1989). The exchange and accumulation of the charges in the void cannot be measured directly. However, they can be detected by the change of voltage on the two electrodes on either side of the insulation (F.H.Kreuger, 1989). This relationship can be analyzed by using the equivalent circuit shown in Figure 2.6.

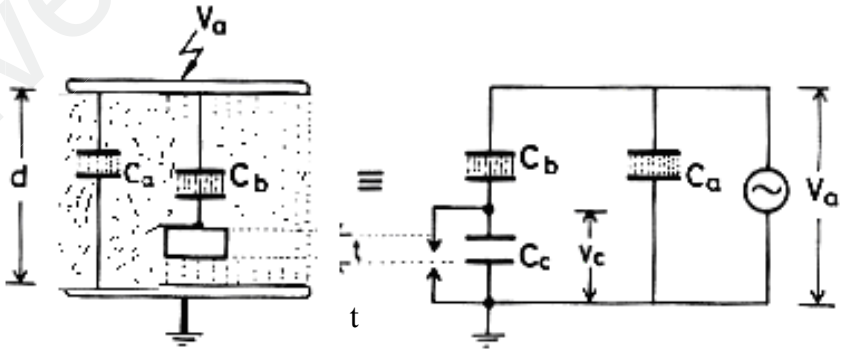


**Figure 2.6: A cavity in the dielectric and its equivalent circuit (N.H. Malik, 1997)**

Figure 2.6 shows a cross-section area of dielectric insulation with thickness d, containing a cavity in the form of a disc with thickness t, together with its corresponding

equivalent circuit. In this circuit the capacitance $C_c$ corresponds to the cavity; $C_b$ corresponds to the capacitance of the dielectric that in the series with $C_c$, and $C_a$ is the capacitance of the rest of the dielectric. For t<<d, which is usually the case, with the assumption that gas has filled the cavity, the field strength across $C_c$ is given by the expression $E_c = \varepsilon_r E_a$ , where $\varepsilon_r$ is the relative permittivity of the dielectric.

Assuming $E_{cbreak}$ is the cavity breakdown stress and treating the cavity as a series of capacitance with the healthy part of the insulation, the voltage across the cavity can be derived as:

$$V_c = \frac{C_b}{C_c + C_b} V = \frac{V}{1 + \frac{1}{\varepsilon_r}\left(\frac{d}{t} - 1\right)} \tag{2.1}$$

Therefore the voltage $V_i$, across the dielectric, which will initiate discharge in the cavity is:

$$V_i = E_{cbreak} t \left\{1 + \frac{1}{\varepsilon_r}\left(\frac{d}{t} - 1\right)\right\} \tag{2.2}$$

The sequence of breakdown under sinusoidal alternating voltage is illustrated in Figure 2.7 The dotted curve, $U_c$, qualitatively shows the voltage across the cavity if it did not breakdown. During the positive half cycle of the applied voltage, as the $U_c$ reached $U_i^+$, a discharge would take place and made the voltage $U_c$ to collapse to residual voltage $U_e^+$ and the gap discharge extinguished. The voltage across the cavity $U_c$ would increase until it reached $U_i^+$ and new discharge would happen. Thus, several discharges may take place during the rising part of the applied voltage. Similarly, during the negative half cycle of the applied voltage, the cavity discharged to residual voltage $U_e^-$ as the voltage across it reached $U_i^-$.

As the discharges happened during the positive half cycle and negative half cycle, it gave rise to the positive and negative current pulses, respectively. The discharge in the insulating medium can be measured with PD detectors.

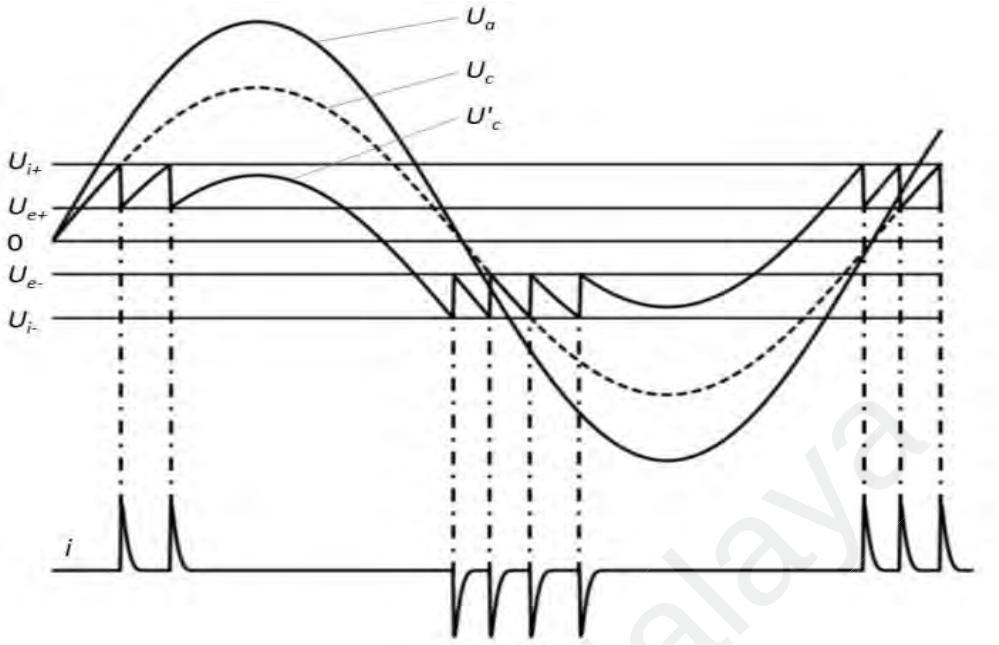


**Figure 2.7: Sequence of cavity breakdown under alternating voltages (N.H. Malik, 1997)**

### 2.8.3 Surface Discharges

A surface discharge happened when a strong electric field ionized the surrounding air on top of the insulation. The surface discharge accelerates by the addition of contamination and moisture, which eventually creates a leakage path to ground. The surface discharge can be intermittent or permanent. The heat generated from the surface discharge results in the burning of the insulation surface into carbon paths and will cause permanent surface tracking. The carbon path on the insulation surfaces results in additional needle-type endpoints. These new needle-type points will result in the stronger electric fields at each of its tips. The stronger electric field will further burn the insulation and the tracking path elongate. This process will continue until the carbon path reaches the ground.

### 2.8.4 Corona Discharges

Corona happens in air insulation at points with the highest electrical stress. The tolerance of dielectric material strength surrounding the conductor to the maximum

strength of the electric field determines the conductivity of the dielectric material. Conductors such as sharp points, or balls with a small radius, are more prone to cause a dielectric breakdown. Corona is sometimes seen as a bluish glow with hissing sound along the high voltage lines (Stone, 2005).

## 2.9 Fiber Optics Sensor

Besides optical communication, optical fiber has been used as a platform to develop fiber optic sensor. Fiber optics sensors have been widely used in many applications such as in medical, biotechnology, marine, environmental analysis, process control and chemical analysis (M. D. Yang, Jixiang, 2012). Recently, fiber optics sensors have been used in arc protection for vacuum circuit breaker, as temperature and partial discharge sensor in power transformer (K. Wang, Tong, Hu, & Zhu, 2013). Fiber optic is preferred in power system because it is a pure insulator and not susceptible to noise and other frequency components in the power system (Blackburn, 2006). Fiber optics sensors have the advantages of multiplexing, can withstand higher temperature, lightweight, and easy integration with the existing fiber optics architecture which enable remote sensing. Fiber optics sensors are preferred for their capability of giving faster response than other types of sensors as well as higher electrical resistance (M. Wang et al., 2012). Fiber optic sensors are also used in detecting gases-in-air such gases are hydrogen and methane. For instance, a fiber optic cable with palladium cladding can detect hydrogen in the air (M. Wang et al., 2012).

### 2.9.1 Light Propagation in Fiber

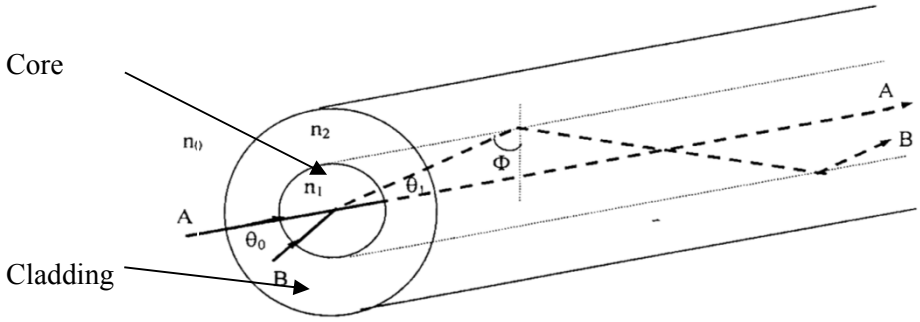


**Figure 2.8: Propagation of light through optical fiber**

An optical electromagnetic wave entering the fiber with an angle will pass through the fiber in a zigzag path in its core (Figure 2.8). This will only happen if the core has a higher reflective index than the cladding and the incident angle Φ is greater than the critical angle, which is defined as $\sin \Phi_c = n_2/n_1$. If both the conditions are not met, the transmitted wave will undergo refraction by penetrating into the cladding and are lost.

The refraction phenomena in fiber follow the Snell's law, $n_0 \sin(\theta_0) = n_1 \sin \theta_1$, where $\theta_0$, $\theta_1$ are the incident and refraction angle, $n_0$, $n_1$ are the refractive index of the air and the core. The Snell's law can be further derived to get the maximum value of incidence angle, which is given by:

$$\theta_0(\max) = \sin^{-1}\left[\frac{\sqrt{(n_1^2 - n_2^2)}}{n_0}\right] \tag{2.3}$$

The sine of the maximum value of the incidence angle is used to figure the merit of the fiber and is defined as the numerical aperture (NA):

$$\sin(\theta_0(\max)) = \frac{\sqrt{(n_1^2 - n_2^2)}}{n_0} \tag{2.4}$$

The NA of fiber is dependent on the refractive indices of the core and the cladding materials and not a function of the fiber dimensions.

### 2.9.2 Modes in an Optical Fiber

A set of guided electromagnetic waves in an optical fiber is called the modes. Each mode will have its own unique pattern of electric or magnetic field repeats at uniform intervals. A monochromatic electromagnetic wave can be represented as:

$$e^{i(\omega t-\beta z)} \tag{2.5}$$

where ω is the angular frequency, β is the wave propagation constant in the z-direction. For a guided mode, the β needs to satisfy the condition of:

$$n_2 k < \beta < n_1 k \tag{2.6}$$

$$k = \frac{2\pi}{\lambda} \tag{2.7}$$

where $n_1$ and $n_2$ are core and cladding refractive index, respectively, and λ is the wavelength.

If the waveguide is planar, the solution of the Maxwell equation at the boundaries yields transverse electric and magnetic modes. However, for cylindrical fiber, the core-cladding boundary condition leads to a coupling of the electrical and magnetic field components. To reduce the complexity of the equation, the refractive index is assumed to be weakly guiding where $(n_1-n_2) \ll 1$. This will give linearly polarized (LP) modes.

### 2.9.3 Fiber Characteristics

The primary motivation to design a fiber is to reduce signal attenuation and dispersion. Attenuation happens due to scattering loss and absorption. The absorption

losses are dependent on the wavelength used and the impurities in the fiber. The impurities can cause signal scattering and loss of signal.

When a fiber is bent, the propagated light will have a possibility of refracting within the cladding than reflecting back into the core. This is called bending losses. Normally, microbends can happen during the manufacturing process.

Signal dispersion happens mainly due to three mechanisms which are modal dispersion, material or chromatic dispersion and waveguide dispersion. The modal dispersion happens in fibers which have more than one modes where the light travels at different path length. This will stretch the light at the receiving end and cause the distortion. Similarly, the chromatic dispersion happens due to the propagation of different wavelength of light at a different speed in the material made up the core. The waveguide dispersion is caused by the different refractive index of the core and cladding because the light can travel in the core as well as the cladding. The light travels in the cladding will reach the end of the fiber sooner than the light travels in the core, thus causing the dispersion.

## 2.10 Fiber Bragg Gratings Theory

Fiber optics sensors have various types such as intensity-modulated, phase modulated, polarized modulated, frequency modulated, wavelength modulated sensors, distributed optical fiber sensors (DOFS), biosensors and chemical sensor (KTV Grattan, 1998). Fiber Gratings are found among the most popular devices widely used in both, optical communications and optical fiber sensing. Within optical communication networks, optical fiber-based devices perform critical operations such as coupling/splitting, wavelength-selective filtering, and optical switching. In the field of

optical sensing, optical fiber sensors, with unique advantages such as immunity to electromagnetic interference, high sensitivity, resistance to corrosion, and high-temperature survivability, are widely used to measure various physical variables such as stress, temperature, pressure, refractive index and chemical parameters.

There are two types of fiber gratings that have been developed so far, including the short-period grating or known as Fiber Bragg Grating (FBG) and the Long Period Fiber Grating (LPG). Fiber Bragg Gratings is known as short period gratings is a conventional optical-based sensor. The period of the FBG is typically small, which is hundreds of nanometers. It consists of a periodic variation of the refractive index along the fiber with a periodic distance of Λ (Figure 2.9). The fundamental principles of the FBG are the Fresnel reflection where light travels through different media with different refractive indices will reflect and refract at the media interface. This will cause some wavelength components to be reflected back to the source. The reflected wavelength ($\lambda_B$) is defined as:

$$\lambda_B = 2n_{eff}\Lambda \tag{2.8}$$

where $n_{eff}$ is the effective refractive index of the grating in the fiber core and Λ is the grating period (Westerwaal et al., 2014). The reflected wavelength is a function of the refractive index and grating period. The refractive index is determined during the production of FBG and will not change during the application. However, the period will change based on the strain applied to the FBG. Maximum flexibility of 2.49% before the FBG break due to strain was reported (Lee, 2017).

Figure 2.9 shows the structure of Fiber Bragg Gratings with core refractive index variations and spectral response of the transmitted signal. The transmitted signal shows a band rejection at wavelength, $\lambda_B$, where this signal is reflected back to the source. The

reflected wavelength $\lambda_B$ is dependent on the effective refractive index and the grating period.

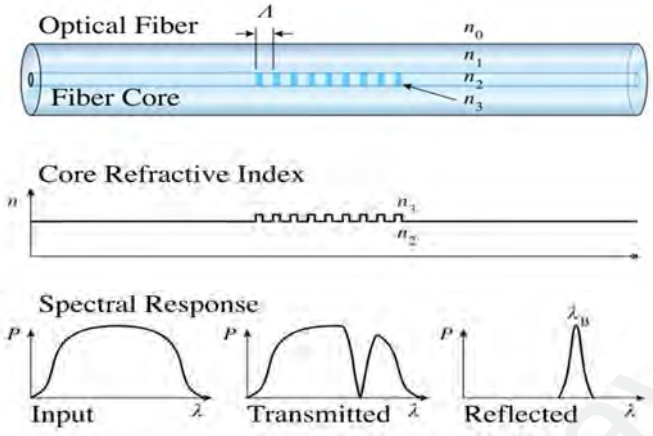


**Figure 2.9: Structure of fiber Bragg gratings with core refractive index and spectral response**

## 2.10 Fabrication of FBG

K.O Hill has demonstrated the first in-fiber gratings in 1978 (Hill, 1978). He has discovered that the germanium doped silica fiber, which is subjected to standing wave from Argon/Ion laser will produce a periodic index change which is the same as the period of the standing wave.

There are two categories of FBG fabrications which are holographic and interferometric. They are done by exposing the piece of fiber periodically to UV radiation (Kashyap, 1999). The holographic technique uses pulsed sources through a spatially period of amplitude mask on a periodic exposure. Besides, the interferometric technique uses a beam splitter to split the UV radiation and brings together the split wave at the fiber.

In the FBG fabrication, germanium doped silica fiber is widely used because it is more photosensitive, where the refractive index of the core will change with the

exposure to UV radiation. Exposure of high energy pulses from sources from Krypton Flouride (KrF) laser normal to the fiber will alter the refractive index of the fiber. If this is done periodically, then the gratings will be formed along the fiber length. The amount of the refractive index change will be determined by the UV radiation intensity, exposure duration and the fiber material (Kashyap, 1999).

### 2.10.1 Interferometric Writing Technique

The interferometric writing technique is the first method used in the fabrication of the FBG. It uses a beam splitter, compensating plate and UV mirrors. The UV radiation light is split to 50% energy and reflected back to fiber by UV mirror. One of the beams passed through the compensating plate to compensate for the path length difference; both beams will be brought together at a mutual angle (θ) at the fiber. Figure 2.10 shows the UV interferometer for FBG writing (Grattan, 1998; Kashyap, 1999).

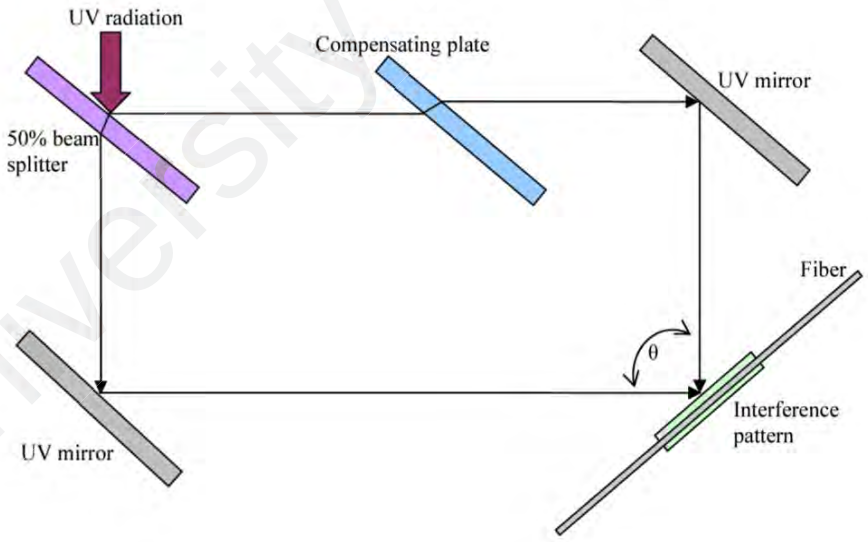


**Figure 2.10: The UV interferometer for FBG writing (Kashyap, 1999)**

This method enables the Bragg wavelength to be chosen independently. However, it is the best method for short length gratings but not for long gratings because it is susceptible to mechanical vibration and air currents. The wavelength is defined as:

$$\lambda_{Bragg} = \frac{n_{eff}\lambda_{uv}}{n_{uv}\sin(\frac{\theta}{2})} \tag{2.9}$$

where $\lambda_{Bragg}$ is the Bragg reflected wavelength, $n_{eff}$is the effective mode index of the fiber, $\lambda_{uv}$ is the wavelength of UV radiation used, and $n_{uv}$ is the refractive index of the silica in UV.

### 2.10.2 Phase Mask Writing Technique

This method is mostly used method in fabricating FBG as it is faster and stable compared to the other methods. Silica phase mask (Figure 2.11) is used for the inscription of fiber gratings. The silica phase mask is constructed on a silica plate by ion beam etching or micro-imprinting technique which is also known as the relief gratings. The etch depth and the phase mask period are the significant features of the phase mask. When UV beam coincides the phase mask, the diffraction of the incident UV beam will be in several orders, m=...,-2,-1,0,1,2,...(Kashyap, 1999).

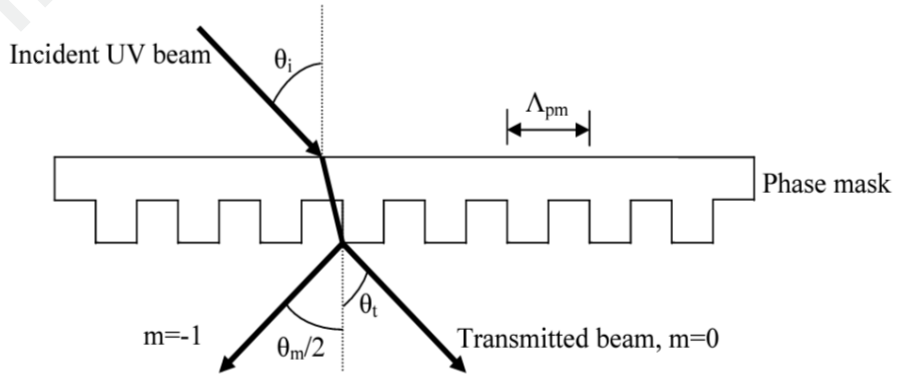


**Figure 2.11: The phase mask and the diffraction of the incident beam (Kashyap, 1999)**

The diffracted beam and the incident beam are correlated based on the general diffraction equation defined as:

$$\Lambda_{pm} = \frac{m\lambda_{uv}}{\sin\left(\frac{\theta_m}{2}\right) - \sin(\theta_i)} \tag{2.10}$$

where $\Lambda_{pm}$ is the period of the phase mask, $\frac{\theta_m}{2}$ is the diffraction angle order, $\lambda_{uv}$ is the wavelength, and $\theta_i$ is the angle of the incident beam. The incident wave is diffracted into a single order (m=-1) if the period of the grating is between 50-100% of $\lambda_{uv}$, where the remaining power is in m=0 order. When $\theta_i = 0$, the incident wave is normal to the phase mask (Figure 2.12). The diffracted beam will be in 3 orders, which are m=-1, 0, 1. Beams with order m=+1 and m=-1 will be brought together by a parallel mirror; the period of the grating $\Lambda_g$ is defined as:

$$\Lambda_g = \frac{\lambda_{uv}}{2\sin\left(\frac{\theta_m}{2}\right)} = \frac{\Lambda_{pm}}{2} = \frac{N\lambda_{Bragg}}{2n_{eff}} \tag{2.11}$$

where $N \geq 1$ is the order of the gratings (Kashyap, 1999).

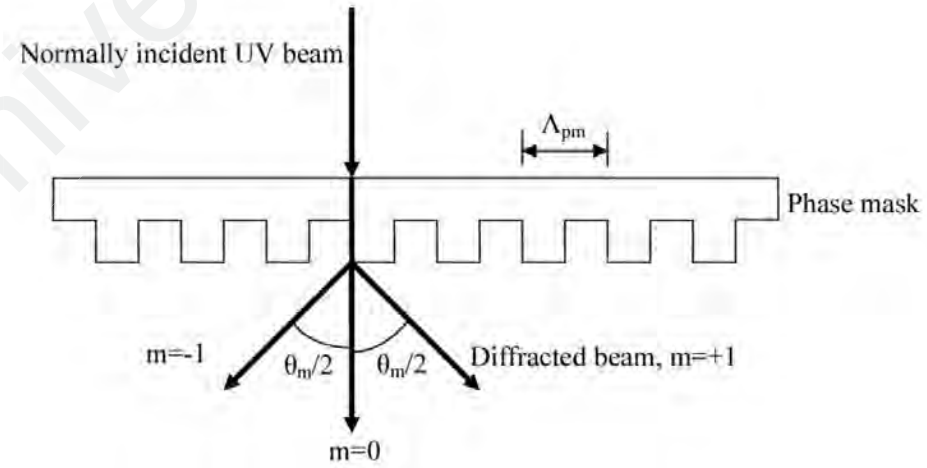


**Figure 2.12: Incident wave at the angle of $\theta_i = 0$. the diffracted wave is split into two orders; m=-1 and m=1 (Kashyap, 1999)**

The photosensitive material will be exposed to the alternating opaque and translucent lines of laser beams from the phase mask to inscribe the gratings. In conclusion, the advantage of the phase mask method is its simplicity of writing and insensitivity to mechanical vibration and stability. However, this method requires a different phase mask for every grating (Krohn, 2000).

### 2.10.3 Point-by-point Writing Technique

Point by point technique offers better flexibility in writing the gratings where the period can be changed in the process of writing. This technique is similar to the phase mask setup, but the laser is focused through a tiny slit on the mask. This technique is suitable for shorter gratings because positioning sensor needs to be linked to the interferometer. The point-to-point writing technique is subjected to the thermal effect where the properties of the fiber will change, thus will create a potential error in gratings. However, for application which does not demand positional accuracy such as long-period gratings, this method is the most suitable (KTV Grattan, 1998).

## 2.11 Previous Work on Gas Detection by using Fiber Optics

Fiber optic is preferred in power system because it is not susceptible to noise and other frequency components in the power system. Successful research of using fiber optics in detecting gas in oil for power transformer was done by (Ho, 2009), where the system developed was able to detect gas concentrations for methane, acetylene and ethylene of 5 ppm, 2 ppm and 50 ppm respectively. This method used a low-cost multi-pass sensor and reference gas cells made of photonic bandgap (PBG), where the detection was based on the absorption spectroscopy (Ho, 2009).

In addition, Argonne National Laboratory has developed a hydrogen sensor based on nanotechnology (Xiao, 2006).This was achieved by applying a thick layer of siloxane molecules to a glass substrate. The siloxane was used because it can bind well with the

glass while some can be left slippery. Then, a thin blanket (2-10 nm) of palladium beads is evaporated to the sticky layer. Palladium, when it is exposed to hydrogen, will produce palladium hydride. The palladium hydride has a different conductivity, and the change of the conductivity will indicate the presence of hydrogen. When the hydrogen content was reduced, the palladium beads will shrink and revert to palladium, and the electrical conductivity will be reduced too.

Applied Nanotech Inc. has attempted to develop a hydrogen sensor by using palladium nanoparticles (Figure 2.13) to detect hydrogen in transformer oil (Pavlovsky, 2008). It is capable of detecting and measuring dissolved hydrogen in concentrations from 50 ppm to 4000 ppm by using the change of the conductivity method too.

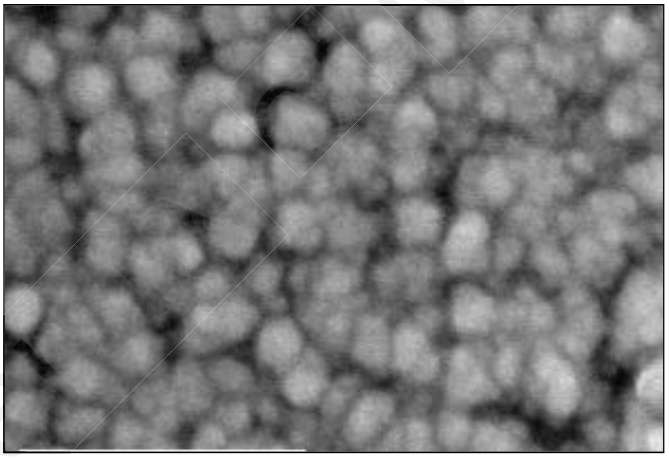

**Figure 2.13: Scanning electron microscopy (SEM) Image of palladium nanoparticles deposited on a sensor substrate (Pavlovsky, 2008)**

Xiao has shown that Pd-H interaction in the sensor is quite complex, where a good fit with analytical function does not produce a simple model of hydrogen sensing effect (Figure 2.14). The sensor response changed monotonously at 1% of $H_2$ in air and saturated at 4% of the concentration in air. In addition, the presence of oxygen has slowed down the absorption of hydrogen in palladium.

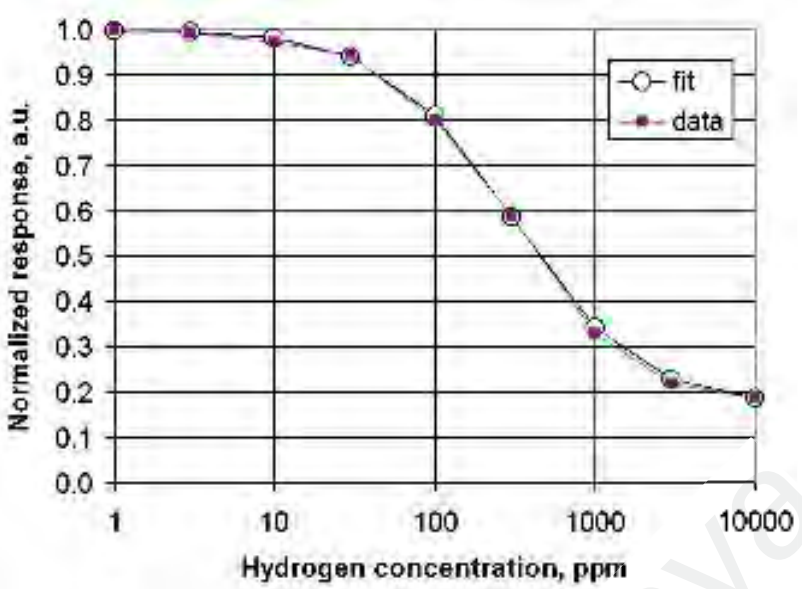


**Figure 2.14: $H_2$ sensor response with respect to $H_2$ concentration (Xiao, 2006)**

The response time was dependent on the hydrogen diffusion, which was influenced by the area of the gas separation membrane. It has been proven that Pd particles did not react with transformer oil. Sensor response time for hydrogen generation inside a transformer is less critical than other application such as hydrogen gas leak detection. The evolution rate of hydrogen in a transformer is 35-132 ppm/year, and pre-failure rates are around 1000 ppm/year. Therefore, response time of FBG within a few hours is acceptable as sampling intervals for transformer application (M. Duval, 2008).

The detection range of the hydrogen sensor is sufficient for the detection of hydrogen content in transformer oil. However, since the detection range is between 50 ppm to 4000 ppm, the development of fault cannot be detected accurately. This is because palladium has its own disadvantages such as low optical response due to hydrogen loading, cross-sensitivity for carbon and oxygen, limited detection range and formation of the micro-cracks on the Pd surface after cyclic absorption/desorption of hydrogen gas (Slaman et al., 2012). The sensor was further improved by using the magnesium of

other rare earth metal-hydrides, which would allow tuning of the hydrogen detection levels over a wide pressure range. The detection level was stable for a concentration of 10% of hydrogen and below, with the presence of oxygen. The developed sensor showed some positive result in detecting dissolved hydrogen in liquids, especially transformer oil.

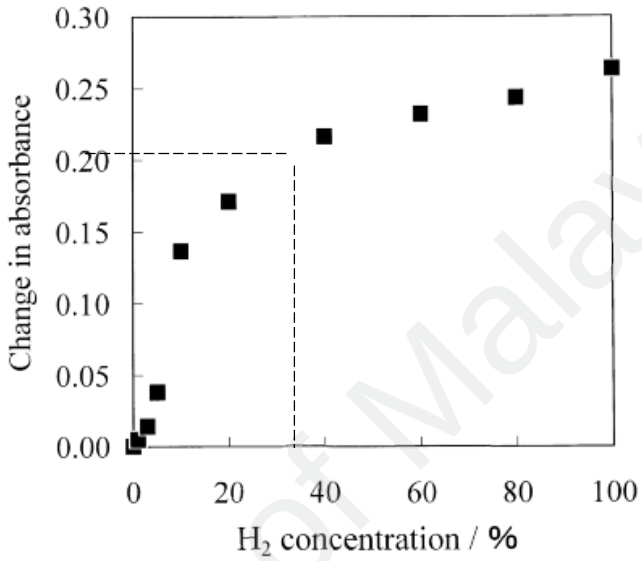


**Figure 2.15: Response of the platinum supported tungsten trioxide sensor (S. Sekimoto, 2000)**

Another material, platinum supported tungsten trioxide thin film, will change colour to blue tungsten bronze when it is exposed to hydrogen at room temperature (S. Sekimoto, 2000). However, the sensor has a slower response and saturated after the concentration of hydrogen exceeded 40%. Figure 2.15 shows the absorption response of the platinum supported tungsten trioxide sensor. This type of sensor showed a higher sensitivity at 1% of hydrogen concentration. However, this sensor was not tested with ageing conditions to assess potential degradation of the surrounding materials on the fiber optics sensor which may have some effects on the accuracy of detection.

Meanwhile, two different fiber optic sensors were developed for the determination of hydrogen sulfide at pretreated filter paper as a solid substrate. In the first type, $CdCl_2$

levels; a probe-type fiber optic sensor coated with polyethylene oxide containing 0.5 M $CdCl_2$ utilizing 0.5 M $CdCl_2$ mixture was coated onto the tip of a fiber optic probe, and the probe was exposed to $H_2$ and a fiber optic sensor –polyethylene oxide (PEO). The methodology is based on the measurement of CdS fluorescence on the surface. Detection time of 3 seconds was reported for the PEO-coated fiber optic system, and the detection limit was 36 ppm for $H_2$ $CdCl_2$S at 0.552 ppb precision. On the other hand, for the fiber optic system utilizing pretreated filter paper, two different configurations were devised and evaluated; a bifurcated fiber optic sensor and a single fiber optic sensor. Similar figures were obtained with these two systems; the detection limit (3s) was 4.0 ppb for the bifurcated fiber optic sensor and 4.3 ppb for the single fiber optic sensor, and both sensors had linear responses in the range 0.032–1.0 ppm. This confirms the linear properties of coatings on the fiber (Eroglu, 2000).

Another work by (Jiachen Yu, 2018) on using tilted FBG sensor to detect hydrogen leakage on the pipeline. A tilted FBG of 8° was coated with pure palladium membrane by using chemical coating method. Membrane was used to serve dual purposes which are as strain sensor and as gas leakage detection sensor. Any crack on the pipeline can be detected by the developed sensor. However, this sensor has a sensitivity of 1 pm drift for 5% of $H_2$ content in 5 minutes. This sensor is suitable to detect $H_2$ gas in air because it has faster response and smaller wavelength shift.

(Hunze, 2018) has attempted to coat 30 nm of titanium layer between the etched fiber and the palladium coating to serve as adhesion layer between them. He has coated a palladium metal with the thickness of 1600 nm by using sputtering method. Testing of the sensor was done with 5% (50,000 ppm) of dissolved hydrogen in oil. A wavelength shift of 25 pm was observed. The sensitivity of sensor is calculated as 0.5fm/ppm. However, the surface of the coating after the test was not inspected for

micro-cracking. In addition, it was shown that sensor with higher cross sectional area has the most sensitivity but reduced response time.

The palladium-based sensor system response has shown reversible properties against hydrogen and oxygen (M. D. Yang, Jixiang, 2012). Besides, the palladium-chromium sensor, coated with a chemical reduction method, showed conductance changes when exposed was to 100 ppm and 300 ppm of oxygen at room temperature (B.K. Miremadi, 1994).

(Jixiang Dai, 2017) has summarized that a few researches that were done on the dissolved gas in transformer oil detection by using palladium metal. Palladium showed a better response to hydrogen in air than in oil. To date, the most sensitive sensor developed to detect dissolved hydrogen in transformer oil was done by (Jiang, 2014). Jiang has used magnetron sputtering method to coat palladium metal on the FBG. He has coated titanium on top of polyimide layer to serve as adhesion layer. The thickness of titanium (Ti) layer was 20 nm and palladium layer was 560 nm. Hydrogen gas was created by discharge method and wavelength shift was recorded. Figure 2.16 shows the response of the sensor with incremental hydrogen content. He has concluded that the sensitivity of the sensor at room temperature is 0.042 pm/ppm follows Equation 2.13 below. At temperature of 80°C, the sensors sensitivity was increased to 0.044 pm/ppm. On the other hand, the thickness of the sensor and the FBG surface area was not inspected after the test.

$$\Delta\lambda(pm) = 0.042 \times H_2(ppm) + 4.253 \quad (2.13)$$

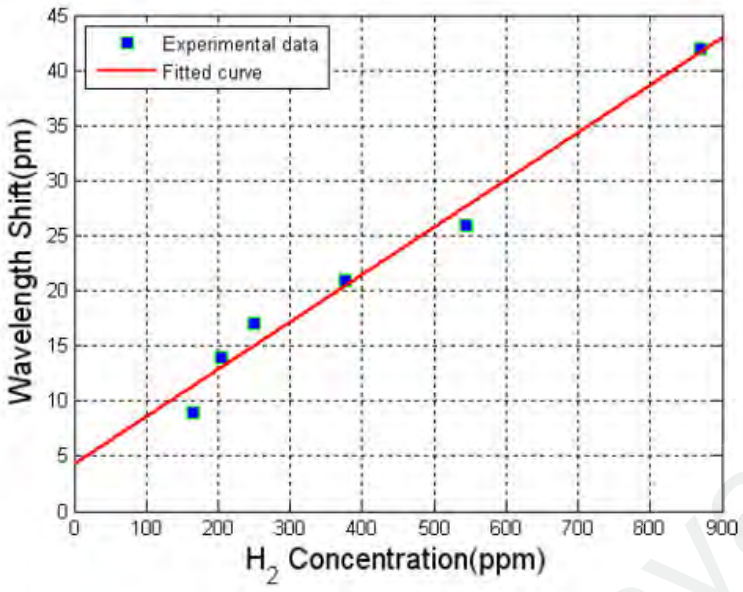


**Figure 2.16: Wavelength shift versus hydrogen concentration in the transformer oil at room temperature**

Palladium serves as an excellent material to detect hydrogen gas. Palladium metal will become palladium-hydride (PdH) when exposed to hydrogen gas and increased its lattice size depends on the dimension of tetrahedral sites the octahedral sites(Kofu, 2016). If the palladium is coated on an FBG, the expansion will cause strain on the FBG and cause wavelength shift. This principle can be used to detect hydrogen gas by using the palladium-coated FBG. Therefore, this research will focus on using palladium as the base material to detect dissolved hydrogen in transformer oil since it has shown some successful research in detecting hydrogen gas. However, the optimization of the sensor is still required for a specific application of the sensor.

Palladium metal was mixed with other alloys like gold and silver to stabilize the reaction of palladium with hydrogen gas. The addition of alloys inside palladium will prevent the hydrogen compound phase transition from α to β phase. Therefore, the coatings with alloy mixture will have good reversibility and rapid response capability at room temperature (Sayago I, 2005). Gold-based palladium sensor has shown promising

detection as in (Shukla, 2003). For most metal hydrides, the reversible reaction to metal is dependent on temperature and pressure of the hydrogen gas (J. Jiang, 2015).

Apart from silver and gold, chromium has shown reaction with hydrogen gas and become chromium hydride by electrical discharge only. The electric discharge breaks up the $H_2$ molecules to become reactive hydrogen atoms. The reactive hydrogen atom reacts with chromium and forms chromium hydride (Dewayne Terrence Halfen, 2008). Besides, chromium hydride was produced by reacting the chromium with methane in an electric arc (Shin, 2005). Therefore, at present, there is no study on chromium reaction with dissolved hydrogen in liquid or gas. In addition, chromium metal does not react with hydrogen or other combustible gasses inside the transformer. On top of these, chromium is cheaper and more available than gold (Rossen, 2015).

Chromium has been used to reduce the dislocation density in silicon iron microstructure which is used to produce transformer core. Addition of chromium into the iron microstructure has reduced the amount of ordered phase (Wensi Chen, 2015). On the other hand, chromium metal reacts with oxygen at room temperature and produce a stable Cr(III) oxide. Therefore, the reaction of Cr with oxygen inside the transformer can be ignored.

## 2.12 Temperature Correction for FBG Sensor

FBG based sensor is widely used for structural health monitoring, such as bridges and buildings (Buric, 2005; J. Da Silva, 2001). However, the FBG also acts as a temperature sensor due to the expansion of the gratings with the temperature. A wavelength shift induced by 1°C is equivalent to 10με of strain (Zhou, 2004). Thus, FBG needs to have temperature compensation whenever it is used as a strain sensor. For strain sensing properties, given that:

$$\lambda_B = 2n_{eff}\Lambda \tag{2.14}$$

Differentiating (2.14) yields:

$$d\lambda_B = 2\Lambda dn_{eff} + 2n_{eff}d\Lambda \tag{2.15}$$

Dividing (2.15) by (2.14), therefore

$$\frac{d\lambda_B}{\lambda_B} = \frac{dn_{eff}}{n_{eff}} + \frac{d\Lambda}{\Lambda} \tag{2.16}$$

where the strain is defined as $\varepsilon = \frac{d\Lambda}{\Lambda}$ , then $n_{eff}$ changes induced by strain is given as (Cho, 2019):

$$\frac{dn_{eff}}{n_{eff}} = -\frac{{n_{eff}}^2}{2}[p_{12} - v(p_{11} - p_{12})]\varepsilon \tag{2.17}$$

where $p_{11}$ and $p_{12}$ are Pockel's coefficient of strain optical sensor, and $v$ is the Poisson's ratio. Defining P = $\frac{{n_{eff}}^2}{2}[p_{12} - v(p_{11} - p_{12})]$, equation (2.16) will be reduced to:

$$\frac{d\lambda_B}{\lambda_B} = (1 - P)\varepsilon = K_\varepsilon\varepsilon \tag{2.18}$$

where $K_\varepsilon$ is the strain sensitivity. A typical value of $P$ , for a wavelength of 1550nm, of a silicon dioxide FBG is 0.22, and the strain sensitivity coefficient is about 1.2 *pm/με* (Zhou, 2004).

Whenever the FBG is affected by temperature, the change of period as well as the refractive index will cause wavelength shift. Deriving equation (2.14) with temperature (*T*) will become:

$$d\lambda_B = 2(\Lambda \frac{n_{eff}}{dT} + n_{eff} \frac{d\Lambda}{dT})d\mathrm{T}) \quad (2.19)$$

dividing equation (2.19) with (2.14) yield:

$$\frac{d\lambda_B}{\lambda_B} = (\frac{1}{n_{eff}} \frac{dn_{eff}}{dT} + \frac{1}{\Lambda} \frac{d\Lambda}{dT})d\mathrm{T} \quad (2.20)$$

Let $\frac{dn_{eff}}{n_{eff}dT} = \zeta$, and $\frac{1}{\Lambda} \frac{d\Lambda}{dT} = \alpha$, which are thermal expansion coefficient and thermal optical tensor, respectively, equation (2.20) will be further simplified to:

$$\frac{d\lambda_B}{\lambda_B} = (\alpha + \zeta)d\mathrm{T} = K_T \quad (2.21)$$

where $K_T$ is thermal sensitivity. If the FBG core is silicon dioxide and affected by temperature only, at the wavelength of 1550 nm, $\alpha + \zeta = 6.67\ X\ 10^{-6}{}^{\circ}\mathrm{C}^{-1}$, and $K_T = 10\ \mathrm{pm}^{\circ}\mathrm{C}^{-1}$ (Zhou, 2004). When the FBG sensor works as a temperature sensor only, the temperature difference, in K, is given as:

$$\Delta\mathrm{T} = \frac{1}{(\mathrm{K}_{\varepsilon}\alpha_{\mathrm{glass}} + \alpha_{\delta})} \frac{\Delta\lambda_{\mathrm{B}}}{\lambda_{\mathrm{B}}} \quad (2.22)$$

where $\alpha_{\mathrm{glass}} = 0.55 \times 10^{-6}/\mathrm{K}$ and $\alpha_{\delta} = 7 \times 10^{-6}/\mathrm{K}$.

## 2.13 Coating Methods Applied for Palladium on Fiber Optics.

In this section coating methods used to coat palladium or equivalent materials are discussed. There are a few methods of applying the palladium coatings on the fiber optic, or glass mainly. The most commonly used methods are chemical reduction, electro-deposition, magnetron sputtering and chemical vapour deposition (CVD). The biggest challenge is to get the metal to stick on the glass surface, without peeling off or losing its properties.

(Alexander, 2013) has attempted to coat palladium nanoparticles on the fabricated titanate nanotubes with chemical reduction method by using sodium borohydride ($NaBH_4$) as a reducing agent. The sizes of the nanoparticles that were used in the studies were between 10-13 nm. The palladium coating was done by preparing the palladium chloride ($PdCl_2$) aqueous solution, with 10 hrs of constant stirring at 10000 rpm, to enable the $PdCl_2$ absorbed to the surface of the nanotubes. Then, the sample was vacuum dried at 80$^oC$ for 5 hrs, to form dried samples. Later, dried samples were dispersed in 10 ml of $NaBH_4$ to form $Pd^{(0)}$. Finally, the nanotubes were washed with ethanol several times and dried under vacuum for 5 hrs at 80$^oC$ (Alexander, 2013).

For chemical evaporation method, a thin palladium coating was applied on top of the glass plate by (Bodzenta et al., 2002). The palladium particles were evaporated directly on the glass surface after 5 nm layer of chromium has been coated on it. In this research, the palladium was not expected to either expand or contract on the glass surface with the presence of dissolved hydrogen. The change of conductivity was used in detecting the presence of dissolved hydrogen. The change of conductivity was measured by passing an electrical current through the palladium layer. In addition, palladium thickness of 10-15 nm was found to have better sensitivity in detecting the presence of hydrogen compared to the palladium with thickness less than 10 nm.

In other studies, (Zagula-Yavorska, 2012) coated 3 μm thickness of the palladium layer on alloy by using the chemical vapor deposition (CVD) method. In order to increase the adhesion between the coatings and the substrate, the CVD was done in the argon atmosphere for 2 hours at the temperature of 1050$^oC$. However, this prolonged temperature treatment would damage to the fiber, thus made the CVD unsuitable for coating palladium on the fiber optics (Trpkovski, 2003).

In addition, Tin Oxide ($SnO_2$) was coated on the surface of the glass slate which was able to detect hydrogen in free air. This was done by applying a thin layer of platinum on the gold-palladium coating, which was coated earlier on the $SnO_2$ layer. The investigation showed that the thickness of 100-150 nm has the best sensitivity for hydrogen detection. Then, the temperature of the hydrogen was raised from 100-700$^oC$, and it was found that the sensor had the highest accuracy at 350$^oC$. However, at room temperature, the sensor was only able to detect $H_2$ concentration between 1-4%, where 4% was considered as the combustible limit. Figure 2.17 shows the coating layers on the glass plate (Shukla, 2003).

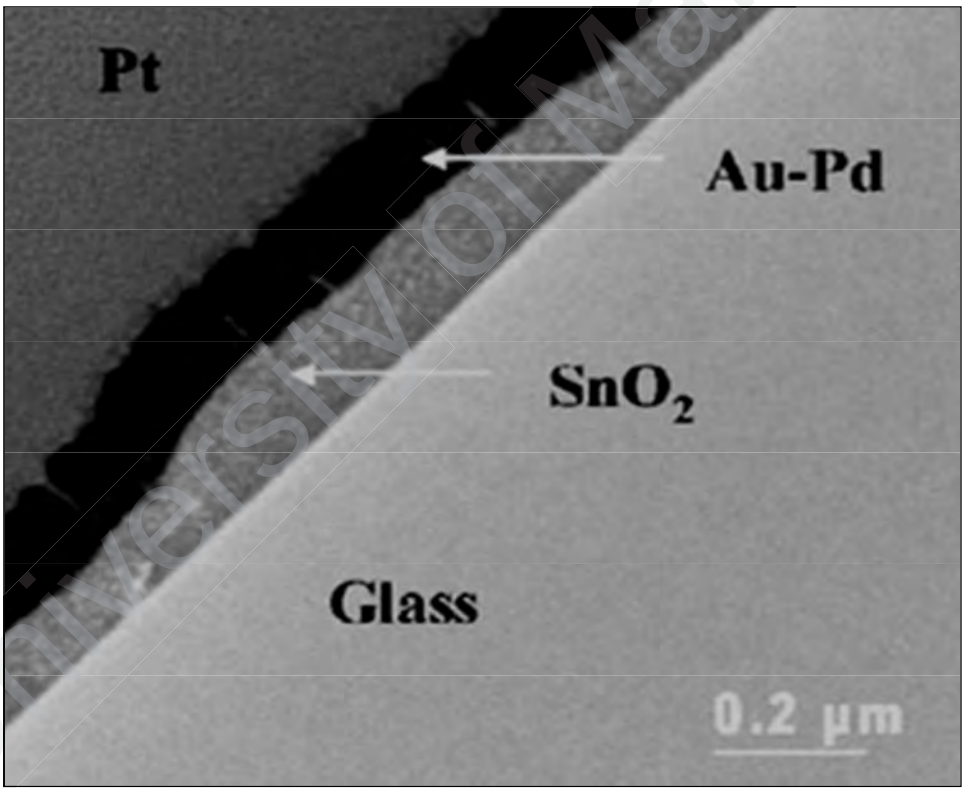


**Figure 2.17: Coatings of Pt-Au-Pd on $SnO_2$ on the surface of the glass (Shukla, 2003)**

Meanwhile, detection of the hydrogen by using palladium coatings could be improved as the thickness of the coating increased (Ma et al., 2012). However, thicker

palladium coating had peeled off after it was exposed to transformer oil. Therefore, a thin titanium layer of 20 nm was applied on the fiber optics to improve the adhesive properties on the palladium (Figure 2.18).

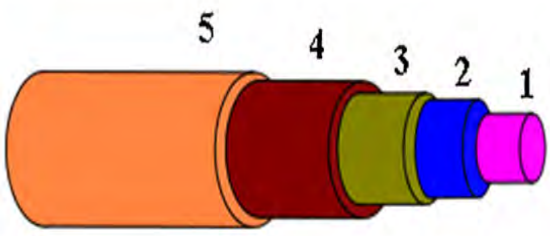


**Figure 2.18: Structure of FBG hydrogen sensor (1: Fiber Core; 2: Fiber cladding; 3: Polyimide layer; 4: Titanium or nickel layer; 5: Palladium layer) (Ma et al., 2012)**

The applied titanium layer can also be replaced with nickel metal. The coating was done by using the magnetron sputtering method. In this work, a palladium layer of 560 nm, and a titanium layer of 20 nm were used to avoid peeling-off of the coatings when it was exposed to transformer oil. Titanium showed excellent adhesion to the fiber when it was exposed to transformer oil. In addition, a polyimide layer which has higher viscosity at the temperature of the magnetron sputtering was used to enhance the adhesiveness of the palladium on the fiber further. This was also improved the detection accuracy of the hydrogen sensor to 13.5 ppm of hydrogen concentration. The added polyimide layer did not significantly improve the sensor accuracy, as shown in Figure 2.19.

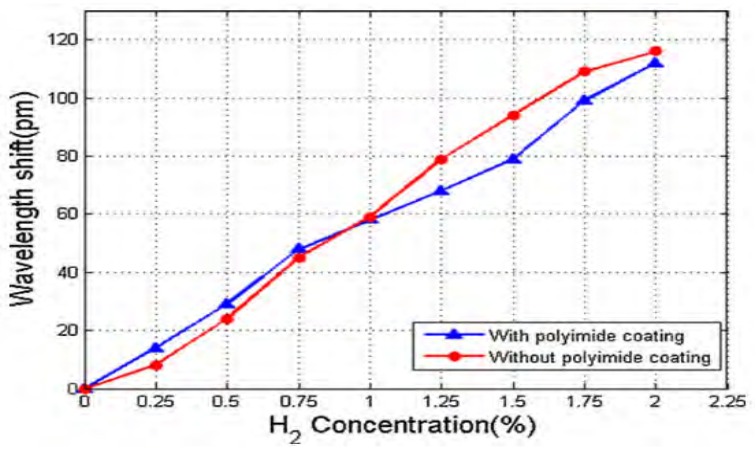


**Figure 2.19: FBG wavelength shift to hydrogen concentration (Jiang, 2014)**

The modification of hydrogen sensor by using polyimide was done by (Li, 2006). The developed sensor was Metal-Insulator-Semiconductor (MIS), where it can detect hydrocarbon gasses such as hydrogen, carbon monoxide, acetylene, methane and ethylene. After the polyimide coating was applied, the selectivity of the sensor towards hydrogen was improved significantly. However, the presence of oxygen still affected the polyimide coated palladium. The polyimide coating acted as a filter to extract the hydrogen from the other hydrocarbon gasses in the sample. In addition, Li has also proved that the detection accuracy of hydrogen is dependent strongly on the thickness of the palladium coating. The coating of the palladium (50 nm) was done by using the electron beam evaporation method.

In other studies, the parameter of coating or coating process has been controlled by varying the length, diameter and the density of palladium. This was done by using porous anodic aluminium oxide. The porous alumina films were prepared by double anodizing high purity aluminium foils in oxalic and sulphuric acids at 40 V and 25 V, respectively. The final pore size of the processed (free-standing) alumina templates

were determined to be ~65 and 35 nm (Kartopu, 2008). However, this process is too complex to be carried out by a non-expert in the field.

Hamagami has prepared photocatalytic titanium coatings with palladium catalyst onto soda limestone glass substrate by using low-temperature synthesis for application of the optical sensor. Titanium coatings were formed on the glass substrate by a sol-gel coating process and followed by a hot water treatment at 55$^{o}$C. Metallic palladium nanoparticles were deposited onto the titania coatings, by means of photo-deposition technique (J. Hamagami, Araki, R., Onimaru, S., Oda, H., 2011). In addition, he demonstrated photo deposition of the palladium on the $TiO_2$ coating by UV method. The normalized transmittance of the Pd/$TiO_2$ thin film at a wavelength of 640 nm decreased to 0.9 within 5 seconds (J. Hamagami, Araki, R., Oda, H., Sakai, M., 2010). However, the sol-gel method is a slow and time-consuming fabrication technique which needs higher furnace temperature to create crystalline form and the thickness cannot be precisely controlled.

For the electrodeposition technique, granular palladium nanowires with 250 nm diameter were electrodeposited on Highly Oriented Pyrolytic Graphite (HOPG). In order to measure the electrical response of the sensor, the nano-wires were transferred to an insulating polystyrene surface. Polystyrene thin films with the thickness of about 150nm were formed on a glass micro-slide by a dip-coating technique from a chloroform solution. Silver microelectrode pads were patterned on the surface of the nano-composite by shadow masking technique. All stages of sensor device fabrication and its mechanism were monitored with the application of atomic force microscopy technique which required sophisticated tools (contact, non-contact, and force modulation modes)(Atashbar, 2005).

In 2013, Dai developed optical hydrogen sensor based on etched FBG sputtered with Pd/Ag composite film by using the magnetron sputtering method. The sensor showed good reversibility for the hydrogen response. X-ray powder diffraction (XRD) results demonstrated the Pd/Ag composite films were mainly cubic phase. The results showed that the FBG with fewer diameters had more wavelength shift under the same hydrogen concentration. When the hydrogen concentration is 4% in volume ratio, the wavelength shifts of FBG-125 lm, FBG-38 lm and FBG-20.6 lm were 8, 23 and 40 pm respectively. And FBG hydrogen sensors showed linearity response for 1.5–4% hydrogen concentrations. As a new solution, etched FBG combined Pd/Ag composite film as a hydrogen sensitive element could be very promising for distributed measurement of hydrogen concentration. The experimental results showed the sensor's hydrogen response was reversible, and the side-polished FBG hydrogen sensor had great potential in hydrogen's measurement (Dai et al., 2013).

Ma developed a highly sensitive and reliable fiber Bragg grating sensor that was suitable for hydrogen sensing in transformer oil. A polyimide layer was successfully used for preventing the thick palladium layer from being peeled off (Figure 2.20). The experimental results demonstrated that the hydrogen sensitivity of the proposed sensor could reach 13.5 ppm/pm in transformer oil. The concept of using FBGs for measuring stress in the sensitive materials could be applied to other types of gases dissolved in the transformer. It provided an ideal solution for gas on-line monitoring and fault location. Hence, the use of polyimide layer revealed another method to improve the reliability of the Pd-based hydrogen sensor (Ma et al., 2012).

**Figure 2.20: Thick palladium peeled off due to no adhesive layer (Ma et al., 2012)**

Yang showed Pd-based hydrogen sensors have a problem of poor reliability due to material instabilities resulting from the significant volume changes that occur during PdH phase transition. Tungsten trioxide, ($WO_3$) is another hydrogen-sensitive material; $WO_3$ film will change its colour from greenish-yellow to blue when it is exposed to hydrogen due to its chemical interaction. However, this chemical interaction between $WO_3$ and hydrogen is not strong enough; $WO_3$ can also chemically interact with other specimens, such as $H_2S$,$C_2H_2$ etc., and therefore does not show selective sensitivity to hydrogen. This will limit its application as a hydrogen sensor.

A solution for improvement is to deposit Pd film on $WO_3$ film, Pd works as catalysts for dissociation of hydrogen. The chemical reaction would proceed faster with the coexistence of Pd. However, the catalyst can only promote the chemical reaction at the interface between Pd and $WO_3$; meanwhile, the mechanical reliability is reduced due to the mismatch of material properties of Pd and $WO_3$. Yang proposed a novel hydrogen sensor based on Pd/$WO_3$ magnetron co-sputtering. A fiber-optic hydrogen gas sensor with composited Pd/$WO_3$ thin film as sensing media was developed. Figure 2.21 shows

the SEM image of $Pd/WO_3$ after exposure to hydrogen cycle (M. H. Yang, Sun, Zhang, & Jiang, 2010). However, this work did not show the response of the sensor for other gasses such as $H_2S$ and $C_2H_2$. Therefore, only palladium can be treated as the most reliable metal to detect hydrogen.

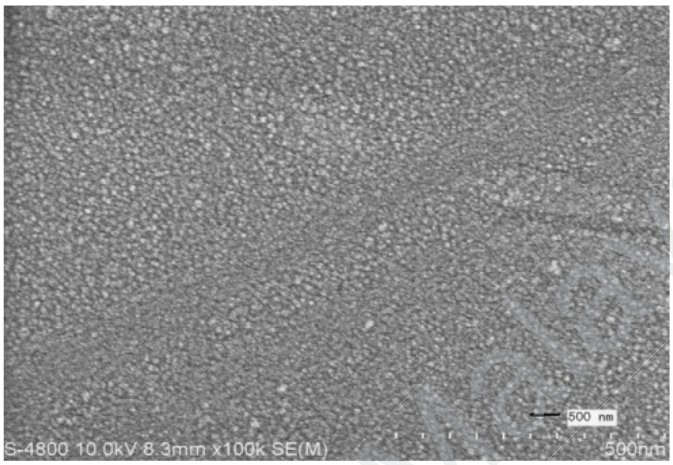


**Figure 2.21: SEM image of $Pd/WO_3$ after exposure to hydrogen cycle (M. H. Yang et al., 2010)**

It is conclusive that the palladium, chromium can adhere to the $TiO_2$ coating, and the latter can adhere to the glass well. The magnetron sputtering method is widely used for coating the palladium on the fiber. Therefore, magnetron sputtering has more significant potential to be used as the coating method for palladium and being used for the latest research.

## 2.14 Novel contribution of this study

During the past three decades, research has focused on using palladium to detect dissolved hydrogen in transformer oil. Various type of alloy composition was used, but there was no study on using chromium mixture.

Chromium was selected because it is comparatively cheaper than the other alloy materials and has shown some reduction in lattice expansion in (Wensi Chen, 2015). This will help in reducing the cost of manufacturing the FBG based sensor. The

application of this type of sensor can be limited to a hermetically sealed transformer because there is less vibration compared to a power transformer. This type of sensor can be produced in the lab. The parameter settings for the physical vapor deposition (PVD) equipment are presented in this work to guide on the future production of the sensor.

However, different compositions of palladium and chromium react differently to dissolved hydrogen. Therefore, all 16 sensors that were developed in this study were tested and validated with measurement result from a certified lab to confirm the accuracy and operability.

They offer various range of detection based on the need of the market. These sensors can be directly mounted to the existing in-service transformer.

In addition, the work carried out in this study has contributed to the body of knowledge in the sensor area and can be further developed to become a fully operational range of products in the industry.

# CHAPTER 3: RESEARCH METHODOLOGY

In this chapter, the sensor development methodology will be discussed. The selection of the base materials and the coating method for the sensors were made based on thorough literature review. The sensors were developed and tested systematically with oil with known hydrogen content generated by diffusion as well as partial discharge. Repeated experiments were conducted to establish the correlation of the wavelength shift and the hydrogen content inside the transformer oil.

## 3.1 Introduction

The following flowchart summarizes the whole project activities. There were a few critical milestones in the projects which were; design the rotator set, selection of the right material, preparation of the traceable gas samples and determination of correct PVD parameter.

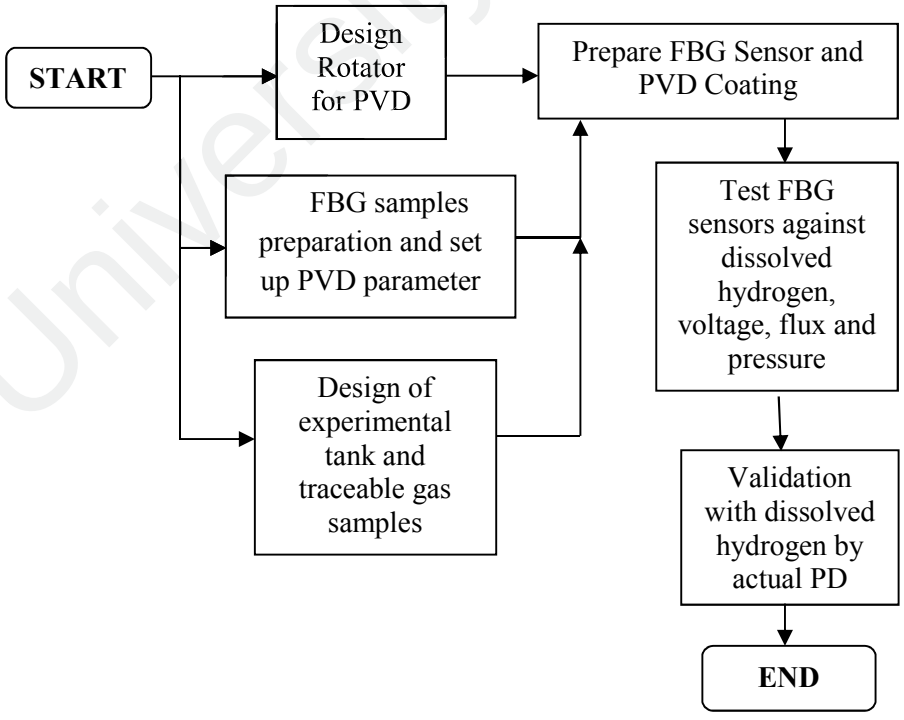


**Figure 3.1: Flowchart on the Project Activities**

## 3.2 Design of the rotator

The PVD machine has a limitation as it can only support z-direction rotation. The distance between the coating substrate and the target was 45cm. This distance had to be maintained to obtain a sufficient coating. In addition, the duration taken to coat a single FBG was around 6 hours. Therefore, to maintain uniformity and the consistency of the samples, a rotator was designed to enable 4 samples to be coated at a time. The rotator rotated at a speed of 120 revolutions per minute by using the friction force from the PVD bottom rotation plate. Figure 3.2 and Figure 3.3 show the 4-tier rotators used in this work.

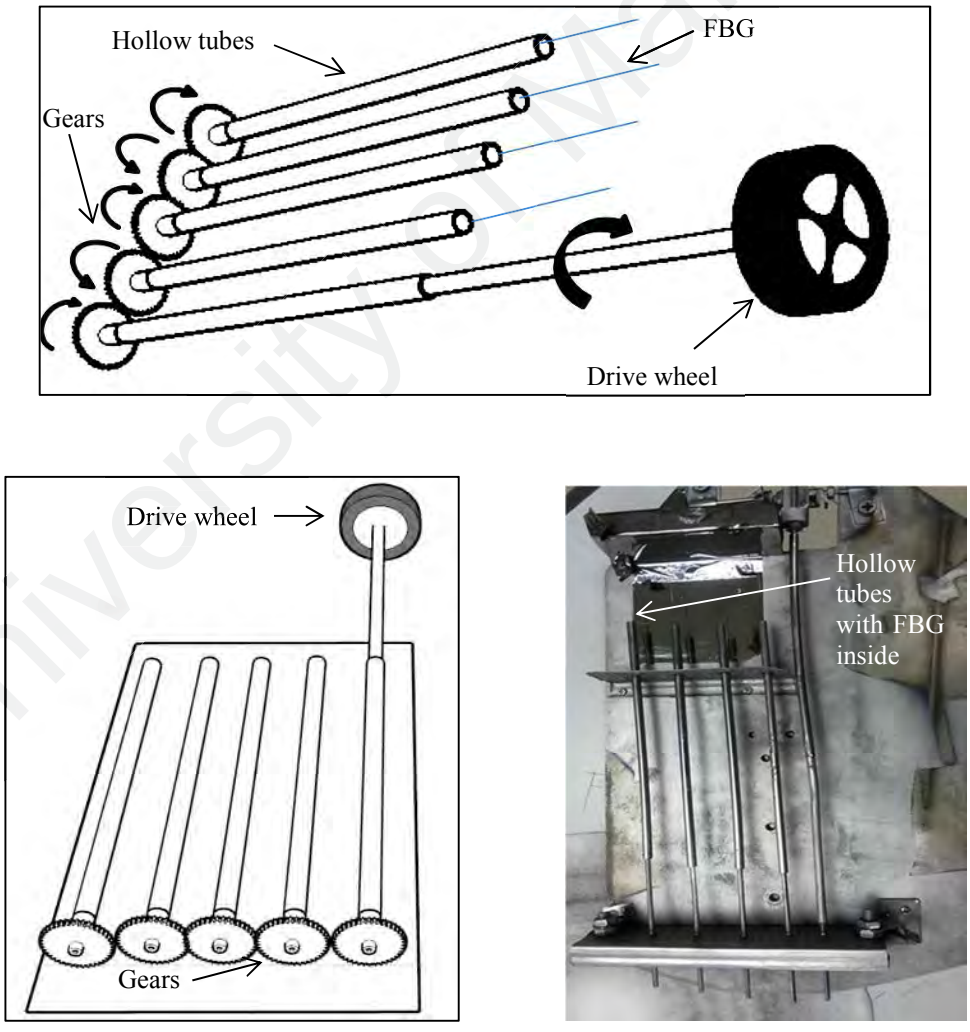


**Figure 3.2: Rotator design (top), gear mechanism placement on a metal plate (bottom left) and actual rotator (bottom right) to be used inside PVD machine**

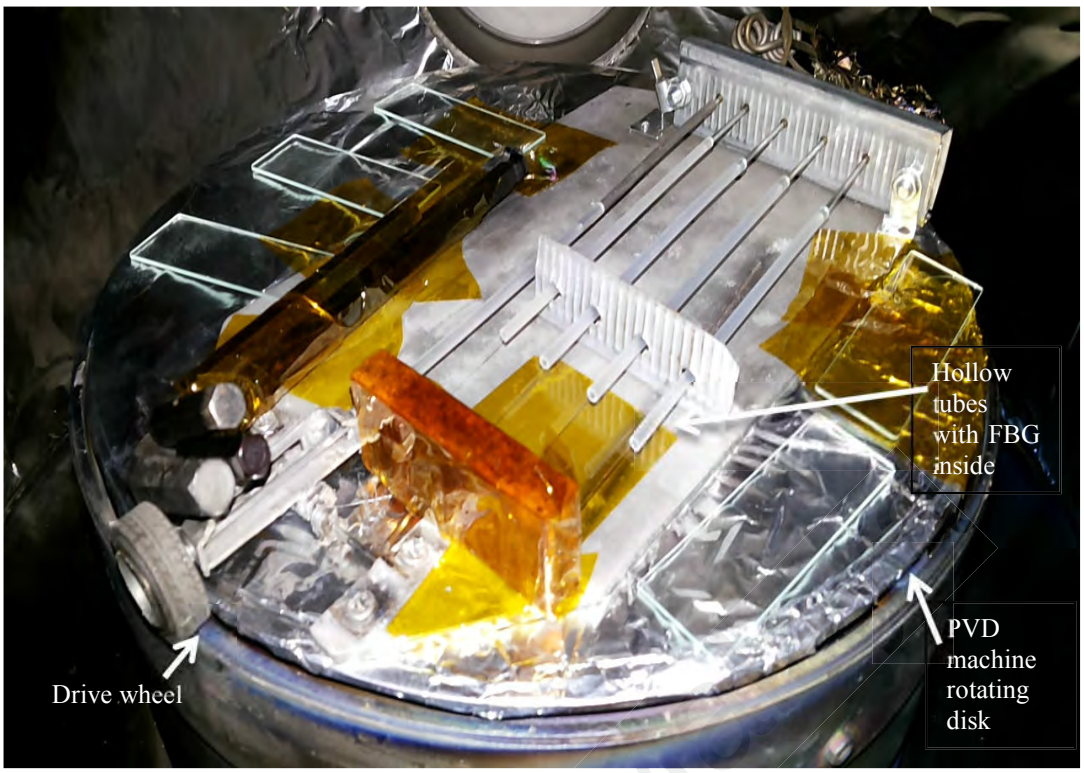


**Figure 3.3: Rotator placed inside the PVD machine**

### 3.3 FBG samples preparation and PVD machine parameter determination

In this work, Physical Vapor Deposition (PVD) method was used to coat the FBG with palladium metal. In order to ensure the adhesion of the Pd to the FBG, a thin layer of $TiO_2$ needed to be applied first. However, due to cost constraints, a test fiber (bare fiber without Bragg gratings) was used to assess the integrity of the $TiO_2$ adhesion strength against the transformer oil before the real FBG was used to coat the $TiO_2$ layer.

The sample preparation was done by removing the outer jacket of a test fiber. Then, it was cleaned with ethanol and chloroform to remove the residues. The test fiber was mounted on a rotator which was placed inside the PVD machine. The coating was done by using the magnetron sputtering method.

The PVD machine has two coating modes which are Radio Frequency (RF) and Direct Current (DC). The latter is used to perform a thicker coating. In this work, the RF

method was used because a thin layer of $TiO_2$ was needed. Next, the $TiO_2$ layer, which had a thickness of 80 nm±10%, was coated on a test fiber and then it was immersed in the mineral oil. The mineral oil was heated in an oven to a temperature of 65ºC to replicate the average in-service transformer oil temperature. Hydrogen gas will be formed due to heat at a temperature more than 150ºC (Arvind et al., 2008).

The inspection of the coating which was immersed in the mineral oil was done once every two days. Once the coating had shown no sign of peeling or micro-cracking for 40 days, the sample was taken out from the oven. $TiO_2$ coating had been verified, and FBGs were coated with palladium and chromium by using the parameter settings in Table 3.1 to Table 3.5, respectively.

**Table 3.1: Parameter setting for $TiO_2$ coating (DC Target)**

| Parameter | Value |
|---|---|
| Pressure | 666 mPa |
| Temperature | 50°C |
| Oxygen | 6 sccm |
| Nitrogen | 6 sccm |
| Power | 250 W |
| Duration | 12 minutes |
| Current | 0.625 A |
| Voltage | 400 V |

The PVD machine had two sputtering targets which were DC and RF. Both sputtering sources (targets) could operate simultaneously. This limited the number of metals for the coating to be two only at one time. For the Pd-Cr coating, the Pd target was mounted on the DC sputtering source whereas the Cr target was mounted on RF sputtering source. On the other hand, the RF sputtering was turned off during the $Pd_{100}$ coating session. In addition, the coating temperature was set to room temperature (25ºC), and the pressure was set at $3x10^{-5}$ Pa. Argon gas was used as the sputtering gas.

The measurement of coating thickness and the composition of the coated FBG were measured by using SEM-EDX method.

Sixteen FBG based sensors with the ratios of 100:0 ($Pd_{100}$), 88:12 ($Pd_{88}Cr_{12}$), 75:25 ($Pd_{75}Cr_{25}$) and 67:33 ($Pd_{67}Cr_{33}$) were prepared. For each composition, there were 4 samples prepared with different coating thickness which were 970 nm, 1060 nm, 1180 nm and 1300 nm. The initial plan was to prepare FBG based sensors with 100:0 ($Pd_{100}$), 90:10 ($Pd_{90}Cr_{10}$), 80:20 ($Pd_{80}Cr_{20}$) and 70:30 ($Pd_{70}Cr_{30}$). However, the uncertain nature of coating plasma in the PVD machine influenced the ratios of the coatings. Different ratios of chromium were chosen to observe the performance of the sensors with respect to dissolved hydrogen and to determine the best ratio for future application.

The FBGs were coated on the fiber for a length of 3cm. The expected coating on the FBG is as in Figure 3.4.

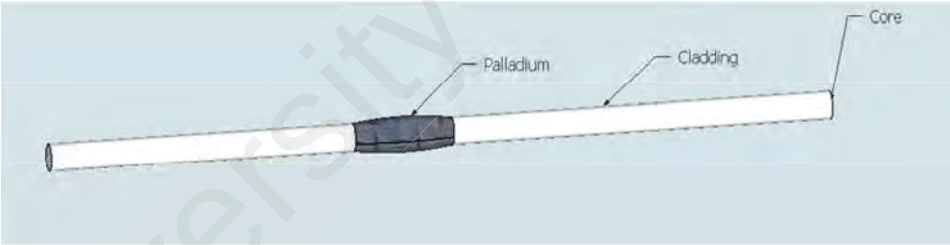


**Figure 3.4: Expected coating on the FBG**

**Table 3.2: PVD parameter setting for 970 nm coating thickness for different Pd-Cr composition**

| | ***Pd (DC Coating)*** | | ***Cr (RF)*** | | ***Pd-Cr*** |
|---|---|---|---|---|---|
| **Duration (min)** | Power (W) | Measured composition (%) | Power (W) | Measured composition (%) | Measured average thickness (nm) |
| **55** | 60 | 100 | - | 0 | 970 ±10 nm |
| **64** | 40 | 88 | 200 | 12 | |
| **76** | 20 | 75 | 400 | 25 | |
| **91** | 15 | 67 | 600 | 33 | |

**Table 3.3: PVD parameter setting for 1060 nm coating thickness for different Pd-Cr composition**

| | *Pd (DC Coating)* | | *Cr (RF)* | | *Pd-Cr* |
|---|---|---|---|---|---|
| **Duration (min)** | Power (W) | Measured composition (%) | Power (W) | Measured composition (%) | Measured average thickness (nm) |
| **66** | 60 | 100 | - | 0 | 1060 ±10 nm |
| **75** | 40 | 88 | 200 | 12 | |
| **87** | 20 | 75 | 400 | 25 | |
| **102** | 15 | 67 | 600 | 33 | |

**Table 3.4: PVD parameter setting for 1180 nm coating thickness for different Pd-Cr composition**

| | *Pd (DC Coating)* | | *Cr (RF)* | | *Pd-Cr* |
|---|---|---|---|---|---|
| **Duration (min)** | Power (W) | Measured composition (%) | Power (W) | Measured composition (%) | Measured average thickness (nm) |
| **72** | 60 | 100 | - | 0 | 1180 ±10 nm |
| **81** | 40 | 88 | 200 | 12 | |
| **95** | 20 | 75 | 400 | 25 | |
| **108** | 15 | 67 | 600 | 33 | |

**Table 3.5: PVD parameter setting for 1300 nm coating thickness for different Pd-Cr composition**

| | *Pd (DC Coating)* | | *Cr (RF)* | | *Pd-Cr* |
|---|---|---|---|---|---|
| **Duration (min)** | Power (W) | Measured composition (%) | Power (W) | Measured composition (%) | Measured average thickness (nm) |
| **80** | 60 | 100 | - | 0 | 1300 ±10 nm |
| **89** | 40 | 88 | 200 | 12 | |
| **103** | 20 | 75 | 400 | 25 | |
| **116** | 15 | 67 | 600 | 33 | |

### 3.4 Selection of dissolved hydrogen range for the experiment

For this experiment, dissolved hydrogen samples up to 700 ppm were required to test all sensors. This was because 700 ppm or less of hydrogen content goes into "Condition 2" in the Total Dissolved Combustible Gas (TDCG) analysis table (IEC, 2015). TDCG is the summation of all dissolved combustible gasses in the transformer. Table 3.6 summarizes the TDCG gasses concentration table extracted from (IEC, 2015). Meanwhile, Table 3.7 summarizes the action required based on transformer oil conditions.

The sensors will serve as monitoring tools until the level of hydrogen inside the transformer reach up to 700 ppm. After 700 ppm, the transformer will require outage and thorough inspection and electrical tests. One can monitor the rate of gas generation inside the transformer to decide on the condition of the transformer. Any hydrogen content more than 101 ppm will go into Condition 2 in Table 3.6, which will require further investigation. This study will focus on the feasibility of using the developed sensor as the early indicator to detect hydrogen gas in Condition 2 range. As mentioned in Table 2.2 and 2.3, higher hydrogen inside transformer oil indicated discharge in the gas-filled cavities resulting from incomplete impregnation, high humidity in the paper, oil super-saturation or cavitation (IEC, 2015). Therefore, a sensor which was operable up to 700 ppm would serve the purpose of monitoring the hermetically sealed transformer.

**Table 3.6: Dissolved gas concentration (IEC, 2015)**

| Status | $H_2$ | $CH_4$ | $C_2H_2$ | $C_2H_4$ | $C_2H_6$ | CO | TDCG |
|---|---|---|---|---|---|---|---|
| **Condition 1** | 100 | 120 | 35 | 50 | 65 | 350 | 720 |
| **Condition 2** | 101-700 | 121-400 | 36-50 | 51-100 | 66-100 | 351-570 | 721-1920 |
| **Condition 3** | 701-1800 | 401-1000 | 51-80 | 101-200 | 101-150 | 571-1400 | 1921-4630 |
| **Condition 4** | >1800 | >1000 | >80 | >200 | >150 | >1400 | >4630 |

**Table 3.7: Actions required based on the condition of the transformer (TDCG level) (IEC, 2015)**

| | TDCG levels (ppm) | TDCG rates (ppm/day) | Sampling intervals and operating procedures for gas generation rates | |
|---|---|---|---|---|
| | | | Sampling interval | Operating procedures |
| **Condition 4** | >4630 | >30 | Daily | • Consider removal of service<br>• Advise manufacturer |
| | | 10-30 | Daily | |
| | | <10 | Weekly | • Exercise extreme caution<br>• Analyze for individual gases<br>• Plan outage |
| **Condition 3** | 1921-4630 | >30 | Weekly | • Exercise extreme caution<br>• Analyze for individual gases<br>• Plan outage<br>• Advise manufacturer |
| | | 10-30 | Weekly | |
| | | <10 | Monthly | |
| **Condition 2** | 721-1920 | >30 | Monthly | • Exercise caution<br>• Analyze for individual gases<br>• Determine load dependence |
| | | 10-30 | Monthly | |
| | | <10 | Quarterly | |
| **Condition 1** | <720 | >30 | Monthly | • Exercise caution.<br>• Analyze for individual gases.<br>• Determine load dependence. |
| | | 10-30 | Quarterly | • Continue normal operation |
| | | <10 | Annually | |

## 3.5 Preparation of gas in oil by diffusion

Transformer oil samples with known dissolved hydrogen contents were prepared separately by dissolving hydrogen gas into oil by using a 90-litre metal tank (Figure 3.5) with perforated copper tube mounted at the inlet valve (Figure 3.6). The tank was constructed by using mild steel which was widely used for transformer tank. The flow of the gasses was controlled by using a precise gas regulator and was set to 1g/hour. First, the hydrogen gas was inserted with a constant flow for 10 minutes and then paused for 20 minutes. The time duration of 20 minutes was required to allow the gas to dissolve in the oil. After that, the cycle was repeated for the 2$^{nd}$ to the 8$^{th}$ samples. At each cycle, 2 samples were taken with a volume of 1000 ml each.

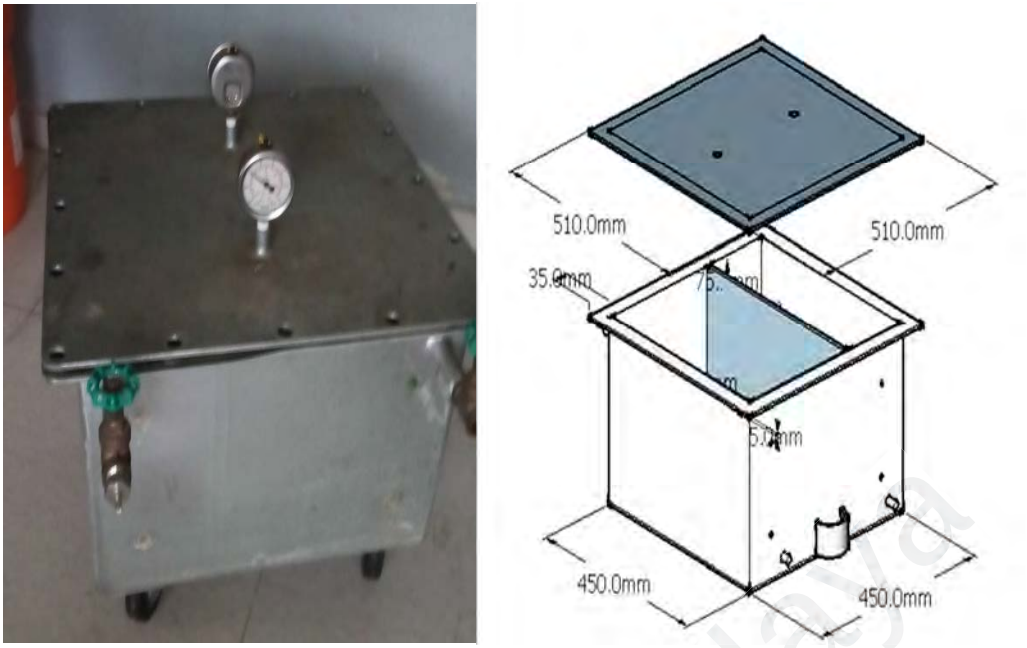


**Figure 3.5: Tank used to dissolve the hydrogen gas inside the transformer oil**

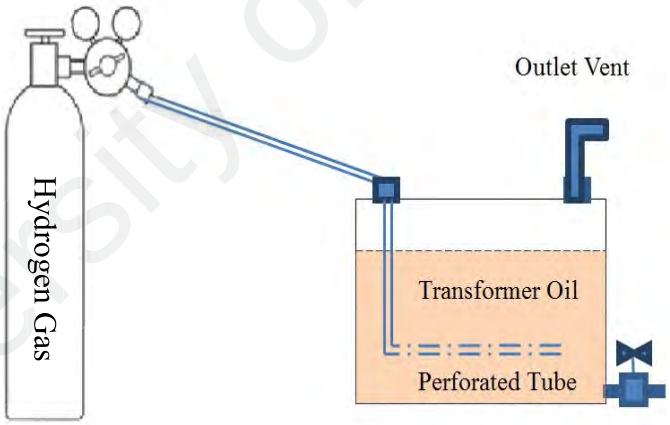


**Figure 3.6: Hydrogen diffusing in the transformer oil**

The diffusion of the hydrogen into the transformer oil was done in a fire-proof lab in TNB Remaco, Connaught Bridge Power Plant, Kelang. The second sample was used for DGA test to measure the amount of dissolved hydrogen in oil. This test was done by using the portable dissolved gas analyzer (Morgan Shaffer mini gas chromatography). The equipment uses gas chromatography technology similar to the lab (Figure 3.7).

Portable equipment was used to get an immediate result and to avoid a false reading. Each oil sample was tested twice for accuracy and repeatability. The equipment complied to ASTM D 3612 or IEC 60567. The equipment took around 2 minutes to complete the measurement of the dissolved gasses inside the oil.


**Figure 3.7: Myrkos - Portable DGA MicroGC**

Once the dissolved quantity of gases was known, the samples were labelled accordingly. All the samples of oil were stored inside a temperature-controlled chamber, where the temperature was set to 25°C. The temperature of the oil samples was controlled by performing the experiment in a controlled temperature lab (IEC 17025 certified lab). This is to reduce the gas in oil activity and gas release rate.

Figure 3.8 shows the hydrogen gas release rate after the diffusion of the hydrogen into the oil. Oil samples (1 litre each) were taken and kept at the right interval for future testing. The DGA test was repeated after 1 month to verify the gas content. In approximation, if the oil was exposed, the hydrogen content inside the oil would reduce to half of its original quantity; depending on the temperature and surface area.

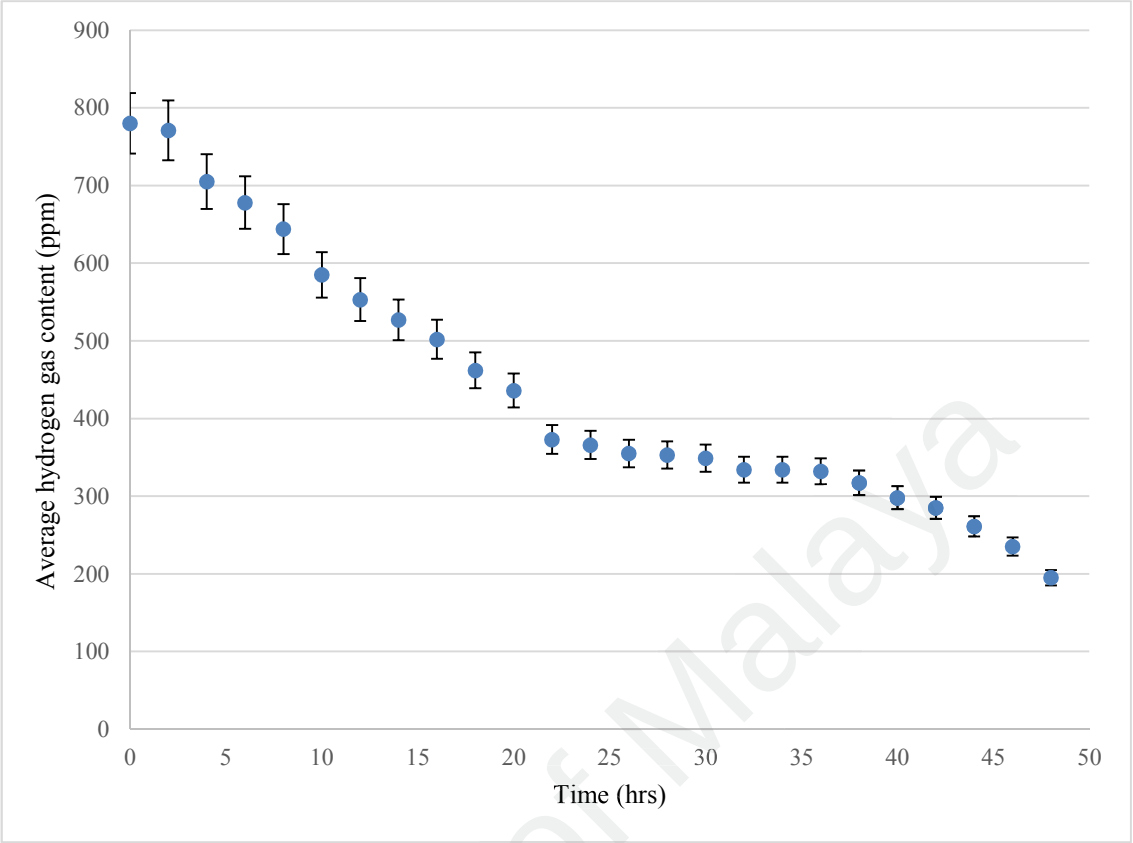


**Figure 3.8: Hydrogen release rate after diffusion**

## 3.6 Preparation of hydrogen gas-in-oil samples by discharge

High voltage generator was developed as a part of the work to simplify the testing of the FBG sensors. A smaller version of a high voltage generator was used to ensure safety to the tester and enhance mobility. The high voltage generator was used to generate corona discharge in transformer oil. The corona discharge will generate hydrogen as the by-product in the oil. This method of generating hydrogen in the oil was preferred because it replicated the real phenomena inside a transformer in service.

The high voltage circuit was developed to be portable and powered by 12 V DC source. The discharge voltage was measured as 20 kV. Figure 3.9 shows the circuit for the high voltage generator.

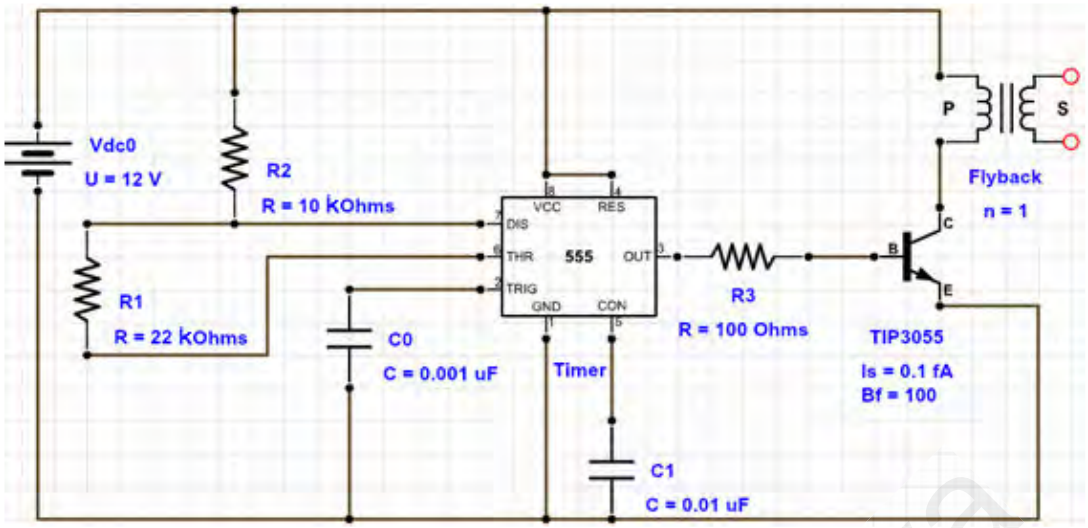


**Figure 3.9: High voltage generator circuit**

The circuit above has three components, namely oscillator, switching stage and step-up stage. The oscillator (Timer 555) generates DC pulses to the base of the transistor TIP3055, which is the switching device. This caused the current from the DC supply flowed through the flyback transformer and induced high voltage up to 20kV at its secondary side. A high voltage up to 20kV is sufficient to generate corona inside transformer oil. The whole circuit was placed inside a plastic container for safety purpose, as in Figure 3.10. There were 2 identical circuits developed for contingency purpose.


**Figure 3.10: High voltage generator inside the plastic container**

The high voltage terminals of the circuits were separated by 10 cm. This was to avoid any air ionization as well as sparking across the terminals. In addition, the sharp edges at the terminals were trimmed to prevent partial discharge/corona. The levels of partial discharge at the terminals were measured by using ultrasonic partial discharge and transient earth voltage detector. The terminals were trimmed and rounded until there was no partial discharge at the terminals.

The high voltage generator was tested to generate corona in the air by placing a thin wire at a distance of 11 mm across the high voltage terminals (Figure 3.11). The ultrasound partial discharge detector was used to detect the presence of corona in the air. Once the ultrasound detector detected the corona, the high voltage generator was brought into a dark room to see the corona discharge. An intense corona was seen as the blue dots in the dark (Figure 3.12).


**Figure 3.11: Spacing between the wires**

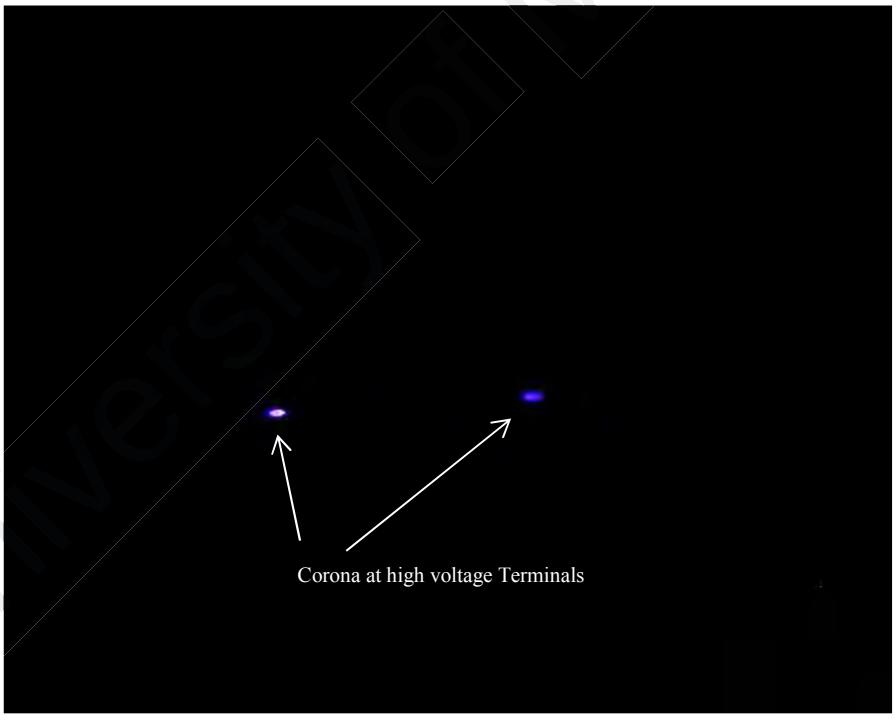


**Figure 3.12: Corona in the dark**

Subsequently, the corona has developed into a complete discharge and was noticed at the gaps at the high voltage terminals (Figure 3.13). This could be due to the intense

ionization of the air at the wire gaps. The discharge had a frequency of 25 kHz with a maximum measured current of 1.8 A.

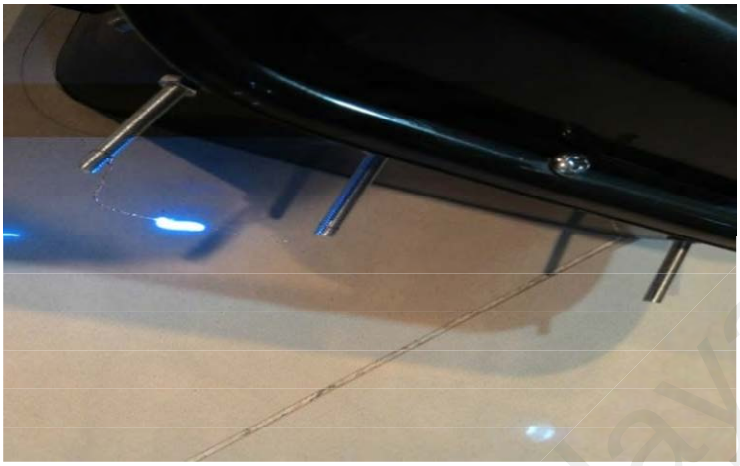

**Figure 3.13: Direct spark**

Then, a spark gap as in Figure 3.14 was constructed to create corona in transformer oil. The spark gap was made by using screws which were mounted on the wood which are commonly used inside the transformer. The transformer wood was treated with transformer oil at high temperature to release voids and other contaminants. The spark gap was placed inside the transformer oil (Figure 3.15), and the terminals were connected to the high voltage generator's terminals. The wires connecting the terminals were insulated with high tension tape.

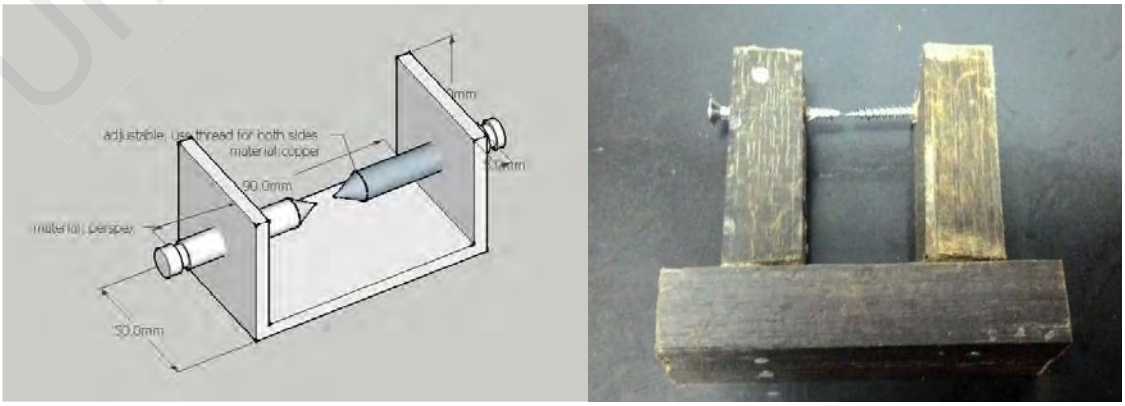


**Figure 3.14: Spark gap to generate discharge in oil**

The transformer oil that was used in the experiment had a breakdown voltage of more than 30 kV/mm, tested by using a spark gap. The spark gap was brought closer inside the transformer oil to create corona. The transformer oil is from the type of uninhibited mineral oil made from hydro-treated wax-free naphthenic oil. This type of treated oil is excellent as dielectric and well as coolant. The transformer oil conforms to the IEC 60296:2003 (Uninhibited), BS 148:1998 (Class 1) and MS 2322: 2010.

Figure 3.15 (a) and (b), show the partial discharge/corona in the oil under the light and dark, respectively. As can be seen, the corona in the oil created a discharge path with voids. These bubbles were gases produced from transformer oil decomposition due to the discharge. The corona occurred at a distance of 5 mm, and when the gaps reduced to 2 mm, a complete streamer discharge occurred.

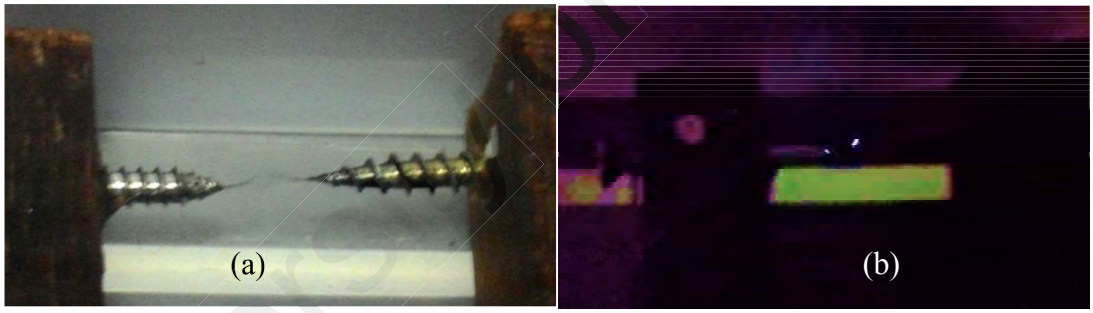


**Figure 3.15: Partial discharge in oil**

Figure 3.16 shows the bubbles produced after the discharge. These bubbles may contain traces of $H_2$, $CH_4$ and $C_2H_2$. All the gasses were tested by using the portable dissolved gas analyser. $H_2$, $CH_4$ and $C_2H_2$ are the key gasses for the electrical fault inside a transformer. The $H_2$ formed at low energy discharge whereas $C_2H_2$ formed at higher energy discharge.

**Figure 3.16: Bubbling in the oil**

The samples were tested consistently by using the portable dissolved gas analyser to obtain desired gas-in-oil content. Figure 3.17 shows the measured amount of dissolved hydrogen, methane and acetylene for every ½ hour of partial discharge for a period of 6 hours. Meanwhile, Figure 3.18 shows the measured amount of dissolved hydrogen, methane and acetylene for every ½ hour of arcing for a period of 6 hours. The oil samples were collected at the predefined interval for validation purpose.

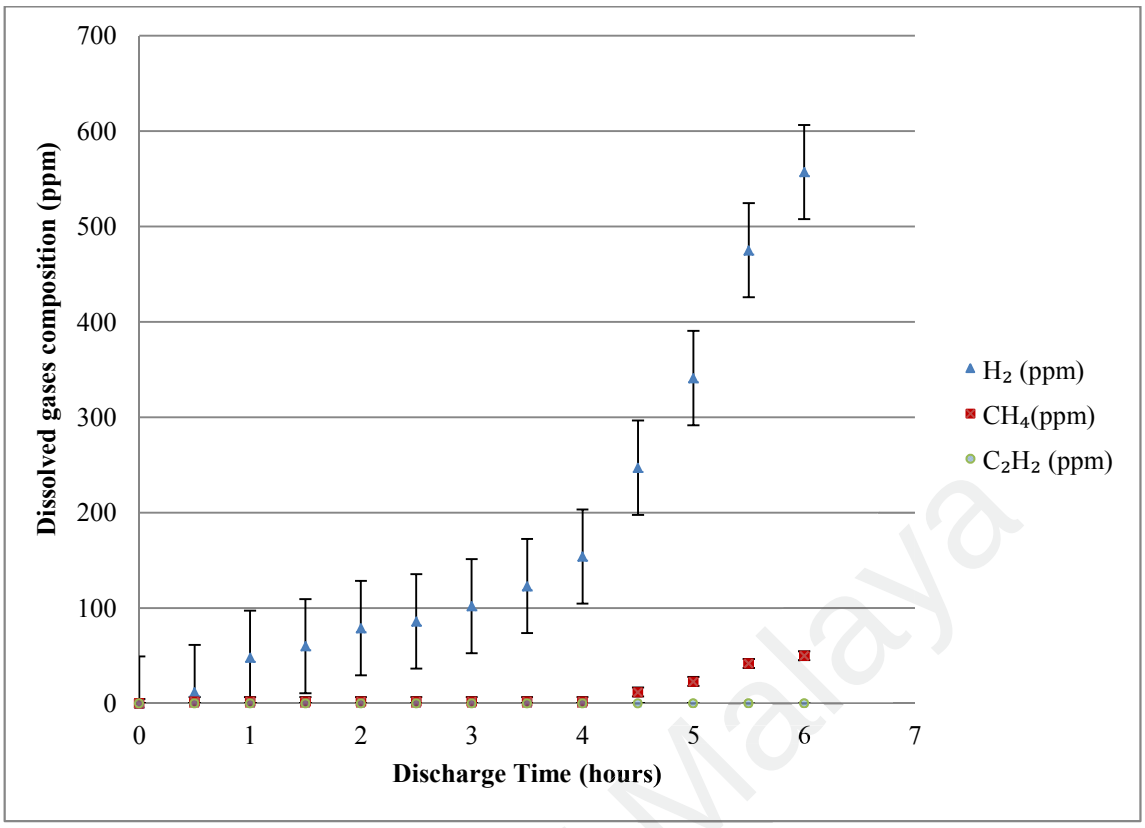


**Figure 3.17: Dissolved gases composition for partial discharge**

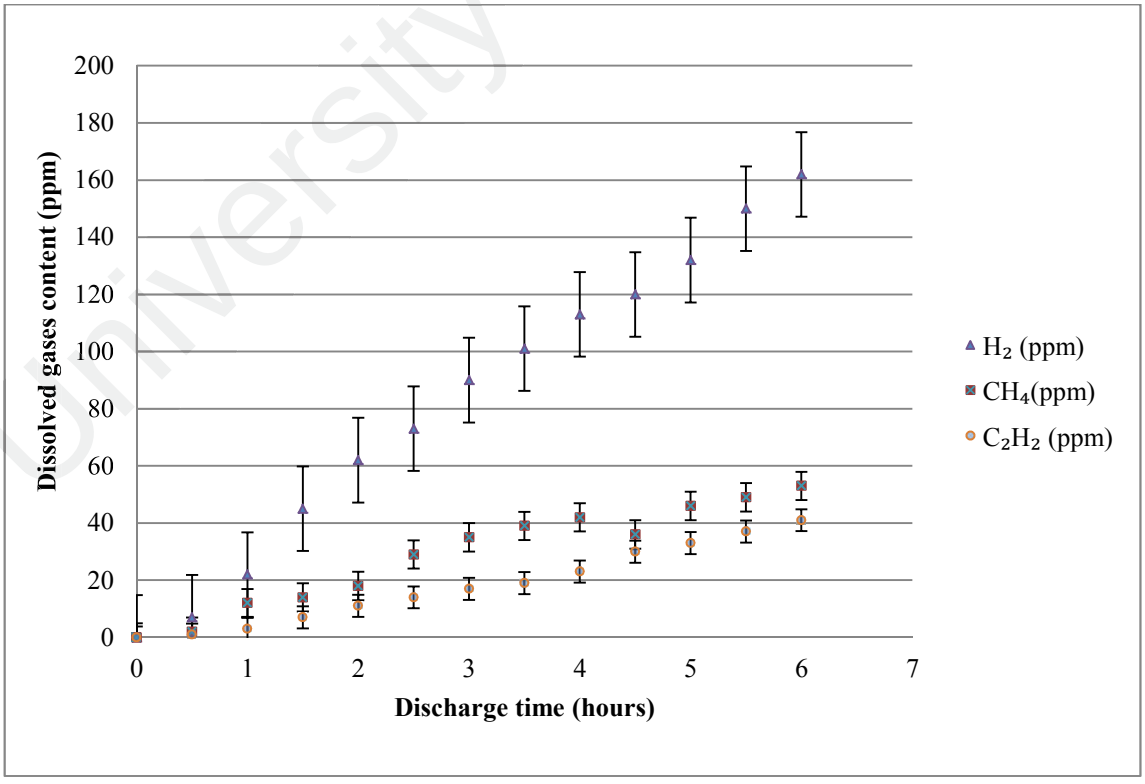


**Figure 3.18: Dissolved gases composition for arcing**

## 3.7 Design of the sensor case

The sensor case was designed to protect the FBG from mechanical stress while handling. The casing was made of aluminium rod with a resin filler. The fiber joints were placed inside the rod and filled with resin for mechanical protection. The tip of the sensor contained the coated FBG. The tip was placed inside a perforated tube for oil circulation purpose during testing. Figure 3.19 shows the sensor case design and the actual sensor. All the sensors were kept inside a plastic container and placed inside a lab with controlled temperature (25°C) and relative humidity (40%-70%).

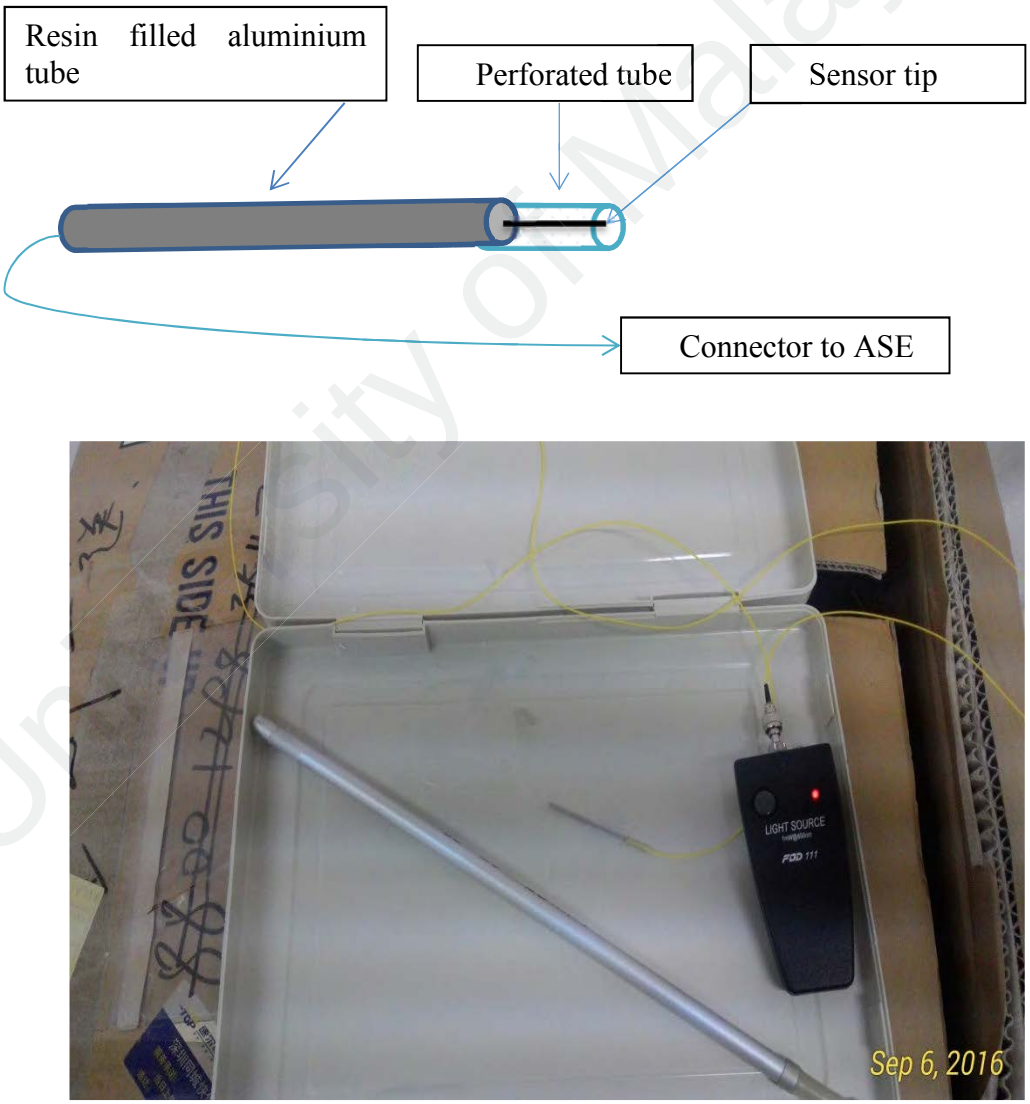


**Figure 3.19: Sensor case**

## 3.8 Experimental setup to measure the wavelength shift

Once the oil samples were ready, the FBG sensors were connected to an amplified spontaneous emission (ASE) source, FBG analyzer and a computer (Figure 3.20). The initial center wavelength for all the sensors was recorded with the temperature compensation. For each test, the readings were taken after the wavelength shift stabilized. The setup was done inside the IEC 17025 lab with controlled temperature and humidity. In addition, a bare FBG was placed for temperature correction.

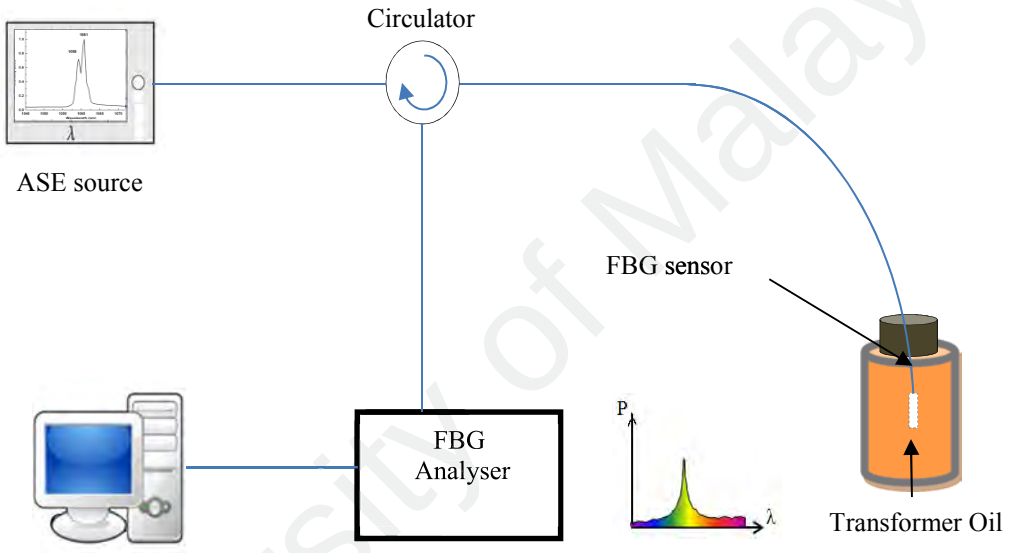


**Figure 3.20: FBG experimental setup for wavelength shift measurement**

## 3.9 Evaluation of the sensors against oil pressure (depth), voltage potential and electromagnetic flux

All the sensors were tested against oil pressure, voltage potential and electromagnetic flux. The evaluations of the sensor's response were done to study and establish boundary condition that could be contributed by oil pressure, voltage and electromagnetic flux in this work. First, the sensors were tested against the pressure inside the oil. The sensor was placed at a predetermined depth inside the experimental

tank. The depth was varied from 0 cm to a maximum depth of 16 cm. In this experiment, new oil with 0 ppm of dissolved hydrogen was used. At 16 cm, a head pressure of 1396 Pa was calculated.

Then, the wavelength shift was recorded. Figure 3.21 shows the placement of the sensor inside the experimental tank. The sensor was supported by using synthetic clay. The sensors were moved slowly towards the bottom of the tank to measure the maximum oil pressure where FBG wavelength shift become saturated and to establish the operating limits.

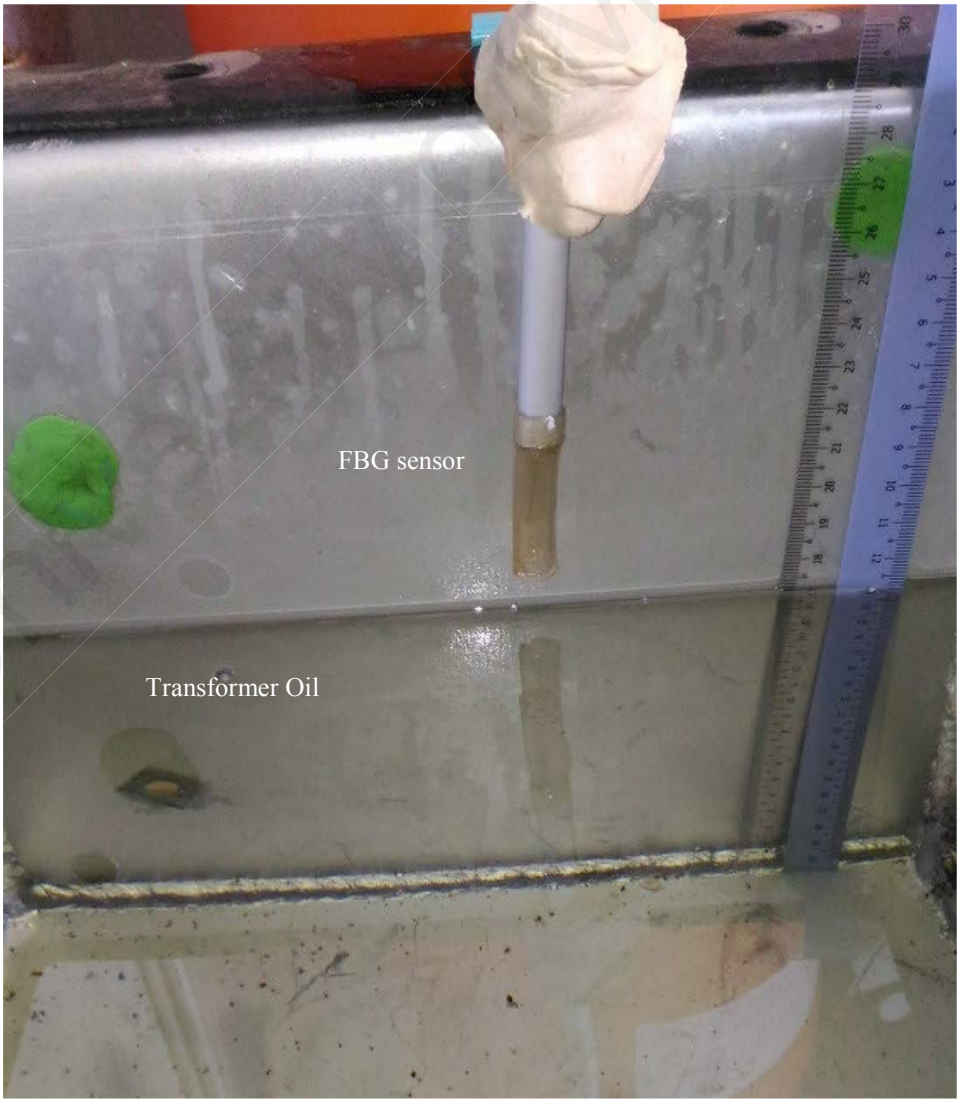


**Figure 3.21: Setup to measure the effect of oil pressure on the FBG**

Next, the sensors were tested again for the influence of voltage potential. This experiment was conducted in a controlled environment which has controlled temperature and humidity too. The sensor was put inside a beaker covered with aluminium foil (Figure 3.20) and was subjected voltage from 0 kV to 25 kV. At each 5 kV step, the wavelength shift was recorded. After each voltage injection, the aluminium foil was discharged to remove any floating charges.

Finally, all sensors were tested again for the influence of electromagnetic flux. The current coil was used to generate the electromagnetic flux across the FBG sensors. The injected current was from 0 mA to 3000 mA, and the wavelength shift was recorded.

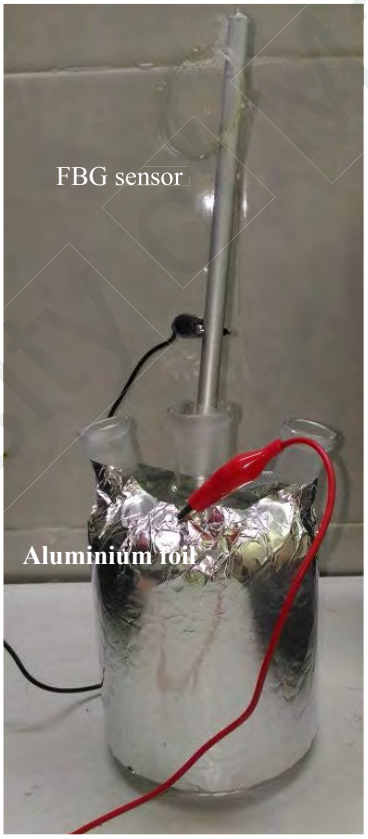


**Figure 3.22: Testing the sensor against potential voltage influence**

### 3.10 Testing of the 16 sensors with known hydrogen content and validation with hydrogen gas generated by partial discharge and previous research work

Once the oil samples were ready, the FBG sensors were connected to a broadband light source, an FBG analyzer and a computer as in Figure 3.20. Then, 4 samples with the same composition and different thicknesses were dipped into the new oil inside the Wolff bottle (Figure 3.23).

A bare FBG was placed alongside with the coated sensors for the temperature correction. It was started with a sample of 0 ppm of hydrogen. The 0 ppm sample was to obtain the baseline of wavelength shift of FBG sensors when it was placed inside transformer oil. Then, the oil was changed to the oil that contained 121 ppm, 243 ppm, 376 ppm, 427 ppm, 485 ppm, 515 ppm, 559 ppm and 683 ppm of dissolved hydrogen. At each oil replacement, the oil was tested for dissolved hydrogen by using the portable DGA analyzer.

At each hydrogen composition, the wavelength shift was recorded for all sensors. The test was repeated for all compositions. The experiment has been conducted inside a temperature (25°C) and relative humidity (40%-70%) controlled lab. The wavelength shifts were recorded 10 times per wavelength shift at a fixed interval of 10 minutes, and the average wavelength shift was calculated. Once all the sensors were tested with known hydrogen content, the correlation of the wavelength shift and the hydrogen content were established via curve fitting formula.

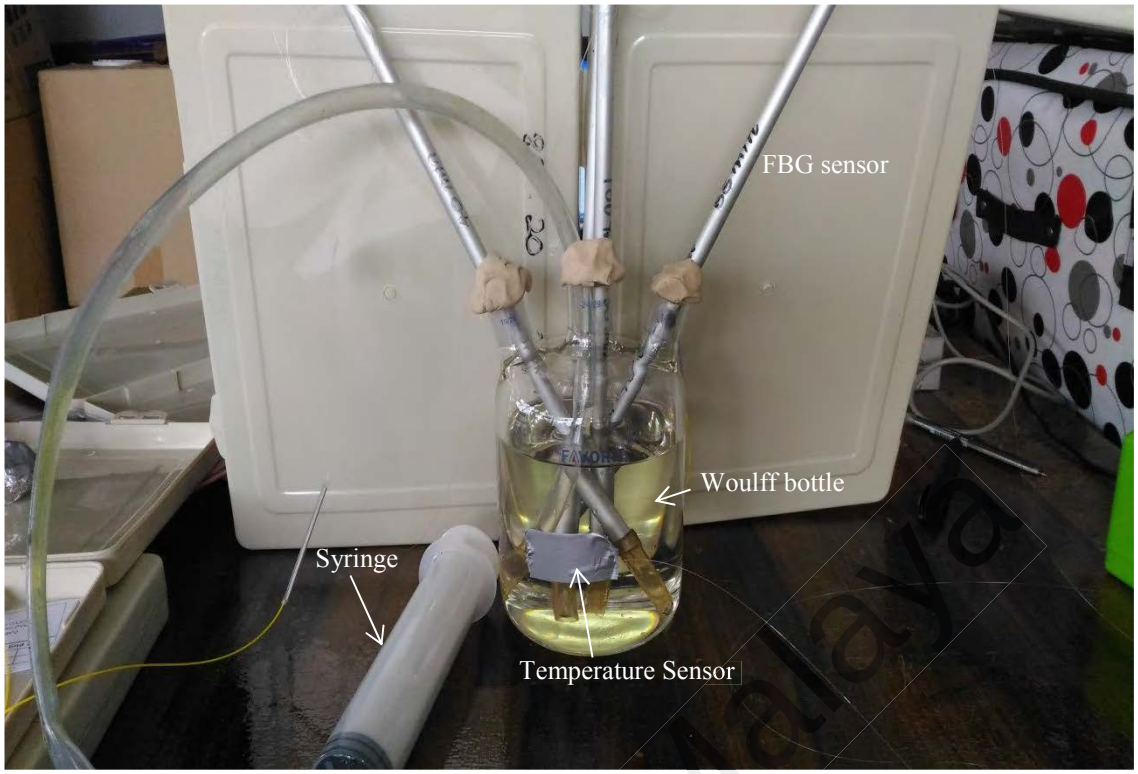


**Figure 3.23: Four sensors placed inside the known dissolved hydrogen content. Syringe to take the oil sample**

On the other hand, all sensors were tested in oil that was produced by partial discharge activity. Wavelength shifts were recorded for all sensors, and the hydrogen contents inside the oil samples were tested by using the gas chromatography method. The gas chromatography method is the most accurate method in measuring the dissolved gas in transformer oil (ASTM, 2009). The validation of the sensors was done by comparing the response of the sensor in the oil with the curve fit formula established earlier. In addition, the response of the sensor was compared with similar work done by (Jiang, 2014)

# CHAPTER 4: RESULTS AND DISCUSSIONS

The experiments were conducted as described in Chapter 3. The results of the experiments are discussed in this chapter. Sensors developed in this study were tested with transformer oil with known dissolved hydrogen quantity. All the experiments were conducted inside an IEC 17025 certified lab which has controlled temperature and humidity. Reference wavelengths (zeroing) of each sensors were obtained from the sensor by dipping all the sensors inside the transformer oil with 0 ppm of hydrogen content. After each test, the sensors were dipped again inside the transformer oil to ensure their repeatability. All the wavelength shifts were temperature corrected to 25°C.

## 4.1 Hydrogen gas release rate from transformer oil

The hydrogen gas was diffused in transformer oil inside the tank and was exposed to the environment. This was to study the gas release rate from the transformer oil. Figure 4.1 shows the hydrogen release rate of exposed hydrogen oil. After 600 ppm, the hydrogen release rate was slower compared to above 600 ppm. This figure was helpful in deciding the right intervals for oil samples extraction for future testing. Oil samples were taken at the right intervals and stored inside sealed bottles for subsequent experiments. The dissolved hydrogen gas amount was measured and the samples were labelled as 121 ppm, 243 ppm, 376 ppm, 427 ppm, 485 ppm, 515 ppm, 559 ppm, and 683 ppm according to the gas concentrations. The error of the measurement was recorded ±2%. All the oil samples were tested before the experiment. This method was used by (Bodzenta et al., 2002) for an experiment to diffuse the hydrogen gas inside the transformer oil. Although the absorption of the hydrogen in the transformer oil was dependent on the amount of dissolved oxygen as reported in (Pavlovsky, 2008) but it

was beyond the scope of the study. The main aim of diffusing hydrogen gas into the oil was to produce traceable gas-in-oil samples for the sensing experiments.

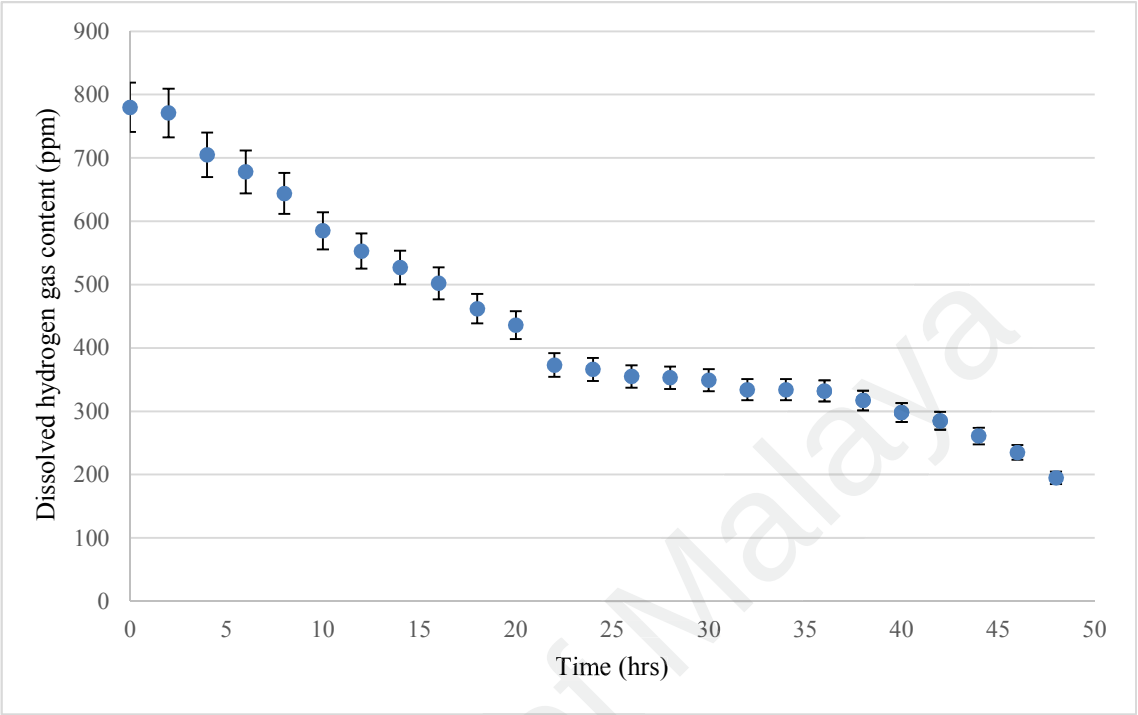


**Figure 4.1: Hydrogen gas release rate**

## 4.2 Wavelength shift against voltage, oil pressure (depth) and electromagnetic flux

Figure 4.2 shows the wavelength shift against voltage exposed to the FBG. A voltage up to 25 kV did not cause any wavelength shift. In addition, Figure 4.3 shows the wavelength shift against electromagnetic flux. There was a wavelength shift noticed at the higher current but this was due to the heat generated by the current in the current transformer. The exact flux was not measured in this experiment because of the measurement equipment limitation. Overall, the effect of wavelength shift conformed to the principle of FBG where its immuned to electromagnetic radiation(A. D. Kersey, 1997).

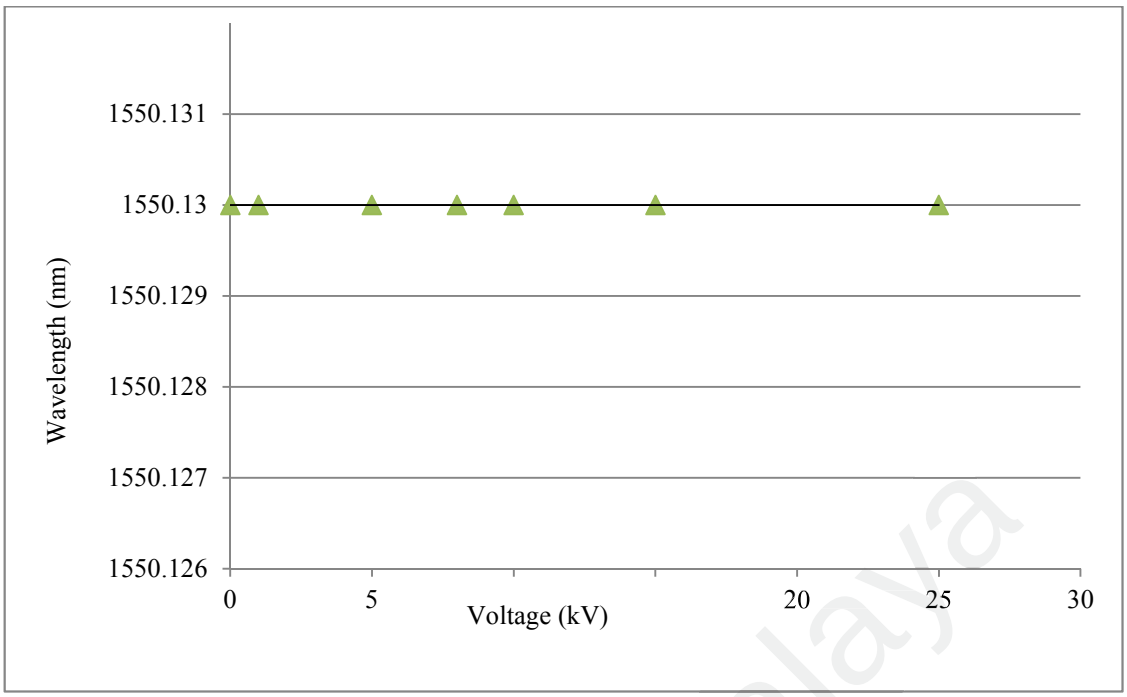


**Figure 4.2: FBG wavelength with respect to voltage**

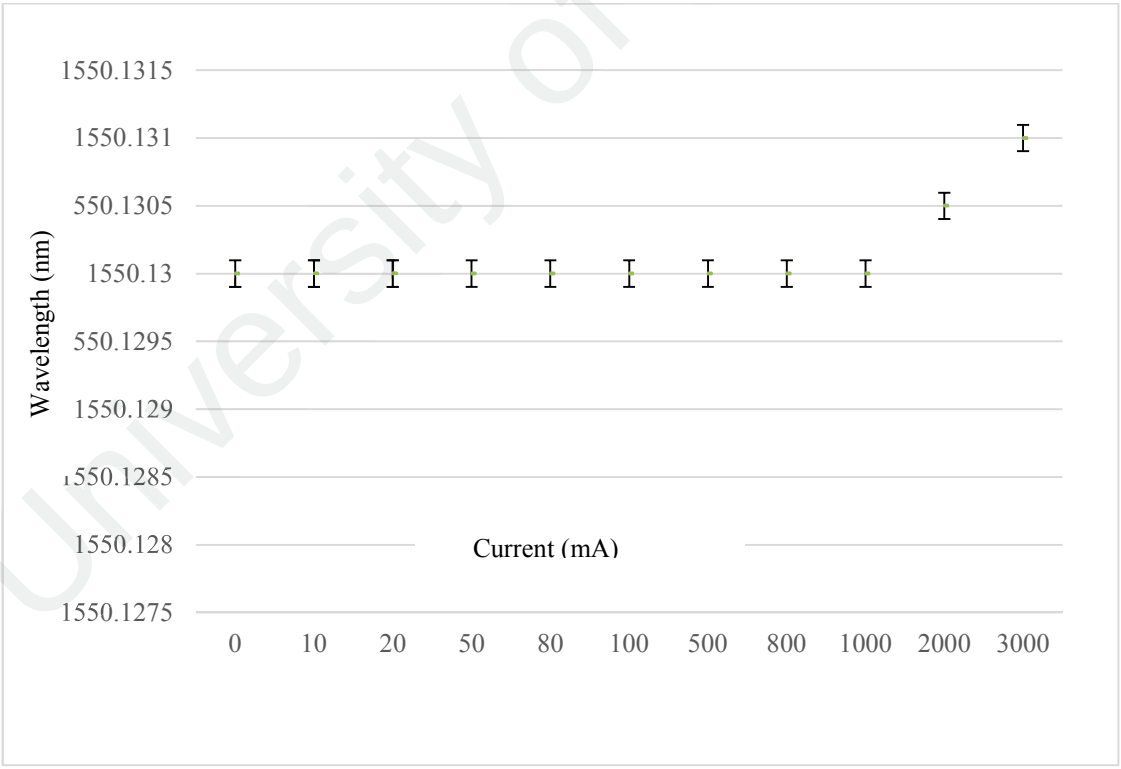


**Figure 4.3: FBG wavelength with respect to electromagnetic flux**

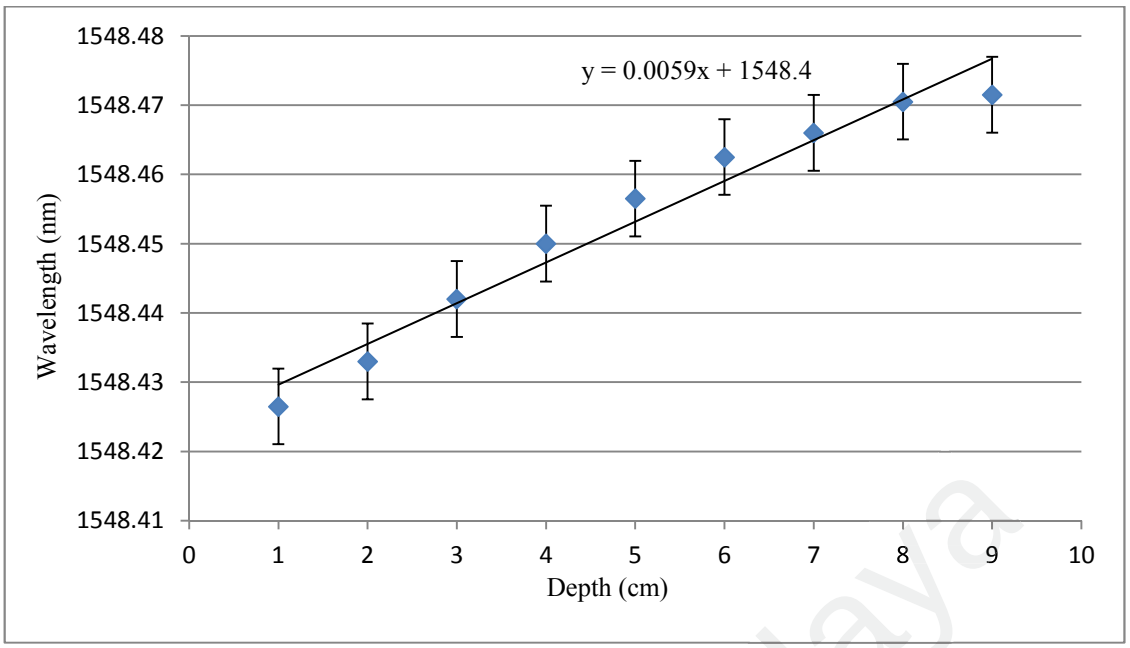


**Figure 4.4: FBG wavelength with respect to the depth of sensor in the transformer oil**

On the other hand, the FBG showed an insignificant wavelength shift when brought deeper inside the oil (Figure 4.4). The calculated oil pressure at the bottom of the tank was 1396 Pa. Meanwhile, the wavelength shift that was measured was 5.9 pm/cm or 50 pm/kPa. In the recent study by (Lim, 2019), a wavelength shift of 117.7 pm/kPa was reported for FBG exposed to pressure. However, the latter has affirmed that the wavelength shift due to pressure change in oil of 16 cm depth yielded no significant information on the placement of the sensor inside the test tank for this work. Therefore, the experiments were conducted at fixed depth of 4 cm to maintain consistency.

## 4.3 Assessment on the $TiO_2$ coating

The inspection of the $TiO_2$ coating which was immersed in the mineral oil was done once every two days. The inspection was done by using a microscope. Figure 4.5 shows the $TiO_2$ on the test fiber before immersing in heated transformer oil for 40 days. The coating was smooth and there was no sign of uneven thickness or breakage. The

thickness of the coating was 80 nm±10%. The transformer oil used has the specification as mentioned in Chapter 1.

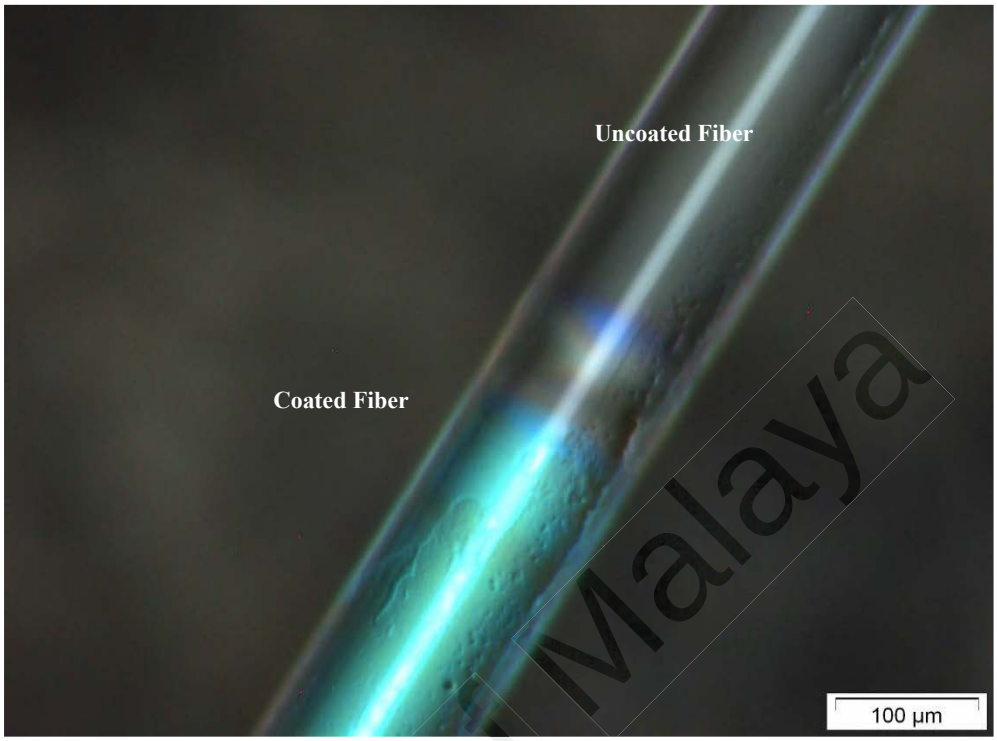


**Figure 4.5: $TiO_2$ coating (blue color) before immersing in transformer oil**

After 40 days of aging inside transformer oil, the coating was inspected again (Figure 4.6). Some discoloration spots on the surface of the titanium were observed. This could be due to the oxidation because of the presence of dissolved oxygen inside the transformer oil. However, a closer inspection at the edge of the coating showed no signs of peeling or micro-cracking after 40 days. This has confirmed that the $TiO_2$ coating adhered to the fiber well although no polyimide layer was used as done by (Ma et al., 2012). This has confirmed that the $TiO_2$ coating on the fiber can be used as the adhesive material between palladium and FBG and the $TiO_2$ coating did not react with transformer oil and degraded after 40 days of exposure.

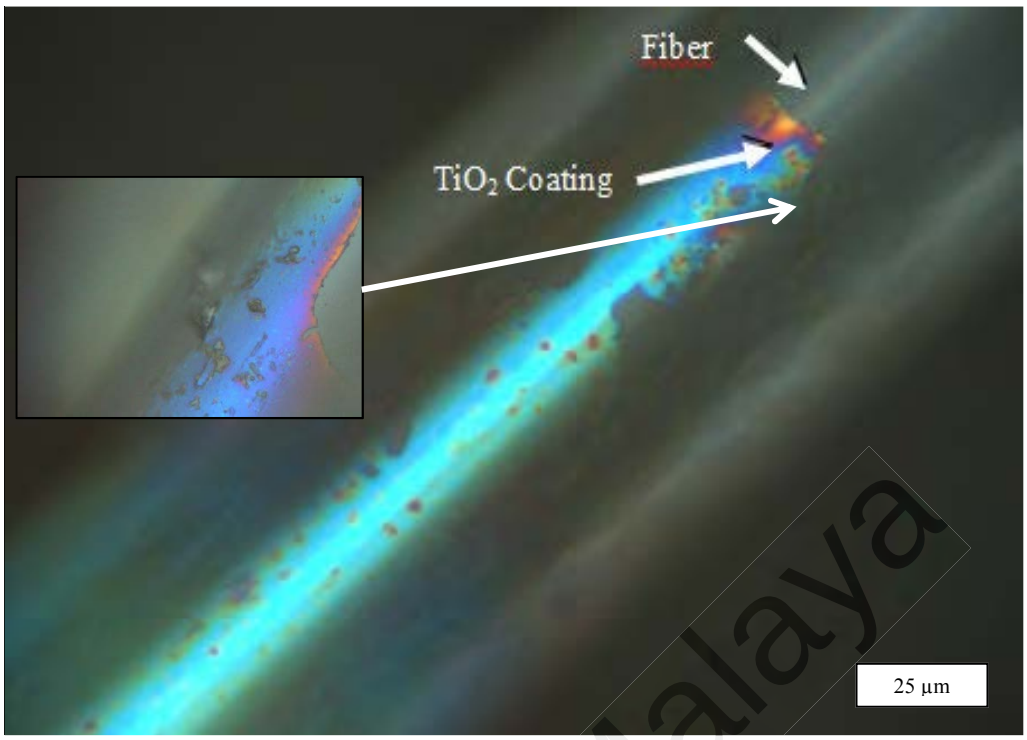


**Figure 4.6: $TiO_2$ coating after 40 days immersed in the transformer oil. Closer examination on the surface(inset).**

## 4.4 Assessment of the Pd-Cr coating before and after experiments

The palladium-chromium coating on the FBG was inspected by using SEM-EDX method before and after the experiments. Figure 4.7 shows the coating before and after the experiments for palladium-chromium alloy coating.

However, the coating of 100% Pd showed micro-cracking after the experiments (Figure 4.8). This is a clear sign that the coating of pure Pd on the $TiO_2$ is not suitable to be used for transformer gas-in-oil detection. In addition, the coating cracked and did not peel-off. This may due to $TiO_2$ coating on the FBG has prevented the peeling off of palladium layer during α-β phase transition (B. Sutapun, 1999).

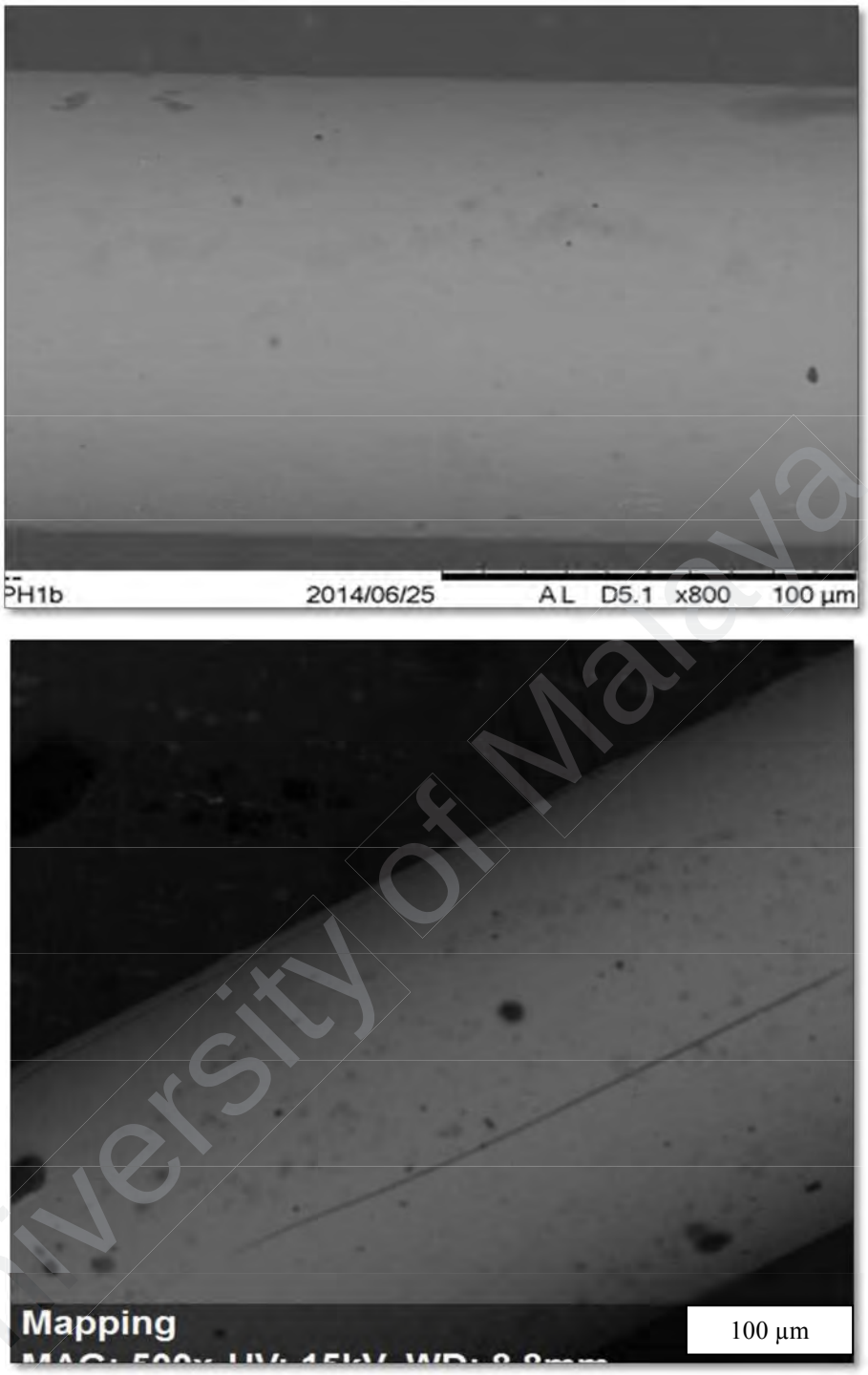


**Figure 4.7: Coating surface before (top) and after (bottom) experiments**

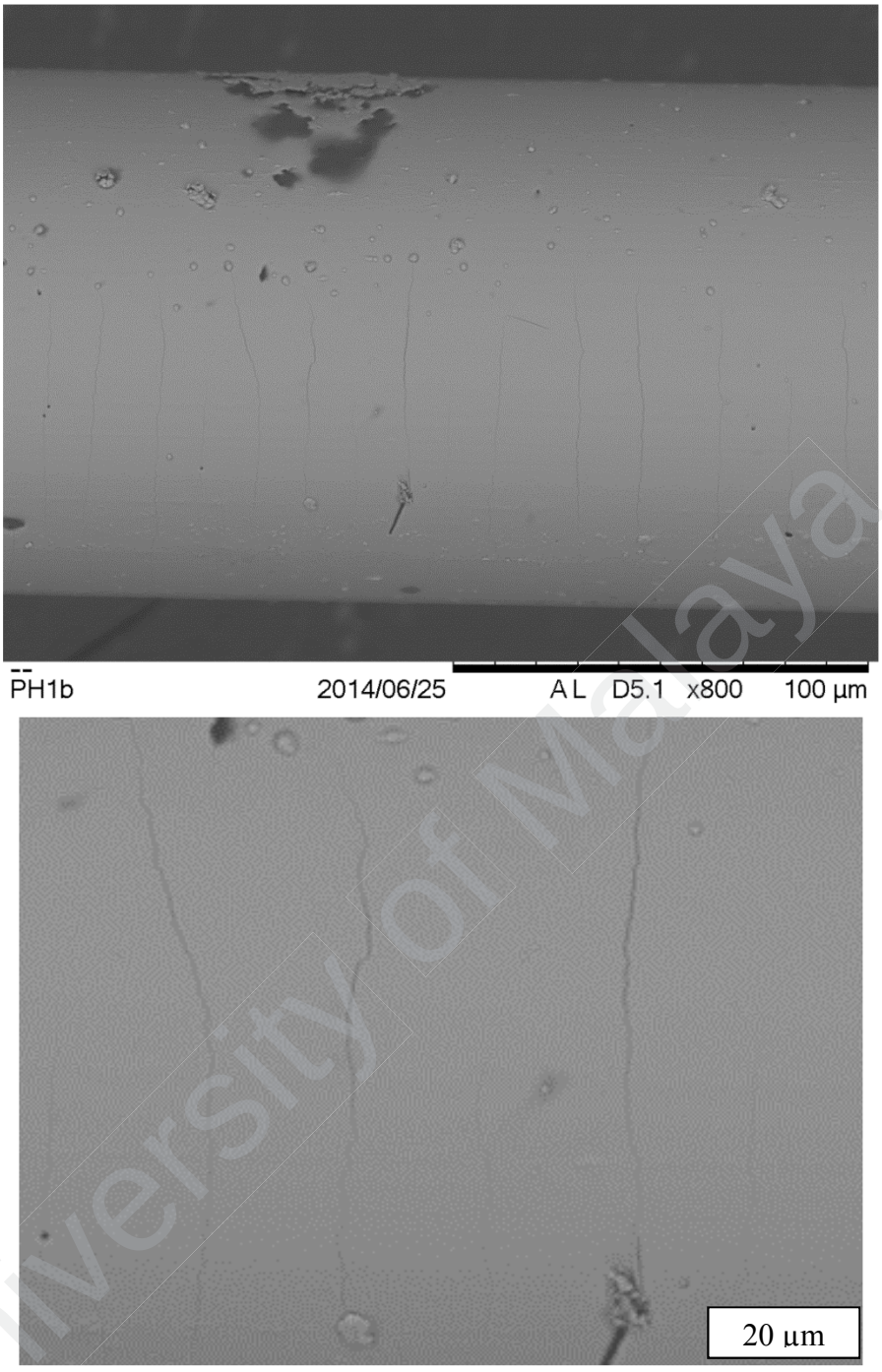


**Figure 4.8: Surface of the 100% palladium coated sensor after test (top) and detailed micro-cracking surface (bottom)**

This confirmed that by allowing palladium to mix with other material such as Ag, Au, Mg, Pt and Ni, the structure of the palladium was still intact after it was exposed to transformer oil (Dai, Yang, Yu, Cao, & Liao, 2012). This coincides with the findings in

this work, where addition of Cr has increased the sensor coating quality and measurability.

In addition, average thickness of the coatings and the percentage composition were determined. Table 4.1 shows the average thicknesses and composition of the developed sensor. The coating thickness was measured by breaking the coating and measuring a few edges of breakage (Figure 4.9). The measurement of the coating thickness is a destructible measurement where the sensor could not be used after the test. However, since four samples were coated per sensor, there was no shortage of sensor for the SEM-EDX measurement. Coating thickness variation of maximum ±10nm was observed during the measurement of the thickness by SEM method.

**Table 4.1: Sensor coating thicknesses and compositions**

| Sensor | Average coating thickness (nm) | Composition (%) | |
|---|---|---|---|
| | | Pd | Cr |
| 1 | 970±10nm | 100 | 0 |
| 2 | | 88 | 12 |
| 3 | | 75 | 25 |
| 4 | | 67 | 33 |
| 5 | 1060±10nm | 100 | 0 |
| 6 | | 88 | 12 |
| 7 | | 75 | 25 |
| 8 | | 67 | 33 |
| 9 | 1180±10nm | 100 | 0 |
| 10 | | 88 | 12 |
| 11 | | 75 | 25 |
| 12 | | 67 | 33 |
| 13 | 1300±10nm | 100 | 0 |
| 14 | | 88 | 12 |
| 15 | | 75 | 25 |
| 16 | | 67 | 33 |


**Figure 4.9: Thickness measurement of the 970 nm coating**

The cross-sectional area of the coating showed uniform distribution of the Pd-Cr material. There were no voids seen inside the coating. Figure 4.10 shows the EDX measurement done on 100% palladium sensor (sensor 1, sensor 5, sensor 9 and sensor 13).

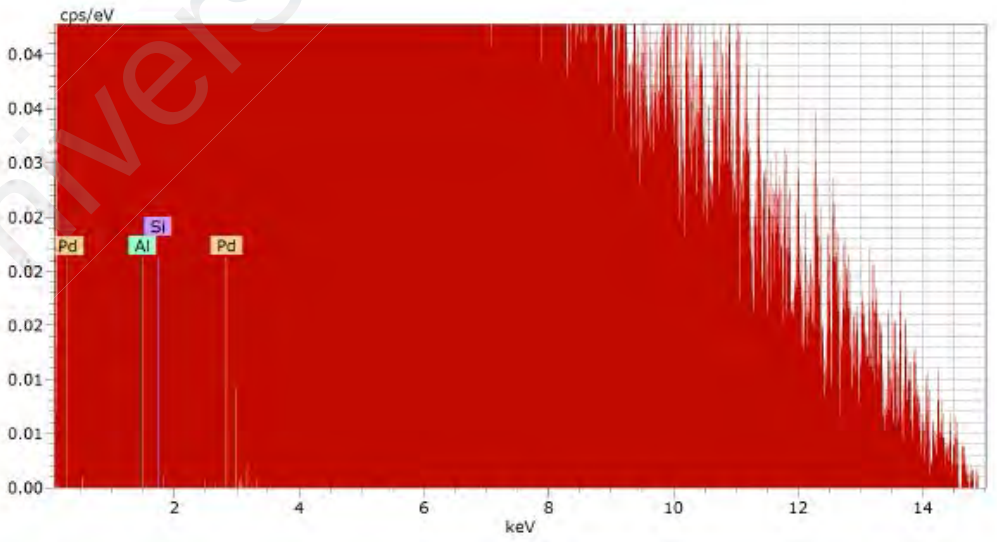


**Figure 4.10: Measurement of composition of the sensors with 100% Pd coating**

It was noticed that there are the presence of silicon and aluminum during the measurement. This was because the base material of the FBG is silicon and it is doped with either germanium oxide ($GeO_2$), aluminum oxide ($Al_2O_3$) or boron trioxide ($B_2O_3$) to alter the refractive index (Kashyap, 1999). In addition, the special holder used inside the EDX machine was made of aluminum too. The aluminum holder was required to support the coated FBG inside vertically the EDX machine. The measurement of metal composition was repeated by using bare fiber without the aluminum holder and only silicon was detected. Therefore, it was suspected that the EDX machine has captured aluminum from the special holder inside the EDX machine and the subsequent measurements, the readings for silicon and aluminum were ignored.

### 4.5 Assessment of the sensors

The detection principle of developed sensor was based on physical change due to chemical reaction of hydrogen sensitive palladium metal. All the sensors were tested with dissolved hydrogen gas inside the transformer oil. The test started with 970 nm coating thickness sensors with different compositions of palladium and chromium (sensor 1, sensor 2, sensor 3 and sensor 4). The wavelength shift was captured at different dissolved hydrogen content. The response time was not captured but it was noticed that the sensor's response stabilized after 10 minutes. Since the sensors were developed for hermetically sealed transformer, response time of 10 minutes is acceptable. This is comparatively faster response compared to commercially available gas-in-oil measurement equipment which takes around 10-60 minutes depending on measurement principle. The latter also uses averaging algorithm to estimate the total quantity of dissolved gasses in the transformer. Therefore, in this study, the response time of 10 minutes is considered good for practical applications.

At coating thickness of 970 nm (Figure 4.11), sensor 1 showed a greater wavelength shift of 0.0289 nm when it was exposed to hydrogen content of 243 ppm. After 243 ppm, sensor 1 did not show any wavelength shift although the hydrogen content was increased to 683 ppm. Sensor 1, which had 100% Pd has showed greater sensitivity at lower hydrogen content. The wavelength shift of sensor 1 could be estimated by using Equation 4.1. All the equations presented in this chapter were temperature corrected as discussed in Chapter 2.

$$\Delta\lambda = -(2.064\text{E}-13)x^4 + (6.291\text{E}-10)x^3 - (6.009\text{E}-07)x^2 + (2.268\text{E}-04)x - (1.49\text{E}-04) \quad (4.1)$$

where $\Delta\lambda$ is the wavelength shift (nm) and $x$ is the hydrogen content (ppm).

Sensor 2 (88% Pd) showed wavelength shift of 0.0254 nm when it was exposed to hydrogen content of 427 ppm. After 427 ppm, sensor 2 saturated and there was no wavelength shift observed. The response of sensor 2 was almost similar to sensor 1 but the wavelength shift was smaller. This could be due to the presence of chromium particles inside the coating. The wavelength shift was distributed between 0 ppm to 427 ppm. The response of the sensor with hydrogen can be correlated by 4$^{th}$ order polynomial as below as in Equation 4.2. This equation lies between the error ranges of the detection.

$$\Delta\lambda = -(5.462\text{E}-13)x^4 + (.9.7171\text{E}-10)x^3 - (6.391\text{E}-07)x^2 + (1.954\text{E}-04)x - (1.425\text{E}-04) \quad (4.2)$$

where $\Delta\lambda$ is the wavelength shift (nm) and $x$ is the hydrogen content (ppm).

On the other hand, sensor 3 (75% Pd) showed almost linear pattern of response up to 559 ppm. The wavelength shift at 121 ppm is 0.0021 nm and it was lower than sensor 4 wavelength shift (0.003 nm). It was expected that the wavelength shift of sensor 3 at 121 ppm to be higher than sensor 4. However, this could be due to measurement

uncertainty during the experiment and the values did not differ much. Equation 4.3 shows the wavelength shift of sensor 3 with respect to hydrogen content.

$$\Delta\lambda = (1.447\text{E}-13)x^4 + (3.634\text{E}-10)x^3 - (2.338\text{E}-07)x^2 - (1.43\text{E}-07)x + (1.297\text{E}-4) \quad (4.3)$$

where $\Delta\lambda$ is the wavelength shift (nm) and $x$ is the hydrogen content (ppm).

Wavelength shift of sensor 3 after 121 ppm was always higher than sensor 4. In addition, sensor 3 become saturated after 559 ppm. On the other hand, sensor 4 showed consistent wavelength shift of 0.003 nm at 121 ppm, 0.0045 nm at 243 ppm, 0.00505 nm at 376 ppm, 0.00563 nm at 427 ppm, 0.00694 nm at 483 ppm, 0.00751 nm at 515 ppm, 0.0835 nm at 559 ppm and 0.00934 nm at 683 ppm.

Sensor 4 did not show any saturation although the hydrogen content was increased to 683 ppm. For hermetically sealed transformer, hydrogen content of 100 ppm was considered alarming. However, the materials used inside the transformer could increase the hydrogen up to a few thousands ppm during initial stage of operation. However, this hydrogen will get saturated inside the transformer oil later. Sensor 4 could serve the purpose of detecting higher range of hydrogen contents. Sensor 4 followed the 4$^{th}$ order equation as in Equation 4.4 respectively.

$$\Delta\lambda = -(3.109\text{E}-13)x^4 + (4.596\text{E}-10)x^3 - (2.181\text{E}-07)x^2 + (4.748\text{E}-05)x - (5.493\text{E}-05) \quad (4.4)$$

where $\Delta\lambda$ is the wavelength shift (nm) and $x$ is the hydrogen content (ppm).

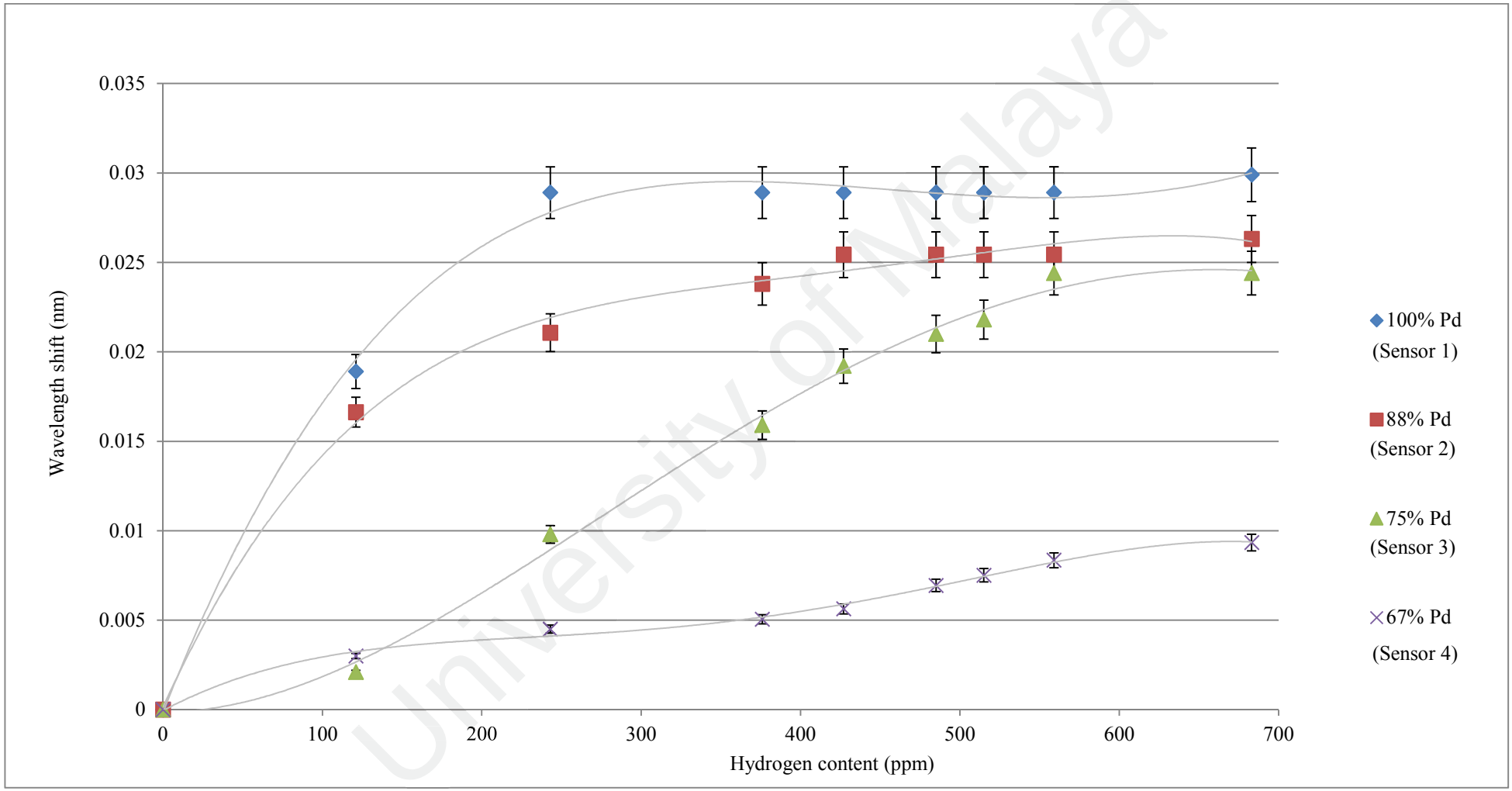


**Figure 4.11: Wavelength shift vs Pd-Cr Compositions (970nm)**

In addition, sensor 5 (100% Pd), sensor 6 (88% Pd), sensor 7 (75% Pd) and sensor 8 (67% Pd) were developed with average coating thickness of 1060 nm (Figure 4.12). Sensor 5 showed greater wavelength shift than sensor 6, sensor 7 and sensor 8. The wavelength shift before saturation was 0.039 nm. The saturation happened after hydrogen content of 427 ppm. Sensor 5 can be used to detect hydrogen up to 427 ppm. Sensor 5 confirms the curve fit equation as in Equation 4.5.

$$\Delta\lambda = -(4.335\text{E}-13)x^4 + (9.854\text{E}-10)x^3 - (8.2\text{E}-07)x^2 + (2.959\text{E}-04)x - (1.246\text{E}-04) \quad (4.5)$$

where $\Delta\lambda$ is the wavelength shift (nm) and $x$ is the hydrogen content (ppm).

On the other hand, sensor 6 reached saturation at hydrogen content lower than sensor 5 at 376 ppm. It could be the most sensitive sensor among the other sensors to detect below 376 ppm but the 4th order polynomial equation as in Equation 4.6 poorly fit to the sensor 6 response.

$$\Delta\lambda = -(5.332\text{E}-13)x^4 + (9.918\text{E}-10)x^3 - (7.143\text{E}-07)x^2 + (2.446\text{E}-04)x - (2.894\text{E}-04) \quad (4.6)$$

where $\Delta\lambda$ is the wavelength shift (nm) and $x$ is the hydrogen content (ppm).

The maximum error recorded by sensor 6 as shown in Table 4.4 was 8.93%. This error was lesser than the acceptable tolerance (10%) in this work, but it was relatively high compared to the other sensors. In addition, sensor 7 reached saturation at 559 ppm of hydrogen content and the effective wavelength shift was 0.02615 nm. The 4th order polynomial equation fits well to sensor 7 responses. The maximum error was 3.33% from Table 4.4. Sensor 7 responses fit in the Equation 4.7 well.

$$\Delta\lambda = -(5.021\text{E}-13)x^4 + (8.558\text{E}-10)x^3 - (5.439\text{E}-07)x^2 + (1.71\text{E}-04)x - (7.328\text{E}-05) \quad (4.7)$$

where $\Delta\lambda$ is the wavelength shift (nm) and $x$ is the hydrogen content (ppm).

In addition sensor 8 did not saturate although the dissolved hydrogen was increased to 683 ppm. The wavelength shift was small but it is better than sensor 4. This type of sensor could be used to detect hydrogen at higher concentration. This sensor had smaller wavelength shift. This is why it may not be applicable for smaller range data measurement application. Sensor 8 responses fit in the Equation 4.8 well.

$$\Delta\lambda = -(2.355\text{E}-13)x^4 + (3.599\text{E}-10)x^3 - (1.868\text{E}-07)x^2 + (4.815\text{E}-05)x - (7.14\text{E}-05) \quad (4.8)$$

where $\Delta\lambda$ is the wavelength shift (nm) and $x$ is the hydrogen content (ppm).

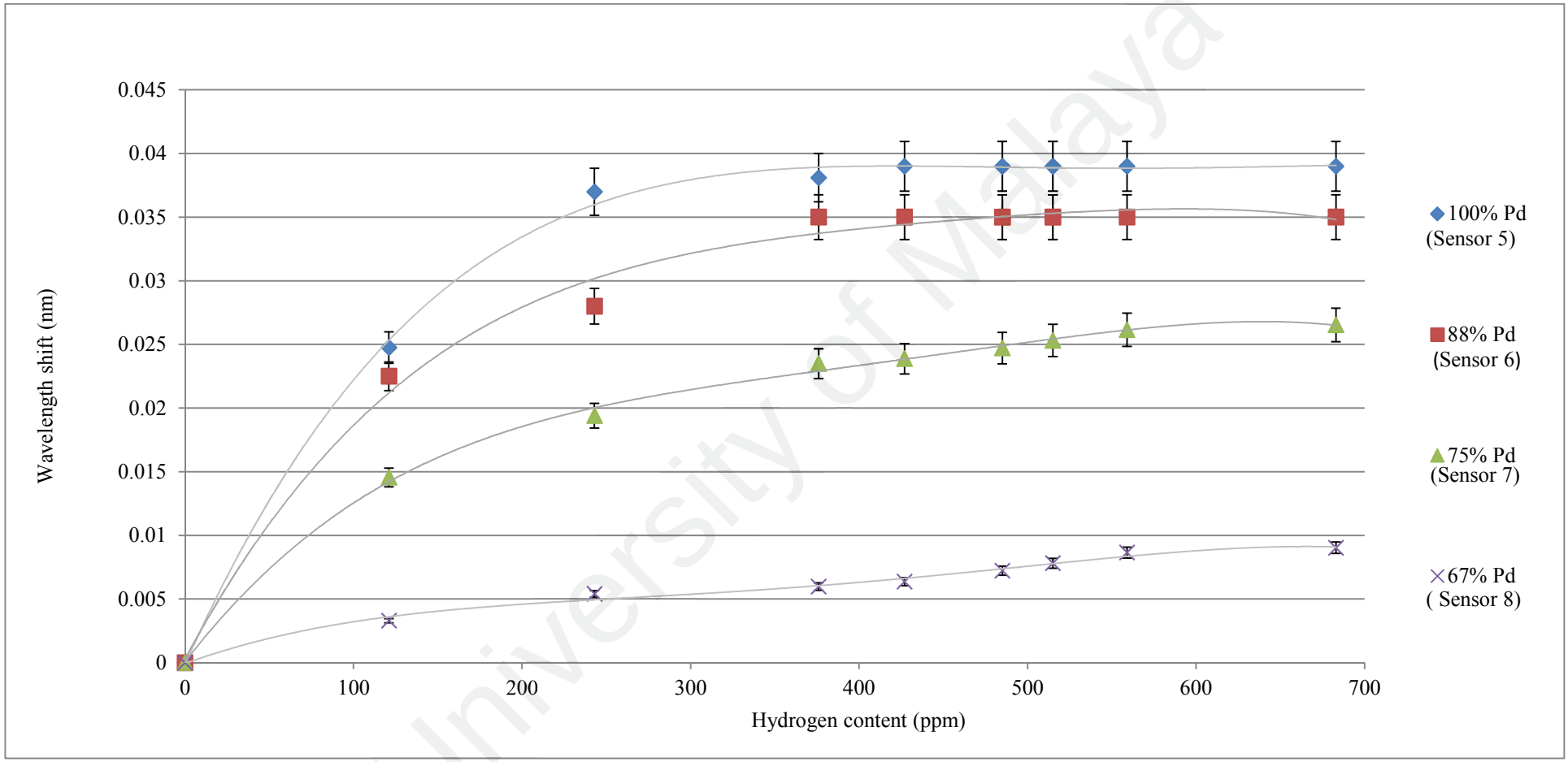


**Figure 4. 12: Wavelength shift vs Pd-Cr Compositions (1060nm)**

Sensor 9 (100% Pd), sensor 10 (88% Pd), sensor 11 (75% Pd) and sensor 12 (67% Pd) were coated with thickness of 1180 nm (Figure 4.13). Sensor 9 and sensor 10 saturated at 376 ppm of hydrogen content. The wavelength shift of sensor 9 and sensor 10 were considerably high which were 0.04105 nm and 0.03704 nm respectively. Both sensor 9 and sensor 10 showed similar pattern of response to the hydrogen. However, sensor 9 surface cracked as in Figure 4.7, therefore it could have limited application to be used in the field. Sensor 9 responses fit in the Equation 4.9 below.

$$\Delta\lambda = -(7.069\text{E}-13)x^4 + (1.428\text{E}-09)x^3 - (1.061\text{E}-06)x^2 + (3.44\text{E}-04)x - (2.216\text{E}-06) \quad (4.9)$$

where $\Delta\lambda$ is the wavelength shift (nm) and $x$ is the hydrogen content (ppm).

On the other hand, sensor 10 has the polynomial formula as in Equation 4.10.

$$\Delta\lambda = -(5.436\text{E}-13)x^4 + (1.145\text{E}-09)x^3 - (8.877\text{E}-07)x^2 + (2.996\text{E}-04)x - (2.44\text{E}-05) \quad (4.10)$$

where $\Delta\lambda$ is the wavelength shift (nm) and $x$ is the hydrogen content (ppm).. Sensor 10 did not show any signs of peeling off or cracking after the testing. Besides, sensor 11 became saturated at 485 ppm of hydrogen content with a wavelength shift of 0.0207 nm. After 485 ppm, the sensor did not show any wavelength shift. Since the temperature was controlled throughout the experiment, the wavelength shift was only expected from stress exerted on FBG by hydrogen-palladium reaction. Sensor 11 confirmed to the Equation 4.11 below.

$$\Delta\lambda = -(1.697\text{E}-13)x^4 + (2.675\text{E}-10)x^3 - (1.563\text{E}-07)x^2 + (4.906\text{E}-05)x - (1.753\text{E}-05) \quad (4.11)$$

where $\Delta\lambda$ is the wavelength shift (nm) and $x$ is the hydrogen content (ppm).. In addition, sensor 12, which had the least palladium content saturated at 559 ppm with a

wavelength shift of 0.0886 nm. This wavelength shift was lower than sensor 9, sensor 10 and sensor 11. It was suspected that the addition of chromium metal into the palladium has restricted the strain on the FBG and caused smaller wavelength shift. However, sensor 12 still had the potential of detecting dissolved hydrogen up to 559 ppm. Sensor 12 confirmed to the Equation 4.12 below.

$$\Delta\lambda = -(1.697\text{E}-13)x^4 + (2.675\text{E}-10)x^3 - (1.563\text{E}-07)x^2 + (4.906\text{E}-05)x - (1.753\text{E}-05) \quad (4.12)$$

where $\Delta\lambda$ is the wavelength shift (nm) and $x$ is the hydrogen content (ppm)..

Sensor 13 (100% Pd), sensor 14 (88% Pd), sensor 15 (75% Pd) and sensor 16 (67% Pd) were coated with thickness of 1300 nm (Figure 4.14). The coating thickness was 22% higher than the sensors coated with 1060 nm of palladium- chromium mixture. Sensor 13 saturated at 243 ppm where the wavelength shift was 0.0437 nm. In addition, sensor 14 saturated at 243 ppm too but the wavelength shift was lower than sensor 13 which was 0.0385 nm. Sensor 13 fit in the polynomial equation of 4$^{th}$ order as in Equation 4.13.

$$\Delta\lambda = -(6.989\text{E}-13)x^4 + (1.49\text{E}-09)x^3 - (1.15\text{E}-06)x^2 + (3.778\text{E}-04)x - (1.436\text{E}-04) \quad (4.13)$$

where $\Delta\lambda$ is the wavelength shift (nm) and $x$ is the hydrogen content (ppm). Sensor 14 fits in the polynomial equation of 4$^{th}$ order as in Equation 4.14.

$$\Delta\lambda = -(6.989\text{E}-13)x^4 + (1.49\text{E}-09)x^3 - (1.15\text{E}-06)x^2 + (3.778\text{E}-04)x - (1.436\text{E}-04) \quad (4.14)$$

where $\Delta\lambda$ is the wavelength shift (nm) and $x$ is the hydrogen content (ppm). However, both sensor 13 and sensor 14 had limitation up to 243 ppm of hydrogen in the oil.

Sensor 15 saturated at 515 ppm where the wavelength shift was 0.0263 nm. In addition, sensor 16 saturated at 515 ppm too but the wavelength shift was lower than sensor 15 which was 0.00886 nm. The wavelength shift of sensor 16 was the lowest compared to all the other sensors coated with 1300 nm of thickness. Sensor 15 fits in the polynomial equation of 6$^{th}$ order as in Equation 4.15.

$$\Delta\lambda = (5.51\text{E}-18)x^6 - (1.055\text{E}-14)x^5 + (7.292\text{E}-12)x^4 - (2.343\text{E}-09)x^3 + (4.034\text{E}-07)x^2 + (1.008\text{E}-05)x + (2.098\text{E}-06) \quad (4.15)$$

where $\Delta\lambda$ is the wavelength shift (nm) and $x$ is the hydrogen content (ppm). Sensor 16 fits in the polynomial equation of 4$^{th}$ order as in Equation 4.16.

$$\Delta\lambda = -(1.196\text{E}-13)x^4 + (2.214\text{E}-10)x^3 - (1.605\text{E}-07)x^2 + (5.739\text{E}-5)x - (7.738\text{E}-06) \quad (4.16)$$

where $\Delta\lambda$ is the wavelength shift (nm) and $x$ is the hydrogen content (ppm). However, both sensor 15 and sensor 16 had limitation up to 515 ppm of hydrogen in the oil. Furthermore, sensor 15 had more limitation because it required one to solve 6$^{th}$ order polynomial to obtain the estimation of dissolved hydrogen in the oil. This will require higher computational power.

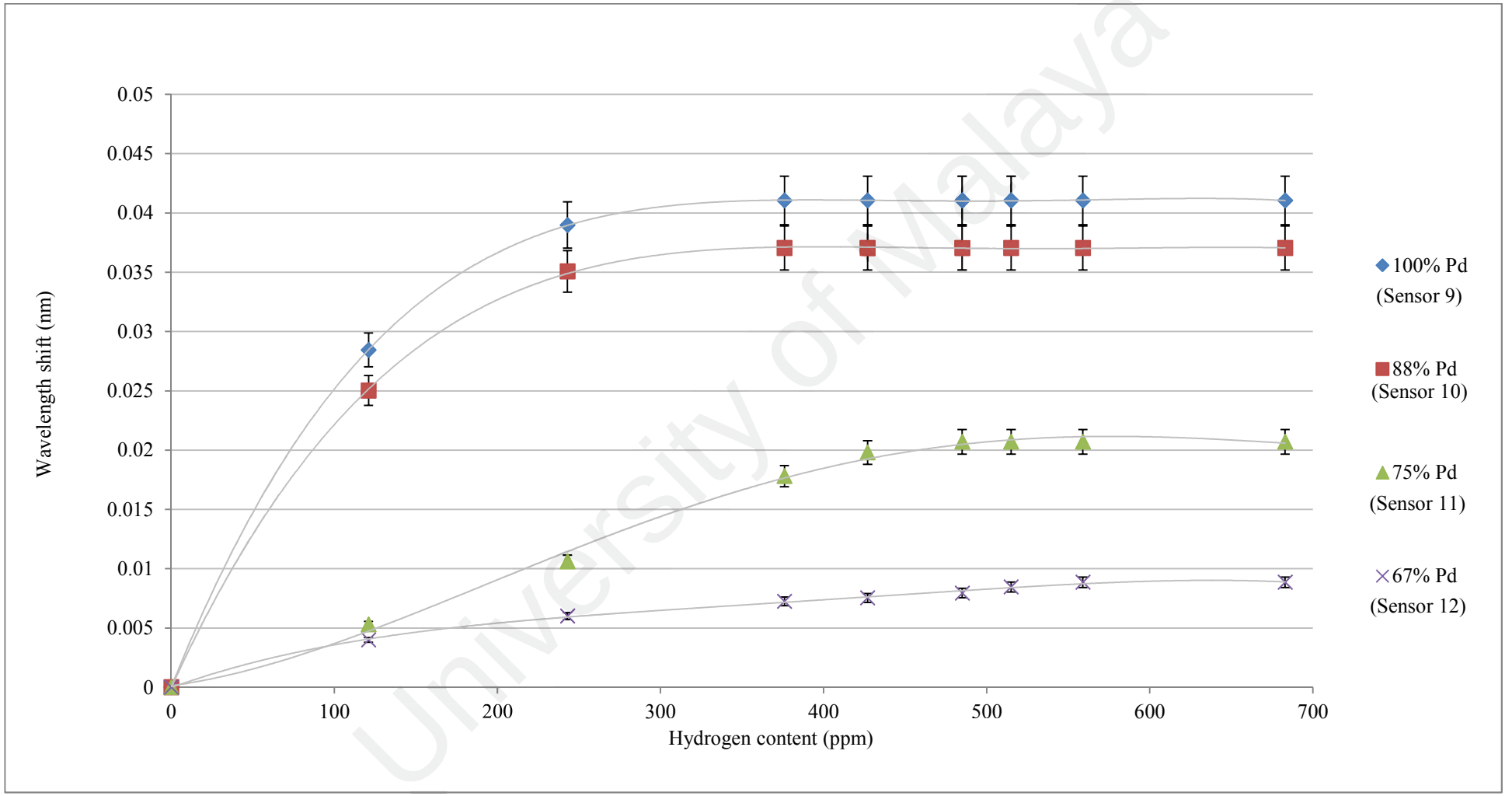


**Figure 4.13: Wavelength shift vs Pd-Cr Compositions (1180nm)**

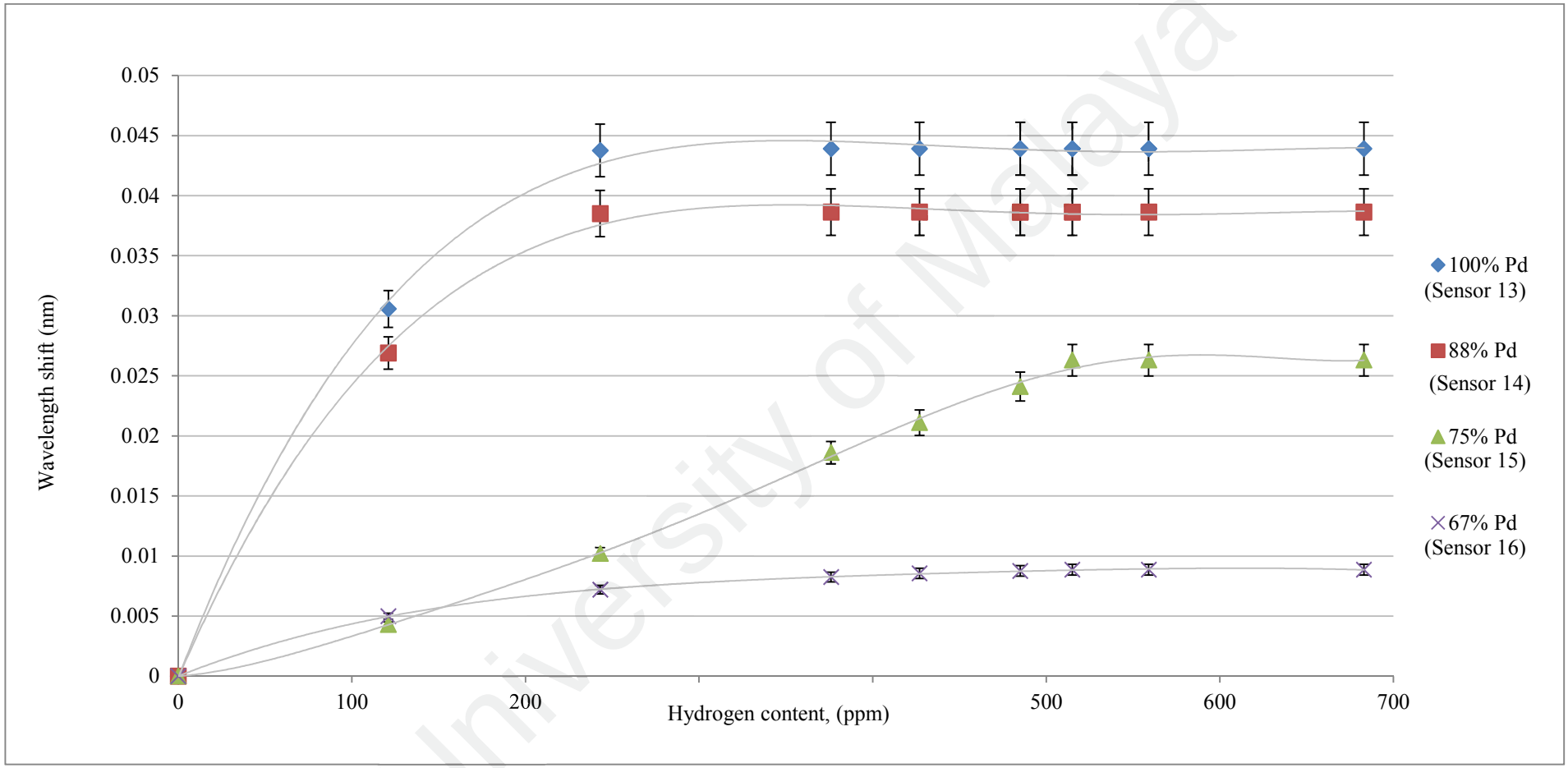


**Figure 4.14: Wavelength shift vs Pd-Cr Compositions (1300nm)**

Figure 4.15 shows the response of the 100% Pd sensors (sensor 1, sensor 5, sensor 9 and sensor 13) plotted based on the thickness of the coatings. It could be observed that sensor 1 and sensor 5 had saturated at 427 ppm of hydrogen content whereas sensor 9 and sensor 13 had saturated at 376 ppm of hydrogen content. Although these sensors showed higher wavelength shift than the other sensors with chromium mixture, it was still limited to range of detection and have problem with coating integrity after the testing.

It was noticed that sensors with 100% palladium coating experienced higher strain due to more palladium content. Palladium which reacted with hydrogen produced palladium hydride which was bigger in lattice size and caused strain on the FBG. Thicker palladium content exerts higher force on the FBG because more palladium hydride particles presented on the FBG. On the other hand, the FBG also exerted counter-force to retain the coating from expanding thus limiting the wavelength shift. This explained why the sensors with thicker palladium coating showed the largest wavelength shift compared to sensors with thinner palladium coatings. In addition, the presence of chromium limited the palladium expansion on the FBG resulting lower wavelength shift.

Although sensor 1, sensor 5, sensor 9 and sensor 13 had cracked and became unusable after the experiments, these sensors have the potential to be used to detect dissolved hydrogen gas within range of 0-250 ppm. However, this range is not sufficient for the monitoring of the transformer within "Condition 2" as in Table 3.6 and the scope of the study needs a sensor which has the uniform response up to 700 ppm of dissolved hydrogen content. On the other hand, these sensors may have the advantage of higher sensitivity and can operate in incremental hydrogen content detection. However, further

measurements are required within the range of 0-250 ppm to study the behaviour of coating and its sensitivity.

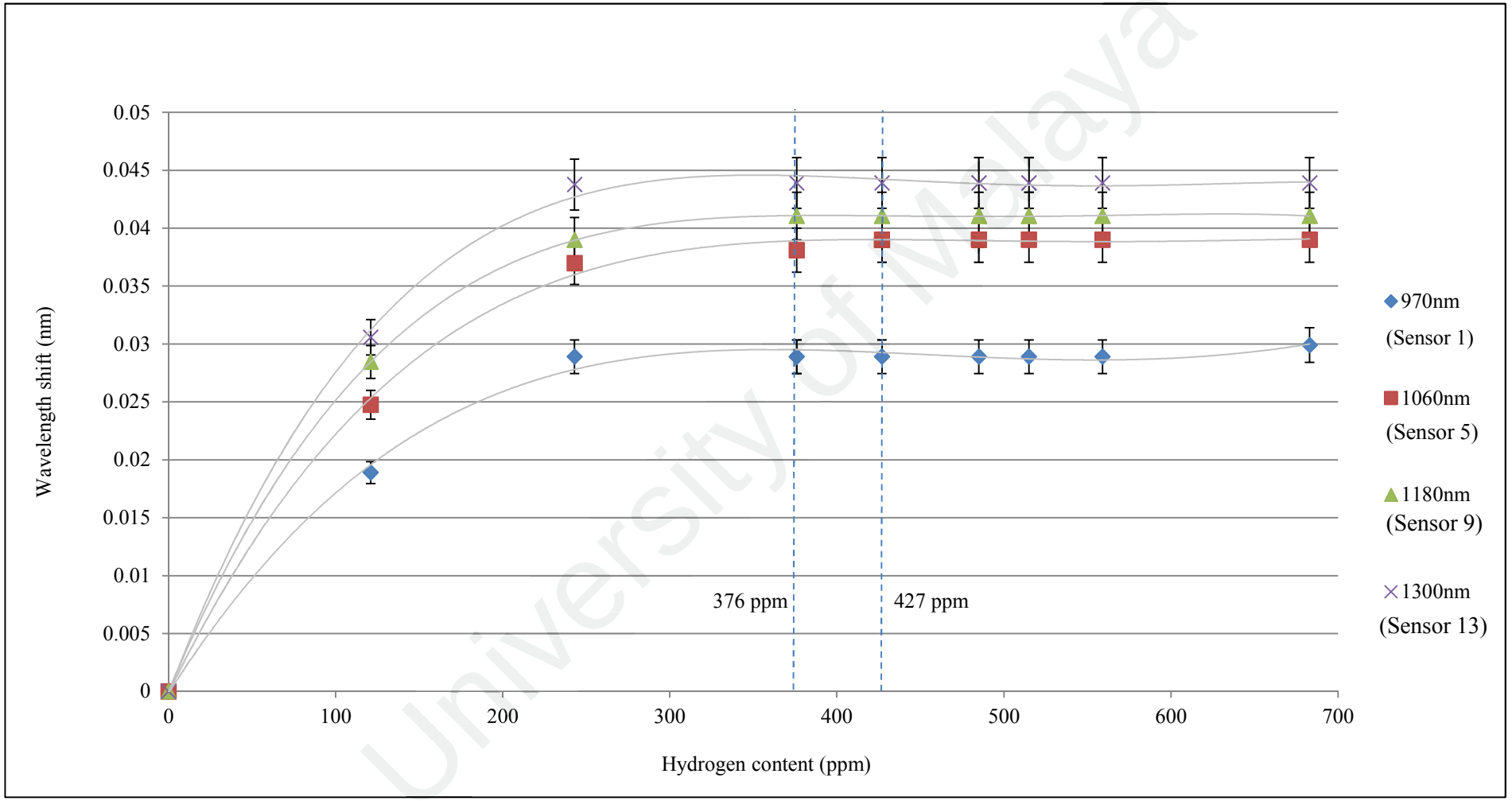


**Figure 4.15: Wavelength shift vs coating thickness (100% Pd)**

Figure 4.16 shows the response of the 88% Pd sensors (sensor 2, sensor 6, sensor 10 and sensor 14) plotted based on the thickness of the coatings. Sensor 6 and sensor 10 saturated at 376 ppm with wavelength shift of 0.035 nm and 0.03704 nm respectively. Sensor 14 which had the coating thickness of 1300 nm saturated at lower hydrogen content (243 ppm). Sensors with 88% Pd had limitation because it reached saturation at 427 ppm (970 nm coating thickness) and 243 ppm (1300 nm coating thickness). This showed that the thickness of the coating influenced the saturation of the sensor. As the thickness increased, the detection range of the sensor shortened but the wavelength shift range was increased. This is because the presence of more palladium metal which exerted greater force on the FBG when it was exposed to dissolved hydrogen.

Figure 4.17 shows the response of the 75% Pd sensors (sensor 3, sensor 7, sensor 11 and sensor 15) plotted based on the thickness of the coatings. Sensor 3 response was not satisfactory at lower hydrogen concentration but had lower deviation error at higher hydrogen content. On the other hand, sensor 7 had consistent response throughout 0 ppm 683 ppm of dissolved hydrogen content. In addition, this sensor did not saturate at tested hydrogen range thus made it the best choice of sensor to be installed inside hermetically sealed transformer. A range of detection up to 683 ppm was sufficient to monitor the partial discharge activities inside the transformer (IEC, 2015).

Figure 4.18 shows the response of the 67% Pd sensors (sensor 4, sensor 8, sensor 12 and sensor 16) plotted based on the thickness of the coatings. Sensor 12 and sensor 16 showed no wavelength shift after 559 ppm of dissolved hydrogen. The maximum wavelength shift for all sensors coated with 67% Pd was 0.00886 nm. This wavelength shift was too small because the sensor could face detection resolution issue during correlating with amount of dissolved hydrogen. Thus, these sensors will require highly sensitive interface which may incur additional cost.

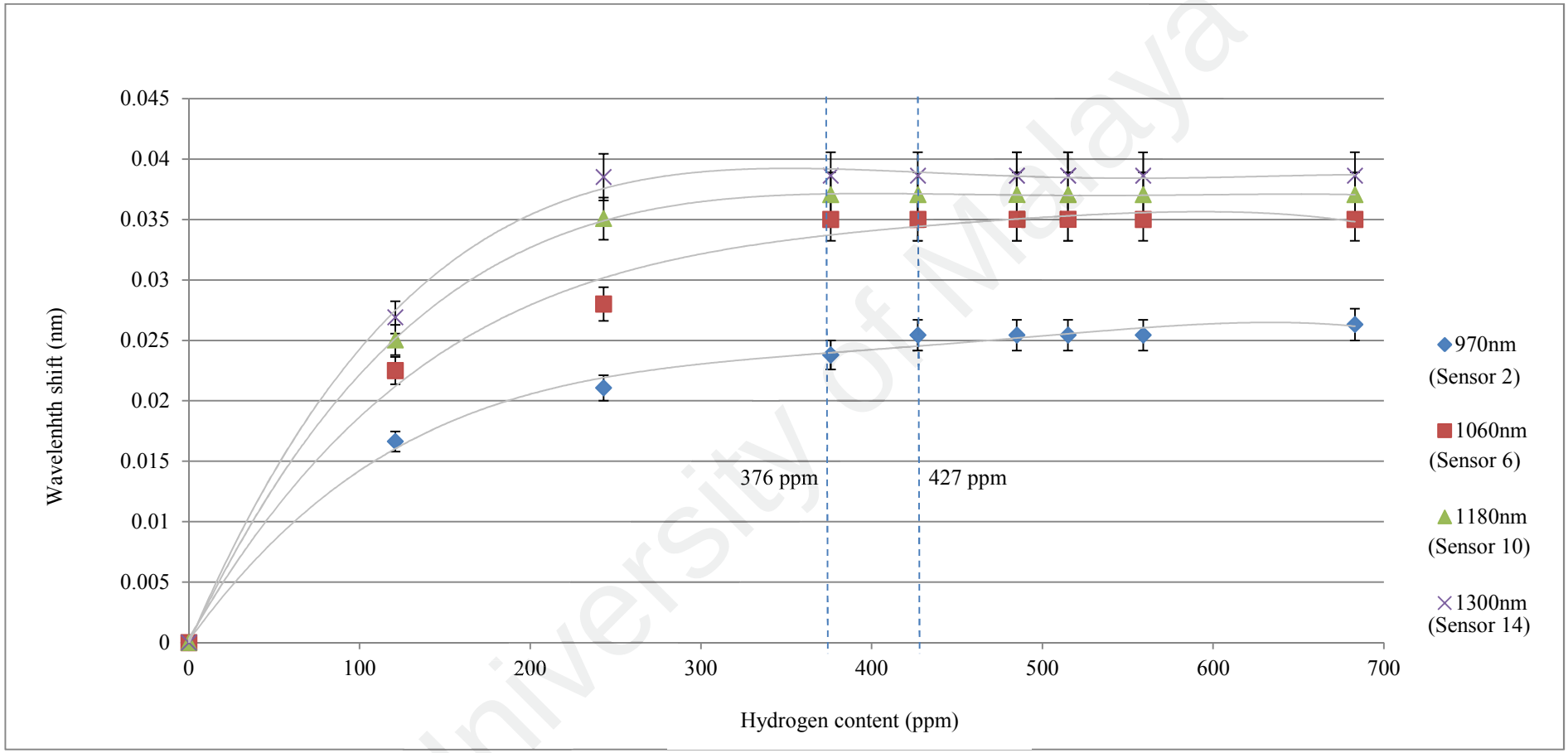


**Figure 4.16: Wavelength shift vs coating thickness (88% Pd , 12% Cr)**

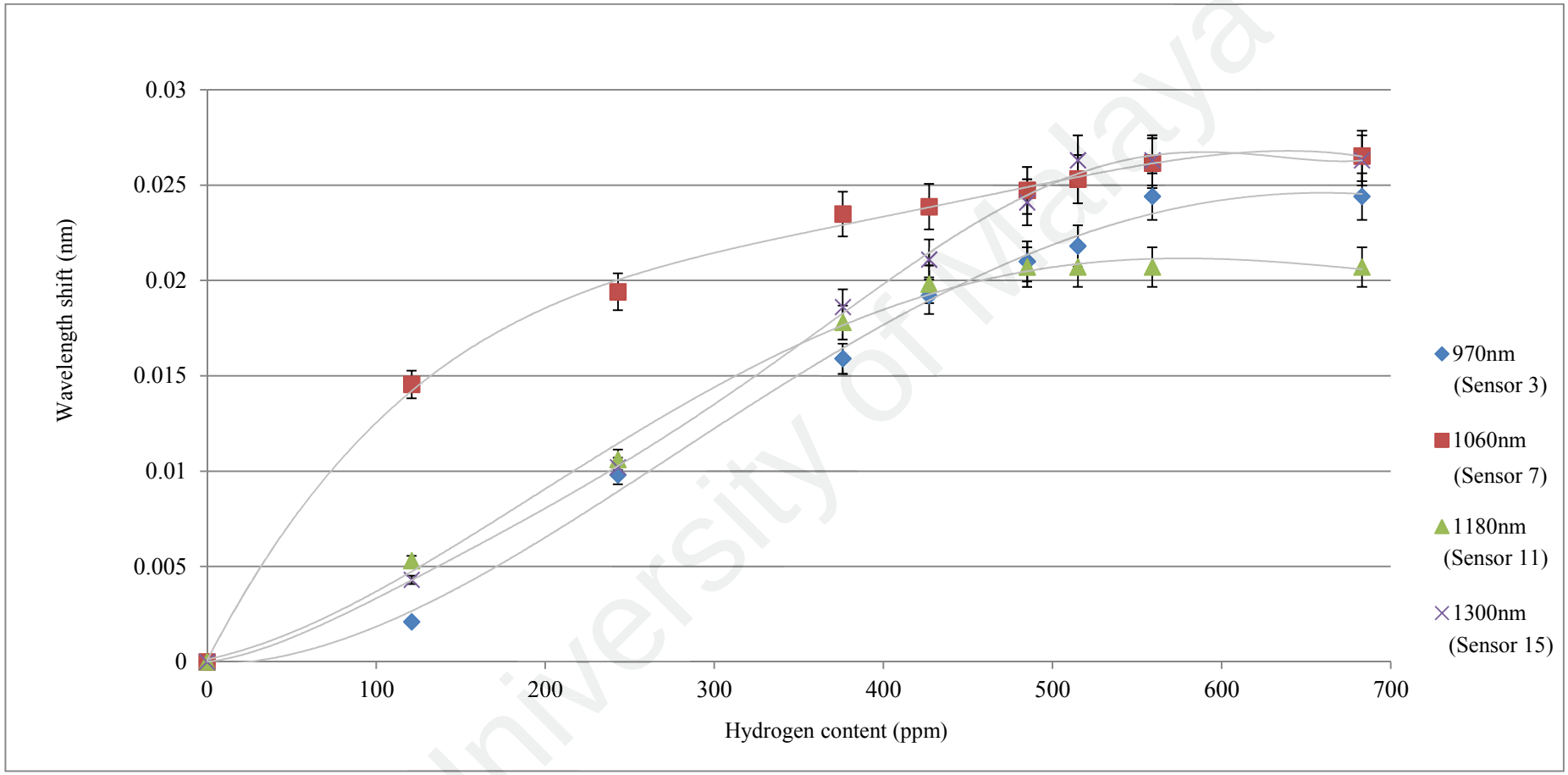


**Figure 4.17: Wavelength shift vs coating thickness (75% Pd , 25% Cr)**

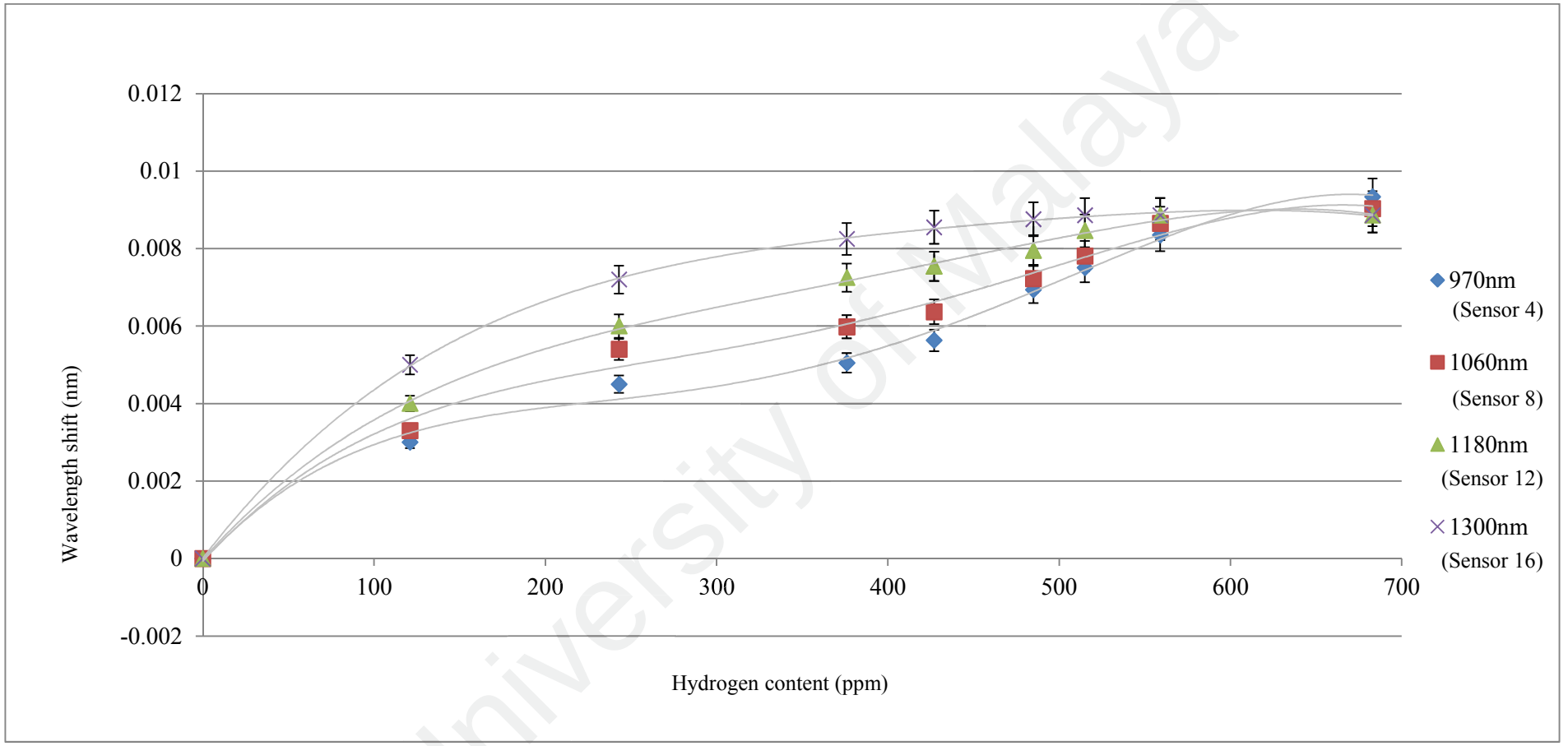


**Figure 4.18: Wavelength shift vs coating thickness (67% Pd , 33% Cr)**

## 4.6 Validation with gas generated by discharge by using spark gap

All the sensors were tested with fault gasses generated by partial discharge activity (Figure 3.17). Hydrogen gasses were formed as by-product of partial discharges. The gasses for the test were taken at calculated interval from the discharge chamber and tested with all the sensors and wavelength shifts were measured. The amounts of dissolved hydrogen were measured by using portable dissolved gas analyser (Figure 3.7). The wavelength shifts were expected caused by the reaction of palladium with hydrogen. The measured wavelengths shift from the sensors which were tested with actual hydrogen generated from partial discharge was compared with calculated wavelength from Equation 4.1 to Equation 4.6 and the percentage differences (error) were calculated. The calculated errors for all sensors are shown in Table 4.2 to Table 4.5 respectively. The wavelength shifts were recorded 10 times per wavelength shift at a fixed interval of 10 minutes, and the average wavelength shift was calculated.

Sensor 6 (88% Pd, 1060 nm) recorded the highest error of 8.93% at 244 ppm of dissolved hydrogen. Besides, the errors were 8.70% and 7.27% at 123 ppm and 349 ppm respectively. In addition, sensor 4 showed persistent error of 5.71% - 8.00% throughout the range of 135 ppm to 501 ppm. On the other hand, sensor 12 showed persistent error of 5.00% - 7.14% throughout the range of 232 ppm to 676 ppm. Sensor 8 showed errors of 6.67% and 5.71% at 123 ppm and 349 ppm respectively. Finally, sensor 1 showed error of 5.24% at 135 ppm of dissolved hydrogen. Meanwhile, sensor 7 (75% Pd, 1060 nm) had the least error with average error of 1.05% to 3.33%. This error is acceptable for gas-in-oil sensing application.

**Table 4.2: Validation of sensor 1, sensor 2, sensor 3 and sensor 4 against dissolved gas generated by partial discharge**

| Measured hydrogen content (ppm) | Sensor 970 nm | | | | | | | | | | | |
|---|---|---|---|---|---|---|---|---|---|---|---|---|
| | Sensor 1 (100 Pd) | | | Sensor 2 (88:12) | | | Sensor 3 (75:25) | | | Sensor 4 (67:33) | | |
| | Measured average wavelength shift (nm) | Calculated from Equation 4.1 | % Error | Measured average wavelength shift (nm) | Calculated from Equation 4.2 | % Error | Measured average wavelength shift (nm) | Calculated from Equation 4.3 | % Error | Measured average wavelength shift (nm) | Calculated from Equation 4.4 | % Error |
| | | | | | | | | | | | | |
| 0 | 0 | 0 | 0.00% | 0 | 0 | 0.00% | 0 | 0 | 0.00% | 0 | 0 | 0.00% |
| 135 | 0.0221 | 0.021 | -5.24% | 0.0186 | 0.018 | -3.33% | 0.0022 | 0.0021 | -4.76% | 0.0032 | 0.003 | -6.67% |
| 273 | 0.0292 | 0.029 | -0.69% | 0.024 | 0.023 | -4.35% | 0.0123 | 0.012 | -2.50% | 0.0054 | 0.005 | -8.00% |
| 349 | 0.0292 | 0.029 | -0.69% | 0.0248 | 0.024 | -3.33% | 0.0144 | 0.014 | -2.86% | 0.0053 | 0.005 | -6.00% |
| 501 | 0.0292 | 0.029 | -0.69% | 0.026 | 0.025 | -4.00% | 0.0232 | 0.023 | -0.87% | 0.0074 | 0.007 | -5.71% |
| 653 | 0.0292 | 0.029 | -0.69% | 0.026 | 0.027 | 3.70% | 0.0251 | 0.024 | -4.58% | 0.0082 | 0.008 | -2.50% |

**Table 4.3: Validation of sensor 5, sensor 6, sensor 7 and sensor 8 against dissolved gas generated by partial discharge**

| Measured hydrogen content (ppm) | Sensor 1060 nm | | | | | | | | | | | |
|---|---|---|---|---|---|---|---|---|---|---|---|---|
| | Sensor 5 (100 Pd) | | | Sensor 6 (88:12) | | | Sensor 7 (75:25) | | | Sensor 8 (67:33) | | |
| | Measured average wavelength shift (nm) | Calculated from Equation 4.5 | % Error | Measured average wavelength shift (nm) | Calculated from Equation 4.6 | % Error | Measured average wavelength shift (nm) | Calculated from Equation 4.7 | % Error | Measured average wavelength shift (nm) | Calculated from Equation 4.8 | % Error |
| | | | | | | | | | | | | |
| 0 | 0 | 0 | 0.00% | 0 | 0 | 0.00% | 0 | 0 | 0.00% | 0 | 0 | 0.00% |
| 123 | 0.0252 | 0.025 | -0.80% | 0.025 | 0.023 | -8.70% | 0.0155 | 0.015 | -3.33% | 0.0032 | 0.003 | -6.67% |
| 244 | 0.0374 | 0.037 | -1.08% | 0.0305 | 0.028 | -8.93% | 0.0192 | 0.019 | -1.05% | 0.0051 | 0.005 | -2.00% |
| 349 | 0.0385 | 0.038 | -1.32% | 0.0354 | 0.033 | -7.27% | 0.0236 | 0.023 | -2.61% | 0.0074 | 0.007 | -5.71% |
| 489 | 0.0395 | 0.039 | -1.28% | 0.0354 | 0.035 | -1.14% | 0.0254 | 0.025 | -1.60% | 0.0082 | 0.008 | -2.50% |
| 687 | 0.0396 | 0.039 | -1.54% | 0.0354 | 0.035 | -1.14% | 0.0274 | 0.027 | -1.48% | 0.0092 | 0.009 | -2.22% |

**Table 4.4: Validation of sensor 9, sensor 10, sensor 11 and sensor 12 against dissolved gas generated by partial discharge**

| Measured hydrogen content (ppm) | Sensor 1180 nm | | | | | | | | | | | |
|---|---|---|---|---|---|---|---|---|---|---|---|---|
| | Sensor 9 (100 Pd) | | | Sensor 10 (88:12) | | | Sensor 11 (75:25) | | | Sensor 12 (67:33) | | |
| | Measured average wavelength shift (nm) | Calculated from Equation 4.9 | % Error | Measured average wavelength shift (nm) | Calculated from Equation 4.10 | % Error | Measured average wavelength shift (nm) | Calculated from Equation 4.11 | % Error | Measured average wavelength shift (nm) | Calculated from Equation 4.12 | % Error |
| | | | | | | | | | | | | |
| 0 | 0 | 0 | 0.00% | 0 | 0 | 0.00% | 0 | 0 | 0.00% | 0 | 0 | 0.00% |
| 142 | 0.0311 | 0.031 | -0.32% | 0.0250 | 0.025 | 0.00% | 0.0052 | 0.005 | -4.00% | 0.0041 | 0.004 | -2.50% |
| 232 | 0.0393 | 0.039 | -0.77% | 0.0353 | 0.035 | -0.86% | 0.0114 | 0.011 | -3.64% | 0.0063 | 0.006 | -5.00% |
| 313 | 0.041 | 0.040 | -2.75% | 0.0367 | 0.036 | -1.94% | 0.0157 | 0.015 | -4.67% | 0.0075 | 0.007 | -7.14% |
| 532 | 0.0413 | 0.041 | -0.73% | 0.0373 | 0.037 | -0.81% | 0.0216 | 0.021 | -2.86% | 0.0084 | 0.008 | -5.00% |
| 676 | 0.0415 | 0.041 | -1.22% | 0.0373 | 0.037 | -0.81% | 0.0219 | 0.021 | -4.29% | 0.0096 | 0.009 | -6.67% |

**Table 4.5: Validation of sensor 13, sensor 14, sensor 15 and sensor 16 against dissolved gas generated by partial discharge**

| Measured hydrogen content (ppm) | Sensor 1300nm | | | | | | | | | | | |
|---|---|---|---|---|---|---|---|---|---|---|---|---|
| | Sensor 13 (100 Pd) | | | Sensor 14 (88:12) | | | Sensor 15 (75:25) | | | Sensor 16 (67:33) | | |
| | Measured average wavelength shift (nm) | Calculated from Equation 4.13 | % Error | Measured average wavelength shift (nm) | Calculated from Equation 4.14 | % Error | Measured average wavelength shift (nm) | Calculated from Equation 4.15 | % Error | Measured average wavelength shift (nm) | Calculated from Equation 4.16 | % Error |
| | | | | | | | | | | | | |
| 0 | 0 | 0 | 0.00% | 0 | 0 | 0.00% | 0 | 0 | 0.00% | 0 | 0 | 0.00% |
| 115 | 0.0320 | 0.030 | -6.67% | 0.0272 | 0.027 | -0.74% | 0.0054 | 0.005 | -3.85% | 0.0053 | 0.0050 | -6.00% |
| 224 | 0.0442 | 0.044 | -0.45% | 0.0393 | 0.039 | -0.77% | 0.0095 | 0.009 | -5.56% | 0.0074 | 0.0070 | -5.71% |
| 368 | 0.0444 | 0.044 | -0.91% | 0.0394 | 0.039 | -1.03% | 0.0187 | 0.018 | -3.89% | 0.0082 | 0.0082 | 0.00% |
| 476 | 0.0444 | 0.044 | -0.91% | 0.0395 | 0.039 | -1.28% | 0.0234 | 0.023 | -1.74% | 0.0090 | 0.0087 | -3.45% |
| 663 | 0.0444 | 0.044 | -0.91% | 0.0394 | 0.039 | -1.03% | 0.0264 | 0.026 | -1.54% | 0.009 | 0.0088 | -2.27% |

## 4.7 Benchmarking with others work on hydrogen detection in transformer oil

Sensor 5 (100% Pd) has a thickness of 1060 nm which is almost twice the thickness of the sensor developed by (Jiang, 2014). He has developed a sensor with 560 nm of palladium coating which has a sensitivity of 0.042 pm/ppm. Sensor 5 has sensitivity of 0.1521 pm/ppm, which is 3.6 times higher than sensor coated with 560 nm of palladium (Figure 2.16).

In addition, the response time of the sensor coated with 560 nm was estimated around 45 minutes, but sensor 5 recorded response time up to 10 minutes. This is because sensor 5 offered twice the surface area than sensor coated with 560 nm of palladium. Higher surface area will allow more hydrogen atom to be absorbed into the sensor. On the other hand, all sensors coated with 100% palladium experienced surface micro-cracking after exposure to transformer oil in this work. Thus, there is a possibility that sensor coated with 560 nm of palladium may have surface cracking in long run.

Sensor 7 which has the same thickness and surface area as sensor 5 showed a sensitivity of 0.0388 pm/ppm and a detection range up to 683 ppm. The addition of chromium has restricted the expansion of palladium thus prevent it from cracking after exposure to the transformer oil. In overall, sensor 7 has improved the response time by three times and reliability of the sensor compared to sensor coated with 560 nm of palladium.

## 4.8 Selection of sensors for hermetically sealed transformer application

Since all the sensors have showed error lesser than the tolerance in this work which is 10%, but the selection criteria to select the most suitable sensor are detection range of 0-700 ppm, least error (<5%) and wider operating range with significant wavelength shift.

Sensor 1, sensor 4, sensor 6, sensor 8, sensor 12, sensor 13, sensor 15 and sensor 16 showed error of more than 5%, therefore not complied to selection criteria. On the other hand, sensor 9, sensor 10, sensor 11 and sensor 12 used 11% more palladium and chromium in weight during coating process than sensors coated with 1060 nm of coating thickness. This indicated that the cost of producing these sensor will be more expensive (11% on material cost) than other thinner sensors. This is not practical for sensors that have limited detection range up to 376 ppm for sensor 9 and sensor 10, 485 ppm for sensor 11 and 559 ppm for sensor 12. These sensors may be sensitive to hydrogen based on their responses and due to higher palladium contents coated on the FBG but these sensors absorbed more hydrogen and saturated. Higher content of chromium restricted the strain on the FBG thus caused the wavelength shift to be limited to certain range. Therefore, this type of sensor with coating thickness of 1180 nm may not be practical for mass production because more palladiums are used. However, this finding has given a baseline on the maximum thickness to coat FBG for practical application dissolved gas sensing application in transformer.

All the sensors coated with 100% palladium cracked after the experiment. This proved that palladium alone on the FBG could not sustain the nature of the transformer oil and expansion of the palladium due to dissolved hydrogen. In addition, all sensors coated with chromium mixture did not crack or peel-off after the experiment. This has proven that addition of chromium metal will strengthen the coating as well as expanding the range of detection. However, there are certain thickness and composition that need to be selected in order to obtain the best hydrogen detection range. Hence, sensors with 100% palladium still can be used for lower range and non-cyclic hydrogen detection in transformer.

Table 4.6 shows the potential operating range, sensitivity, advantages and disadvantages for all sensors. Typical values of hydrogen gas in transformer are between 50-150 ppm. However, for transformers with electrical fault inside, the value of hydrogen can go up to 2000 ppm (IEEE, 2015). Therefore, the range more than 150 ppm to 700 ppm is of concern for this work. The average sensitivity of the sensors was calculated by dividing maximum wavelength shift of the sensor with the hydrogen when the saturation happened. Sensors with the highest sensitivity saturated at lower hydrogen content than the sensors with the lower sensitivity.

All sensors coated with 88% Pd except sensor 2 (970 nm) saturated after 376 ppm whereas sensor 2 was saturated after 427 ppm (Figure 4.16). All sensors coated with 85% Pd did not crack after the testing. These sensors had limitation because they would get saturated at lower hydrogen content. In addition, sensor 6 recorded highest error when tested with actual dissolved hydrogen generated by partial discharge activities. Finally, sensor 3 saturated after 559 ppm and showed uncertainty at lower hydrogen concentration. Sensor 3 has shown higher error (2.5-4.76%) compared to error of sensor 7 (1.05-3.33%).

Sensor 7 coated with 75% Pd with a thickness of 1060 nm demonstrated a good response throughout the 0 ppm to 683 ppm. As the coating thickness for this composition increased from 1060 nm to 1180 nm and 1300 nm, the sensor would get saturated at lower hydrogen content. Meanwhile, as the coating thickness reduced, the sensor seemed to higher error at lower hydrogen content (sensor 3). Sensor 7 has the right composition and mixture of palladium-chromium alloy for detection range of hydrogen that could be applicable for hermetically sealed transformer. However, further studies are required to investigate the response of the thickness and composition and for the fine-tuning and optimizing the sensor.

The presence of chromium metal has restricted the expansion of palladium. Chromium presence in the coating has changed the lattice expansion performance of the coating which can be observed by the wavelength shifts of the FBG. However, the lattice strength of palladium with chromium needs further analysis to identify the maximum strain on the FBG. This kind of sensor is suitable to be used for wider range of dissolved hydrogen detection where resolution of measurements (±1 ppm) is not critical.

Higher content of chromium mixture in the coating caused the sensors sensitivity to reduce which good for higher range hydrogen gas detection, but is not suitable for precise measurement. Therefore, sensor 7 is the most suitable and economical sensor for the hermetically sealed transformer application due to the sensitivity and the selectivity. Besides, other sensors which do not comply with the criteria may have different application.

Although sensor 7 operating range is between 0- 683 ppm as per measurement, this is sufficient to serve the purpose of detecting dissolved hydrogen in hermetically sealed transformer. Due to the large number of hermetically sealed transformer in the electricity distribution system, an alarm setting for hydrogen content more than 650 ppm will assist the utility manager to plan shutdown of the transformer for further investigation.

**Table 4.6: Potential operating range, sensitivity, advantages and disadvantages for all the sensors sorted based on sensitivity**

| Sensor | Advantage | Disadvantage | Coating thickness (nm) | Composition | | Potential operating range | | Average sensitivity (pm/ppm) |
|---|---|---|---|---|---|---|---|---|
| | | | | Pd | Cr | min (ppm) | max (ppm) | |
| 1 | High wavelength shift | Coatings cracked after test | 970 | 100 | 0 | 0 | 243 | 0.1801 |
| 5 | High wavelength shift | Coatings cracked after test | 1060 | 100 | 0 | 0 | 243 | 0.1604 |
| 14 | High wavelength shift | Saturates above 376 ppm | 1300 | 88 | 12 | 0 | 243 | 0.1584 |
| 9 | High wavelength shift | Coatings cracked after test | 1180 | 100 | 0 | 0 | 376 | 0.1521 |
| 10 | High wavelength shift | Saturates above 376 ppm | 1180 | 88 | 12 | 0 | 243 | 0.1443 |
| 13 | High wavelength shift | Coatings cracked after test | 1300 | 100 | 0 | 0 | 376 | 0.1189 |
| 6 | High wavelength shift | Saturates above 427 ppm and high error | 1060 | 88 | 12 | 0 | 376 | 0.0931 |
| 15 | Moderate wavelength shift | Saturates above 515 ppm | 1300 | 75 | 25 | 0 | 515 | 0.0511 |
| 11 | Moderate wavelength shift | Saturates above 485 ppm | 1180 | 75 | 25 | 0 | 485 | 0.0463 |
| 2 | High wavelength shift | Saturates above 559 ppm | 970 | 88 | 12 | 0 | 427 | 0.0454 |
| 3 | None | Possible uncertainty at lower hydrogen content | 970 | 75 | 25 | 0 | 559 | 0.0429 |
| 7 | Uniform wavelength shift throughout 0 ppm to 683 ppm | None | 1060 | 75 | 25 | 0 | 683 | 0.0388 |
| 16 | Low wavelength shift | Saturates above 515 ppm | 1300 | 67 | 33 | 0 | 515 | 0.0172 |
| 12 | Low wavelength shift | Saturates above 559 ppm | 1180 | 67 | 33 | 0 | 559 | 0.0158 |
| 4 | Possibly wider range of hydrogen detection | Low wavelength shift may introduce uncertainty in the measurement | 970 | 67 | 33 | 0 | > 683 | 0.0137 |
| 8 | Possibly wider range of hydrogen detection | Low wavelength shift may introduce uncertainty in the measurement | 1060 | 67 | 33 | 0 | > 683 | 0.0131 |

# CHAPTER 5: CONCLUSION AND FUTURE DIRECTION

The detection of dissolved hydrogen content in transformer oil was proven by using the optical method. Although the measurements were done with indirect method by using reactants (palladium and chromium), the accuracy is still acceptable compared to most online monitoring systems in the market. The developed sensor has a potential to be commercialized after a few fields trial and improvement. The sensor has showed consistency throughout experiments but the repeatability in the actual transformer condition with many uncontrolled parameter is yet to be explored. Therefore, the current thesis aimed to explore the potential use of optical FBG for hydrogen monitoring and contribute to the body of knowledge especially on operation technology (OT). The findings and contributions of this research are summarized below.

## 5.1 Summary and conclusions

To conclude, it is clear that the findings of this research could be used for the detection of the hydrogen in transformer oil with various range of detection. The sensor can open up evolutionary road towards operational technology (OT) and information technology (IT). Accordingly, the following conclusions are drawn for each objective.

**i. FBG is feasible to be used as the base material to detect dissolved hydrogen in transformer oil.**

The capability and feasibly of the FBG sensor as the base material for the dissolved hydrogen in transformer oil detection has been proven through this study. The strain caused by the reactant on the FBG sensor caused wavelength shift the magnitude can be quantified. Furthermore, the FBGs showed repeatability of the measurements and stability after they were exposed to prolong temperature degradation. To the author's best knowledge, this is the first attempt of using FBG together with Pd-Cr reactant to detect dissolved hydrogen in the transformer. The

promising result has encouraged the author to further investigate on the other gas detection in the transformer.

ii. **$TiO_2$ coating performed well as the adhesion layer to coat 16 units of FBG sensors with various coating thicknesses and compositions of palladium-chromium alloy by using physical vapour deposition equipment.**

Significant contribution to the body of engineering knowledge is the formula to coat the palladium and chromium on the FBG. In addition, the PVD machine parameter settings were presented in this paper. $TiO_2$ showed good adhesion strength on the FBG and Pd-Cr layer. The coating did not show any sign of surface roughness, uneven thickness, peeling off or micro-cracking after it was immersed in transformer oil throughout the experiment. This has given further confidence in using the same material for advanced research related to dissolved gas sensing in the transformer oil.

iii. **Evaluation of performance on developed FBG sensors against hydrogen gas dissolved in transformer oil and to assess the accuracy of the palladium-chromium sensors against and the dissolved hydrogen generated by the sharp edges.**

All the 16 sensors developed in this work were tested with transformer oil with diffused hydrogen as well as transformer oil exposed to partial discharge. The sensors showed good repeatability and error less than 10%. This work has shown the potential of using alloy metal like chromium to the palladium metal to enhance dissolved hydrogen detection range. In addition, all the sensors response followed certain behavior which adhered to fourth order polynomial formula. The results have confirmed that the sensors can be used on the hermetically transformer to detect dissolved hydrogen.

iv. **Recommendation on the most suitable sensor for hermetically sealed transformer application based on the detection range and accuracy.**

The study showed that the developed sensor can be used inside the hermetically sealed transformer to detect dissolved hydrogen. Sensors with higher palladium content has the potential of detecting the hydrogen for lower range, whereas sensor with lesser palladium content can be used to detect hydrogen at higher range. All sensors showed a reversible response after removing them from the transformer oil. This work has identified the optimum and cost effective thickness and composition to develop the FBG sensor to detect hydrogen in transformer oil. The findings in this study will help in mass production of the sensor later.

## 5.1 Direction for future research

This work can be continued by looking into the reaction of hydrogen with other cheaper materials such as silver and aluminium. More compositions of the palladium and the alloy material range can be studied. In addition, this sensor can be incorporated with existing fibre cable to monitor all the parameters in transformer such as pressure and temperature. The sensor can be placed near the active component of transformer to measure temperature and gassing activities. A hybrid FBG sensor could be developed to detect various gases inside transformer. This sensor may have different composition of the palladium and alloy material, and other reactants to detect other gases inside transformer.

Although this research was done at 25°C, further research is required to look into the sensitivity and accuracy of the sensor at higher temperature. This study also needs to look into the effect of vibration, mechanical stress and oil flow inside the transformer. The mechanical stress on the sensor can cause wavelength shift and can confuse the detection of preferred parameter inside transformer. Therefore, further research is

required on the sensor array to segregate the measured parameters based on the unique wavelength. In addition, more studies are also needed to position the sensors inside the transformer to get the best range of detection because of the effect of oil pressure on the wavelength shift.

At the same time, additional research is required to inspect the suitability of using the sensor developed in this project for newly developed transformer oil types such as paraffinic, vegetable oil and bio-degradable oil. The reactant on the sensor may react with these oils and generate stray gasses in transformer. In addition, the chemical compound in the oil may cause the coating to peel off.

Besides, hermetically sealed transformer is smaller in size compared to power transformer. Therefore, there is a need to look into smaller rates of gas generation and gas limits inside hermetically sealed transformer and updates the IEC and IEEE standards related to transformers. This is because established standards like IEC and IEEE standards are developed by using statistical data obtained from power transformer although it is usable selectively for smaller transformers.

Finally, the research can also focus in developing micro integrated circuit modules to enable interface between the sensors and fiber optic network. Thus, the interface should be able to raise fault alarm if the fault gasses inside the transformer exceed the pre-set value.

## REFERENCES


A. D. Kersey, M. A. D., H.J. Patrick, M. LeBlanc, K.P. Koo, C.G. Askins, M.A. Putnam , E.J. Friebele. (1997). Fiber Grating Sensors. *Journal of Lightwave Technology, Vol 1*, pp. 1442-1463.

A. D'Amico, A. P., and E. Verona. (1982). Palladium-surface acoustic wave interaction for hydrogen detection. *Applied Physics Letters 41*, pp. 300-301.

Alexander, M., & Pandian, K. (2013). Linen fiber template-assisted preparation of TiO2 nanotubes: palladium nanoparticle coating and electrochemical applications. *Journal of Solid State Electrochemistry, 17(4)*, 1117-1125.

Arshad, M., & Islam, S. M. (2011). Significance of Cellulose Power Transformer Condition Assessment. *IEEE Transactions on Dielectrics and Electrical Insulation, 18*(5), 1591-1598.

Arvind, D., Khushdeep, S., & Deepak, K. (2008). Condition monitoring of power transformer: A review. *IEEE/PES Transmission & Distribution Conference & Exposition, 1-3*, 1599-1604.

ASTM. (2009). Standard Test Method for Analysis of Gases Dissolved in Electrical Insulating Oil by Gas Chromatography. West Conshohocken, PA, USA: ASTM.

Atashbar, M. Z., Banerji, D., Singamaneni, S., & Bliznyuk, V. (2005). Polystyrene palladium nanocomposite for hydrogen sensing. *Molecular Crystals and Liquid Crystals, 427*, 529.

B. Sutapun, M. T. A., A. Kazemi. (1999). Pd-coated elastooptic fiber optic Bragg grating sensors for multiplexed hydrogen sensings. *Sensors and Actuators B60*, pp. 27-34.

B.K. Miremadi, R. C. S., Z.Chen. (1994). Chromium oxide gas sensors for the detection of hydrogen, oxygen and nitrogen oxide *Sensors and Actuators B21*, pp 4.

Bandyopadhyay, M. N. (2007). Condition Monitoring for power transformer. *Proceedings of 2008 International Conference on Condition Monitoring and Diagnosis*, 983-988.

Blackburn, T. R. (2006). Optical Fibre Sensor For Partial Discharge Detection. *IEEE Electrical Insulation Journal, 2*(6), 23-29.

Bodzenta, J., Burak, B., Gacek, Z., Jakubik, W. P., Kochowski, S., & Urbanczyk, M. (2002). Thin palladium film as a sensor of hydrogen gas dissolved in transformer oil. *Sensors and Actuators B-Chemical, 87*(1), 82-87.

Boggs, S. A. (1990). Partial Discharge: Overview and Signal Generation. *IEEE Electrical Insulation Magazine, Vol. 6*, pp 11-20.

Buric, M. (2005). *Wavelength modulation spectroscopic chemical sensing using a piezo-electric tunable fiber Bragg grating laser.* (MS Thesis), University of Pittsburgh.

Cheng, Z., Cheng, L., Li, W., Zhou, J. H., Yang, K. C., & Zhang, X. H. (2012). An on-line transformer windings temperature measurement system based on fiber Bragg grating. *Photonics and Optoelectronics Meetings (POEM) 2011: Optoelectronic Sensing and Imaging, 8332*.

Cho, K. C. S. T. K. Y.-H. P. J. R. (2019). Measurement of Mechanical and Thermal Strains by Optical FBG Sensors Embedded in CFRP Rod. *Journal of Sensors, 2019*, 6.

Dai, J. X., Yang, M. H., Chen, Y., Cao, K., Liao, J. S., & Zhang, P. C. (2012). Hydrogen Performance of Side-Polished Fiber Bragg Grating Sputtered with Pd/Ag Composite Film. *Sensor Letters, 10*(7), 1436-1439.

Dai, J. X., Yang, M. H., Yu, X., Cao, K., & Liao, J. S. (2012). Greatly etched fiber Bragg grating hydrogen sensor with Pd/Ni composite film as sensing material. *Sensors and Actuators B-Chemical, 174*, 253-257.

Dai, J. X., Yang, M. H., Yu, X., & Lu, H. (2013). Optical hydrogen sensor based on etched fiber Bragg grating sputtered with Pd/Ag composite film. *Optical Fiber Technology, 19*(1), 26-30.

Dewayne Terrence Halfen, L. M. Z. (2008). The submillimeter spectrum of CrH and CrD (X6Σ +). *The Astrophysical Journal, 611*(1), L65.

Duval, M. (2002). A review of faults detectable by gas-in-oil analysis in transformers. *IEEE Electr. Insul. Mag., 18*(3), pp. 8-17.

Duval, M. (2003). New Techniques for Dissolved Gas-in-Oil Analysis. *IEEE Electrical Insulation Magazine, 19*(2), pp 6-15.

Duval, M. (2008). Calculation of DGA limit values and sampling intervals in transformers in service. *IEEE Elect. Insul. Magazine, 24*(5).

Duval., M. (1989). Dissolved Gas Analysis: It Can Save Your Transformer. *IEEE Electrical Insulation Magazine, 5*(6), pp. 22-27.

E. Kuffel, W. S. Z., J. Kuffel. (2000). *High Voltage Engineering Fundamentals* (2nd ed. Vol. 1). Great Britain: Reed Educational and Professional Publishing Ltd.

Eroglu, A. E., Volkan, M., Ataman, O. Y. (2000). Fiber optic sensors using novel substrates for hydrogen sulfide determination by solid surface fluorescence. *Talanta, 53*(1), 89-101.

F.H.Kreuger. (1989). *Discharge Detection in High Voltage Equipment* (Vol. 1). United States: Temple Press Book.

Flanagan, W. M. (1992). *Handbook of Transformer Design & Application* (Vol. 2). United States: McGraw Hill.

Godswill, O., Ubeka, E. U., Mesharun, C. E. (2008). Large power transformer condition assessment and life extension. *Conference Record of the 2008 IEEE International Symposium on Electrical Insulation, 1*, 197-200.

Grattan, K. T. V. (1998). *Optical Fiber Sensor Technology*. London: Kluwer Academic Publisher.

H.Harlow, J. (2004). *Electric Power Transformer Engineering* (J. H. Harlow Ed. Vol. 1): CRC Press LLC.

Haema, J., Phadungthin, R. (2012). Power Transformer Condition Evaluation by the Analysis of DGA methods. *2012 Asia-Pacific Power and Energy Engineering Conference (Appeec)*.

Hamagami, J., Araki, R., Oda, H., Sakai, M. (2010). Preparation and characterization of Pd-Based optical hydrogen sensor operated at room temperature by using photodeposition process. *Electroceramics in Japan Xiii, 445*, 100-104.

Hamagami, J., Araki, R., Onimaru, S., Oda, H. (2011). Low Temperature Preparation and Optical Hydrogen Response of Pd/Titania Composite Film. *Electroceramics in Japan Xiv, 485*, 275-278.

Hernández, J. V. a. D. M. (2005). Fast detection of hydrogen with nano fiber tapers coated with ultra thin palladium layers. *Optics Express 13*, pp. 5087-5092.

Hill, K. O. (1978). Photosensitivity in optical fiber waveguides: Application to Reflection Filter Fabrication. *Applied Physics Letters 32(10)*, pp 647-649.

Ho, H. L. J., J.; Jin, W. . (2009). *Fiber optic gas detection system for health monitoring of oil-filled transformer.* Paper presented at the 20th International Conference on Optical Fibre Sensors, Edinburg, United Kingdom.

Hunze, M. F. R. A. B. A. (2018). Palladium-Based Hydrogen Sensors Using Fiber Bragg Gratings. *Journal of Lightwave Technology, 36*(4).

I. Lundstrom, S. S., C. Svensson, L. Lundkvist. (1975). A hydrogen-sensitive MOS field effect transistor. *Applied Physics Letters 26*, pp. 55-57.

IEC. (2015). Mineral Oil-Impregnated Electrical Equipment in Service-Guide to the Interpretation of Dissolved and Free Gases Analysis: IEC Publication.

IEEE. (2015). IEEE Guide for Interpretation of Gases Generated in Oil Immersed Transformer *Standard C57.104.2008*.

J. Da Silva, H. K. (2001). *Strain Studies in Electrical Energy Transmission Cables using an Optical Fiber Bragg Grating Sensor.* Paper presented at the Microwave and Optoelectronics Conference.

J. Deng, H. X., W. Huo, M. Luo, R. May, A. Wang, and Y. Liu,. (2001). Optical fiber sensor-based detection of partial discharges in power transformers. *Optics & Laser Technology, vol. 33,*, pp. 305-311.

J. Jiang, H.-T. S., G.-M. Ma, C. Li, Y.-T. Luo, H.-B. Wang. (2015). Dissolved hydrogen detection in power transformer based on etched fiber Bragg grating. *Proc. 2015 IEEE Int. Instrum. Meas. Technol. Conf.*, 422-427.

Jiachen Yu, Z. W., Xin Yang, Xiuyou Han, Mingshan Zhao. (2018). Tilted Fiber Bragg Grating Sensor Using Chemical Plating of a Palladium Membrane for the Detection of Hydrogen Leakage. *MDPI Sensors 2018, 18*(1).

Jiang, G.-M. M. C.-R. L. R.-D. M. J. (2014). Fiber Bragg Grating Sensor for Hydrogen Detection in Power Transformers. *IEEE Transactions on Dielectrics and Electrical Insulation, 21*(1), 380-385.

Jixiang Dai, L. Z., Gaopeng Wang, Feng Xiang, Yuhuan Qin, Min Wang, Minghong Yang. (2017). Optical Fiber Grating Hydrogen Sensors: A Review. *MDPI Sensors 2017, 17*(577), 15.

Kartopu, G., Habouti, S., & Es-Souni, M. (2008). Synthesis of palladium nanowire arrays with controlled diameter and length. *Materials Chemistry and Physics, 107(2-3)*, 226-230.

Kashyap, R. (1999). *Fiber Bragg Gratings*. San Diego CA: Academic Press.

Kofu, H. A. H. K. M. (2016). Nanometer-Size Effect on Hydrogen Sites in Palladium Lattice. *Journal of the American Chemical Society, 138*(32).

Krohn, D. A. (2000). *Fiber Optics Sensors-Fundamental and Applications* (3rd ed.). New York: ISA, 2000.

KTV Grattan, B. M. (1998). *Optical Fiber Sensor Technology* (Vol. 1). London: Kluwer Academic Publisher.

Kulkarni, S. V. (2004). *Transformer Engineering* (Vol. 1). New York, USA: Marcel Dekker Inc.

Lee, J.-M. K. C.-M. K. S.-Y. C. B. Y. (2017). Enhanced Strain Measurement Range of an FBG Sensor Embedded in Seven-Wire Steel Strands. *Sensors (Basel, Switzerland), 17*(7), 1654.

Li, D. M., McDaniel, A. H., Bastasz, R., & Medlin, J. W. (2006). Effects of a polyimide coating on the hydrogen selectivity of MIS sensors. *Sensors and Actuators B-Chemical, 115(1)*, 86-92.

Lim, Z. M. H. E. V. A. M. A. K. S. (2019). High-Resolution Fibre Bragg Grating (FBG) Pressure Transducer for Low-Pressure Detection. *International Journal of Automotive and Mechanical Engineering, 16*(2), 6783-6795.

Liu, H. L., Yang, M. H., Dai, J. X., Cao, K. (2011). Hydrogen sensor based on side-polished fiber Bragg gratings coated with thin palladium film. *21st International Conference on Optical Fiber Sensors, 7753*.

M. Benounis, T. A.-N., N. Jaffrezic, and J. P. Dutasta. (2008). NIR and optical fiber sensor for gases detection produced by transformation oil degradation *Sensors and Actuators A: Phys., 141*, pp. 76-83.

M. Mirzaie1, A. G. A. H. T. (2007). *Thermal Degradation of Cellulose Paper Insulation In Power Transformers.* Paper presented at the 2007 International Conference On Solid Dielectrics, Winchester, UK.

M. Tabib-Azar, B. S., R. Petrick, A. Kazemi. (1999). Highly sensitive hydrogen sensors using palladium coated fiber optics with exposed cores and evanescent field interactions. *Sensors and Actuators B56, 43*, pp. 158-163.

M. Wang, A. J. V., and K.D. Srivastava. (2002). Review of Condition Assessment of Power Transformers in Service. *IEEE Electrical Insulation Magazine*, pp 12-25.

M.C. Steele, B. A. M. (1976). Palladium/cadmium-sulfide Schottky diodes for hydrogen detection. *Applied Physics Letters 28*, pp. 687-688.

Ma, G. M., Li, C. R., Luo, Y. T., Mu, R. D., & Wang, L. (2012). High sensitive and reliable fiber Bragg grating hydrogen sensor for fault detection of power transformer. *Sensors and Actuators B-Chemical, 169*, 195-198.

Mayoux. (2000). The Degradation of Insulating Material Withstanding Electrical Stress. *IEEE Transactions on Dielectrics and Electrical Insulation, Vol 7*.

Mohd Iqbal Ridwan, M. R. S., Young Zaidey Yang Ghazali. (2011). Reliability Analysis of Premature Failed 11/0.433kV Hermetically Sealed Distribution Transformers *2011 IEEE Colloquium on Humanities, Science and Engineering Research (CHUSER 2011)*.

N.H. Malik, A. A. A.-A., M.I Qureshi. (1997). Electrical Insulation in Power System. *Marcell Dekker, Inc*, pp 30-35 , pp 214- 218.

Naphthenics, N. (2008). Transformer Oil Handbook. In N. N. AB (Ed.), (1 ed., Vol. Vol. 1, pp. pp 32). Sweden: Nynas Naphthenics AB.

Palais, J. C. (2001). *Fiber Optics Communication* New Delhi: Pearson Education.

Pavlovsky, I. (2008). *Hydrogen Sensor for Oil Transformer Health Monitoring*. Paper presented at the 2008 8th IEEE Conference on Nanotechnology, Arlington, Texas USA.

Petersen, A. (2010). The Risk of transformer fires and strategies which can be applied to reduce the risk. *Paris: A2-101 CIGRE Session*.

Pradhan, M. K. (2006). Assesment of Status of Insulation during Thermal Stress Accelerated Experiments on Transformer Prototypes. *IEEE Transactions on Dielectrics and Electrical Insulation, Volume 13*(Issue 1), pp 227-237.

R. Schwarz, M. M. a. S. P. (2005). *Partial discharge detection in oil with optical methods*. Paper presented at the IEEE International Conference on Dielectric Liquids, Coimbra, Portugal.

Rojas, A. (2006). *Power factor testing in transformer condition assessment - Is there a better way?* Paper presented at the 2006 IEEE/PES Transmission & Distribution Conference & Exposition, Latin America, Caracas.

Rossen, A. (2015). What are metal prices like? Co-movement, price cycles and long-run trends. *Resources Policy, 45*, 255-276.

S. Sekimoto, H. N., S. Okazaki, K. Fukuda, S. Asakura, T Shigemori ,S. Takahashi. (2000). A fiber-optic evanescent-wave hydrogen gas sensor using palladium-supported tungsten oxide. *Sensors and Actuators, Sensors and Actuators(B66), 3*.

Sayago I, T. E., Lafuente E. (2005). Hydrogen sensors based on carbon nanotubes thin films. *Synthetic Metals, 148*(1), 15-19.

Shin, S., Dale J. Brugh ,Michael D. Morse. (2005). Radiative Lifetime of the v = 0, 1 Levels of the A 6Σ+ State of CrH. *The Astrophysical Journal, 618*, 407-411.

Shukla, S., Patil, S., Kuiry, S. C., Rahman, Z., Du, T., Ludwig, L. (2003). Synthesis and characterization of sol-gel derived nanocrystalline tin oxide thin film as hydrogen sensor. *Sensors and Actuators B-Chemical, 96(1-2)*, 343-353.

Slaman, M., Westerwaal, R., Schreuders, H., & Dam, B. (2012). Optical hydrogen sensors based on metal-hydrides. *Photonic Applications for Aerospace, Transportation, and Harsh Environment Iii, 8368*.

Stone, G. C. (2005). Partial Discharge Diagnostics and Electrical Equipment Insulation Condition Assessment. *IEEE Transactions on Dielectrics and Electrical Insulation, 12*(5).

Suwanasri, T., Haema, J., Phadungthin, R., Suwanasri, C. (2009). Diagnostic Techniques to Evaluate Internal Condition of Power Transformer. *Ecti-Con: 2009 6th International Conference on Electrical Engineering/Electronics, Computer, Telecommunications and Information Technology,, 2*, 19-22.

Takeshita, T., Tanaka, K., Ishizaki, A., & Stanbury, P. F. (1993). Development of a Dissolved Hydrogen Sensor and Its Application to Evaluation of Hydrogen Mass-Transfer. *Journal of Fermentation and Bioengineering, 76*(2), 148-150.

Trpkovski, S. W., S. A.; Baxter, G. W.; Collins, S. F. . (2003). Dual temperature and strain sensor using a combined fiber Bragg grating and fluorescence intensity ratio technique in Er3+-doped fiber. *Review of Scientific Instruments, 74*.

Vecchio, R. M. D. (2001). *Transformer Design Principles* (Vol. 1). United States of America: Taylor & Francis Group.

Wang, K., Tong, X. L., Hu, J., & Zhu, X. L. (2013). On-line power transformer partial discharge monitoring based on the optical fiber sensing technology. *Fourth Asia Pacific Optical Sensors Conference, 8924*.

Wang, M., Cheng, J., Yu, X., Dai, J. X., Zhang, G. L., & Yang, M. H. (2012). Optical Fiber Hydrogen Sensor based on Micro Interferometer. *22nd International Conference on Optical Fiber Sensors, 8421*.

Wensi Chen, J. L., Zhaoyang Cheng, Xifeng Lin, Jiachen Zhu. (2015). Effect of chromium on microstructure, ordered phase and magnetic properties of Fe-6.5 wt %Si alloy. *Materials Science and Engineering, 2*, S314 - S318.

Westerwaal, R. J., Gersen, S., Ngene, P., Darmeveil, H., Schreuders, H., Middelkoop, J., & Dam, B. (2014). Fiber optic hydrogen sensor for a continuously monitoring of the partial hydrogen pressure in the natural gas grid. *Sensors and Actuators B-Chemical, 199*, 127-132.

X. Bevenot, A. T., C. Veillas, H. Gagnaire, M. Clement. (2000). Hydrogen leak detection using an optical fibre sensor for aerospace applications. *Sensors and Actuators B67*, pp. 57-67.

X. Bevenot, A. T., C. Veillas, H. Gagnaire, M. Clement. (2002). Surface Plasmon resonance hydrogen sensor using an optical fiber. *Measurement Science and Technology 13*, pp.118-124.

Xiao, Z. (2006). Hydrogen Sensor Fast, Sensitive, Reliable, and Inexpensive to Produce. Retrieved 5-June-19, 2019, from http://web.anl.gov/techtransfer/pdf/Profile_HydrogenSensor9_06.pdf

Xue, J. H., Yang, Z., Wang, L. Y., Wang, M. J. . (2013). On-line Monitoring of Air Cooler in Transformer by Using Fiber Bragg Grating Temperature Sensors. *Advances in Applied Science and Industrial Technology, 798-799*, 565-569.

Y. Yun, W. C., Y. Wang, and C. Pan, . (2008). Photoacoustic detection of dissolved gases in transformer oil. *European Trans. Electr. Power, vol. 18*, pp. 562-576.

Yang, F., Jung, D., & Penner, R. M. (2011). Trace Detection of Dissolved Hydrogen Gas in Oil Using a Palladium Nanowire Array. *Analytical Chemistry, 83*(24), 9472-9477.

Yang, M. D., Jixiang. (2012). Review on optical fiber sensors with sensitive thin films. *Photonic Sensors, 2*(1), 14-28.

Yang, M. H., Dai, J. X., Cao, K., Liao, J. S., & Zhang, P. C. (2012). Side-polished fiber Bragg grating hydrogen sensor with different sensitive thin films. *Third Asia Pacific Optical Sensors Conference, 8351*.

Yang, M. H., Sun, Y., Zhang, D. S., & Jiang, D. S. (2010). Using Pd/WO3 composite thin films as sensing materials for optical fiber hydrogen sensors. *Sensors and Actuators B-Chemical, 143*(2), 750-753.

Yang, M. T., Hu, L. S. (2013). Intelligent Fault Types Diagnostic System for Dissolved Gas Analysis of Oil-immersed Power Transformer. *IEEE Transactions on Dielectrics and Electrical Insulation, 20*(6), 2317-2324.

Zagula-Yavorska, M., Sieniawski, J., & Gancarczyk, T. . (2012). Some Properties of Platinum and Palladium Modified Aluminide Coatings Deposited by Cvd Method on Nickel-Base Superalloys. *Archives of Metallurgy and Materials, 57(2)*, 503-509.

Zhou, Z. (2004, September 13-16 ,2004). *Techniques for Temperature Compensation for FBG Strain Sensors.* Paper presented at the Proceeding of Asian Pasific Fundamental Problem of Opto- and Microelectronics (APCOM 2004), Khabarovsk, Russia.

## LIST OF PUBLICATIONS AND PAPERS PRESENTED

- **Published paper**

1. M. R. Samsudin, Y. G. Shee, F. R. M. Adikan, B. B. A. Razak, and M. Dahari, "Fiber Bragg gratings hydrogen sensor for monitoring the degradation of transformer oil," IEEE Sens. J. **16**(9),2993 - 2999 (2016).

- **Submitted paper**

1. M. R. Samsudin, Y. G. Shee, F. R. M. Adikan, B. B. A. Razak, "Hydrogen and Oxygen Detection Application for Hermetically Sealed Transformer Oil by using Palladium-Chromium Coated Fiber Bragg Gratings" submitted to IEEE Dielectric Journal on 16th January 2019. Second submission on 6th Dec 2019.
2. M. R. Samsudin, Y. G. Shee, F. R. M. Adikan, "Analysis of Mechanical and Electrical Strains on Flat Fibers Straight and S-Bend Bragg Gratings Channel by Using Finite Element Method" submitted to Jurnal Teknologi Universiti Teknologi Malaysial on 6th December 2019.